

**SCALE-UP IN CARBON-IN-PULP ADSORPTION PROCESS
SYSTEMS**

KODJO ISAAC AFEWU

A dissertation submitted to the Faculty of Engineering,
University of the Witwatersrand, Johannesburg, in
fulfilment of the requirements for the degree of Master
of Science in Engineering.

Johannesburg, 1992

To my dear wife, Gladys and our daughter,
Kekeli

'Now to Him who is able to do immeasurably
more than we ask or imagine, according to His
power that is at work within us, to Him be
glory in the church and in Christ Jesus
throughout all generations, for ever and
ever! Amen.'

DECLARATION

I declare that this dissertation is my own unaided work, except where specific acknowledgement is made. It is being submitted for the degree of Master of Science(Engineering) to the Faculty of Engineering, University of the Witwatersrand, Johannesburg. It has not been submitted before for any degree or examination in this or any other University.



KODJO I. AFEWU

18TH day of SEPT. 1992.

ABSTRACT

An investigation was undertaken into the influence of agitation intensity on the adsorption of aurocyanide from slurries onto activated carbon. This involved estimating the film mass transfer coefficient from kinetic experiments and the power input for agitation from measurements of the torque exerted by the agitator drive.

It was found - as expected - that the rate of transfer of aurocyanide onto carbon increases sharply as the speed of agitation is increased up to the point where all the carbon particles in the system are just assimilated into the slurry. Thereafter, the rate increases only slowly as the speed of agitation is increased further.

For all the vessel-impeller configurations tested, it was found that the film mass transfer coefficient at the 'just assimilated' condition is approximately the same though the speed and power required to achieve that condition vary from one configuration to another.

A model was developed for scaling up the value of the film mass transfer coefficient as determined at one scale so that its value at a different scale can be predicted. The model applies to typical CIP systems. The scale-up model represents adequately the data above the 'just assimilated' condition, with all the data lying within 5% of the predicted values. A procedure is recommended for scaling up the values of the film mass transfer coefficient from laboratory to larger scales.

ABSTRACT

An investigation was undertaken into the influence of agitation intensity on the adsorption of aurocyanide from slurries onto activated carbon. This involved estimating the film mass transfer coefficient from kinetic experiments and the power input for agitation from measurements of the torque exerted by the agitator drive.

It was found - as expected - that the rate of transfer of aurocyanide onto carbon increases sharply as the speed of agitation is increased up to the point where all the carbon particles in the system are just assimilated into the slurry. Thereafter, the rate increases only slowly as the speed of agitation is increased further.

For all the vessel-impeller configurations tested, it was found that the film mass transfer coefficient at the 'just assimilated' condition is approximately the same though the speed and power required to achieve that condition vary from one configuration to another.

A model was developed for scaling up the value of the film mass transfer coefficient as determined at one scale so that its value at a different scale can be predicted. The model applies to typical CIP systems. The scale-up model represents adequately the data above the 'just assimilated' condition, with all the data lying within 5% of the predicted values. A procedure is recommended for scaling up the values of the film mass transfer coefficient from laboratory to larger scales.

ACKNOWLEDGEMENT

I wish to express my heartfelt gratitude to the following people who have played distinguished roles in this investigation:

- Mr L.C. Woollacott for supervising every aspect of this work;
- Professor L. Fatti, Head of Department of Statistics, University of the Witwatersrand for useful discussions on the statistical analysis of this work;
- Mr G. Gibbon of Electrical Engineering Department for modifying the load cell circuit;
- The managements of FRD-CSIR, University Senior Bursary and Bradlow Postgraduate Award for financial support;
- The staff of Kemix (Pty) Ltd. for the impellers;
- Genmin Laboratories for the 690 mm vessel and the frame;
- Mr R. Fletcher of Wits Technikon, Messrs J. Morffitt, J.J. Bezuidenhout, A. Armstrong and J. Ndegenza of the workshop in our department for various instances of assistance in the equipment set-up;
- The staff of Western Deep Levels Gold Mines 1 and 2 for the activated carbon and residue for this work;
- Mr M. Ramotsehoa of Chemical Engineering Department, for the analysis on AAS.
- Messrs G. Banini, B. Naidu, B. Mothibeli, P. Sesinyi and Dr W. Assibey-Bonsu for the help in fetching the residue from Western Deep Levels Gold Mine, and for their assistance on uncountable number of occasions;
- My christian brethren and the Ghanaian community in Johannesburg.
- My dear wife Gladys and our daughter Kekeli, for their encouragement and support.

TABLE OF CONTENTS

	PAGE
DECLARATION	i
ABSTRACT	ii
ACKNOWLEDGEMENT	iii
TABLE OF CONTENTS	iv
LIST OF FIGURES	viii
LIST OF TABLES	xiii
CHAPTER ONE	1
INTRODUCTION	1
1.1 OVERVIEW	1
1.2 A BRIEF HISTORY OF THE CIP PROCESS	2
1.3 A TYPICAL MODERN CIP PLANT	4
1.4 THE MODELLING OF ADSORPTION	5
1.4.1 Empirical Rate Models	7
1.4.2 Mechanistic Rate Models	8
1.4.3 More Complex Adsorption Models	9
1.5 THE SCALE-UP PROBLEM	11
1.6 OBJECTIVES AND SCOPE OF THIS RESEARCH	13
1.6.1 Objectives	13
1.6.2 Scope	13
CHAPTER TWO	14
MIXING AND AGITATION THEORY	14
2.1 INTRODUCTION	14
2.1.1 Degree of Agitation	15
2.2 CONTACTOR GEOMETRY AND POWER FOR AGITATION	16
2.2.1 The Vessel	16
2.2.2 Power and Flow Numbers of Impellers	16
2.2.3 Circulation and Types of Impellers	18
2.3 SUSPENSION CRITERION AND MODELLING	20
2.3.1 Complete Suspension Criteria	20
2.3.2 Homogenous Suspension Criteria	22
2.3.3 Assimilation of Floating Solids Particles	22

2.3.4	Suspension Modelling	23
	CHAPTER THREE	26
	MASS TRANSFER AND SCALE-UP MODELS	26
3.1	THE FILM MASS TRANSFER COEFFICIENT	26
3.1.1	Definition	26
3.1.2	Classical Film Transfer Theory	27
3.1.3	Estimation of the Film Mass Transfer Coefficient	27
3.1.4	Problems of Intraparticle Mass Transfer	29
3.2	THE FILM MASS TRANSFER COEFFICIENT AND DIMENSIONLESS MASS TRANSFER CORRELATIONS	30
3.3	DEVELOPMENT OF A SCALE-UP MODEL	35
3.3.1.	Basis	35
3.3.2	Derivation of Scale-up Equations from Mass Transfer Correlations	38
3.3.3	Other Approaches for the Development of a Scale-up Model	40
3.3.4	Summary	41
3.4	DETERMINATION OF THE POWER TO JUST ASSIMILATE THE CARBON	41
	CHAPTER FOUR	44
	EXPERIMENTAL	44
4.1	INTRODUCTION	44
4.2	THE DESIGN OF THE ADSORPTION CHEMISTRY	44
4.2.1	Initial Gold concentration	44
4.2.2	Solution Chemistry	45
4.2.3	Carbon	45
4.2.4	Inert Solids	47
4.3	GEOMETRICAL CONSIDERATIONS	48
4.4	THE MEASUREMENT OF SPEED AND POWER	49
4.4.1	Dealing with Friction	50
4.4.2	Dealing with Fluctuations	52
4.5	THE AGITATION SYSTEMS USED	52

4.5.1	185, 305 and 300 mm diameter vessels	52
4.5.2	690 and 1200 mm diameter vessels	54
4.6	KINETIC TESTS	54
4.7	REPRODUCIBILITY TESTS	58
4.8	RESULTS	61
	CHAPTER FIVE	69
	DISCUSSIONS OF RESULTS	69
5.1	KINETIC DATA	69
5.2	THE INFLUENCE OF AGITATION SPEED AND POWER ON THE MASS TRANSFER COEFFICIENTS	69
5.3	QUANTIFYING THE INFLUENCE OF AGITATION ON THE MASS TRANSFER COEFFICIENT	81
5.4	TESTING THE POTENTIAL SCALE-UP MODELS	85
5.5	THE FILM MASS TRANSFER COEFFICIENT AT THE 'JUST ASSIMILATED' CONDITION	89
5.6	THE SPEED/POWER TO JUST ASSIMILATE THE CARBON	93
5.7	SOURCES OF ERROR IN THIS INVESTIGATION	98
	CHAPTER SIX	102
	CONCLUSIONS AND SCALE-UP PROCEDURE	102
6.1	CONCLUSIONS	102
6.2	SCALE-UP PROCEDURE	103
6.3	LIMITATIONS OF THE SCALE-UP MODEL	104
6.4	RECOMMENDATIONS FOR FUTURE WORK	105
	REFERENCES	107
	APPENDICES	114
1A	POWER DATA	114
1B	DATA FROM KINETIC TESTS	117
2A	DETERMINATION OF FRICTIONAL TORQUE IN THE TORQUE MEASURING EQUIPMENT	

	- Small Vessels	139
2B	DETERMINATION OF FRICTIONAL TORQUE IN THE TORQUE MEASURING EQUIPMENT	
	- Large Vessels	146
3A	BI-LINEAR MODEL - THEORY	152
3B	COMPUTER PROGRAM FOR ESTIMATION OF PARAMETERS IN THE BI-LINEAR MODEL	157
4A	FITNESS OF THE BI-LINEAR MODEL - THEORY	161
4B	COMPUTER PROGRAM TO DETERMINE THE FITNESS OF THE BI-LINEAR MODEL	163

LIST OF FIGURES**PAGE**

Figure 1.1	Schematic diagram of a typical CIP circuit	6
Figure 2.1	Diagram of radial flow pattern	19
Figure 2.2	Diagram of axial flow pattern	19
Figure 3.1	Non-linear film diffusion model: Dimensionless time-concentration profiles for different initial gold concentrations (After Le Roux et al(19))	31
Figure 3.1	Non-linear film diffusion model for an initial gold concentration of 8.73 mg/dm ³ (After Le Roux et al(19))	31
Figure 4.1	Calibration curve for the load cell	51
Figure 4.2	Schematic diagram of the modification of the load cell circuit	53
Figure 4.3	Schematic diagram of the agitation system for the 185, 305 and 330 mm diameter vessels	55
Figure 4.4	Schematic diagram of the agitation system for the 690 mm diameter vessel	56
Figure 4.5	Schematic diagram of the	

	agitation system for the 1200 mm diameter vessel	57
Figure 4.6	Kinetic tests for 185 mm diameter vessel: impeller diameter = 110 mm	63
Figure 4.7	Kinetic tests for 305 mm diameter vessel: impeller diameter = 110 mm	63
Figure 4.8	Kinetic tests for 305 mm diameter vessel: impeller diameter = 130 mm	64
Figure 4.9	Kinetic tests for 305 mm diameter vessel: impeller diameter = 142 mm	64
Figure 4.10	Kinetic tests for 330 mm diameter vessel: impeller diameter = 110 mm	65
Figure 4.11	Kinetic tests for 330 mm diameter vessel: impeller diameter = 130 mm	65
Figure 4.12	Kinetic tests for 330 mm diameter vessel: impeller diameter = 142 mm	66
Figure 4.13	Kinetic tests for 690 mm diameter vessel: impeller diameter = 275 mm	
Figure 4.14	Kinetic tests for 1200 mm diameter vessel:	

impeller diameter = 480 mm

67

- Figure 5.1 The effect of the speed of agitation on the film mass transfer coefficient of (vessel diameter = 185 mm) 70
- Figure 5.2 The effect of power of agitation on the film mass transfer coefficient (vessel diameter = 185 mm) 71
- Figure 5.3 The effect of the speed of agitation on the film mass transfer coefficient (vessel diameter = 305 mm) 72
- Figure 5.4 The effect of power of agitation on the mass transfer coefficient (vessel diameter = 305 mm) 73
- Figure 5.5 The effect of the speed of agitation on the film mass transfer coefficient (vessel diameter = 330 mm) 74
- Figure 5.6 The effect of power of agitation on the film mass transfer coefficient (vessel diameter = 330 mm) 75
- Figure 5.7 The effect of speed of agitation on the film mass transfer coefficient (impeller diameter = 275 mm vessel diameter = 690 mm) 76

Figure 5.8	The effect of power of agitation on the mass transfer coefficient (impeller diameter = 275 mm vessel diameter = 690 mm)	77
Figure 5.9	The effect of speed of agitation on the mass transfer coefficient of (impeller diameter = 480 mm vessel diameter = 1200 mm)	78
Figure 5.10	The effect of power of agitation on the film mass transfer coefficient (impeller diameter = 480 mm vessel diameter = 1200 mm)	79
Figure 5.11	The exponent x_1 (Equation 3.32) on E vrs vessel diameter	83
Figure 5.12	The effect of power input on the mass transfer coefficient for the various vessel-impeller configurations	84
Figure 5.13	Observed and Predicted values of k_f using Scale-up model Equation 5.1	88
Figure 5.14	The film mass transfer coefficient vrs speed of agitation at the 'just assimilated' condition for the different impeller-vessel configurations.	90

Figure 5.15	The film mass transfer coefficient vrs the specific power input for agitation for different impeller- vessel configurations.	91
Figure 5.16	The effect of scale (vessel diameter) on E_{j_a} and N_{j_a} for systems of similar T/D ratios	97
Figure 2A.1	Schematic diagram for the determination of the static frictional torque in the set-up for the 185,305 and 330 m vessels	140
Figure 2A.2	Schematic diagram for the determination of Bollard friction on the crossbar	143
Figure 2B.1	Schematic diagram for the determination of the static frictional torque in the set-up for the 690 and 1200 mm vessels	147
Figure 3A.1	A sketch of the relationship between the film mass transfer coefficient and the power input for agitation during the adsorption of aurocyanide onto activated carbon	152

	LIST OF TABLES	PAGE
Table 3.1	Dimensionless Mass Transfer Relationships Reported for Stirred Reactors	34
Table 4.1	Particle size distribution of the solids used for the slurry	48
Table 4.2	Baffle Design for the vessels used	49
Table 4.3	Reproducibility in the estimation of mass transfer coefficient (130 mm diameter impeller in the 305 mm diameter vessel)	60
Table 4.4	Reproducibility in the estimation of power input (130 mm diameter impeller in the 305 mm diameter vessel)	61
Table 4.5	The power data for the various the impeller-vessel configurations	62
Table 4.6	The film mass transfer coefficient for the various impeller-vessel configurations	68
Table 5.1	Fitting the Bi-linear Model	80
Table 5.2	Values of the exponents of N and E for the various impeller-vessel geometries- ($N > N_{j2}$ - Equation 3.30 and $E > E_{j2}$ - Equation 3.32)	82

Table 5.3	Testing of the Scale-up Models	86
Table 5.4	$k_{f,ja}$ values obtained from the speed and power data for the various impeller/vessel geometries	89
Table 5.5	Speed and Power to just assimilate the carbon in the slurry	94
Table 5.6	Predicted and measured values for N_{jz}	96
Table 5.7	The values of E_{ja} and N_{ja} for systems with similar T/D ratios	96
Table 5.8	Power numbers determined for the various mixing configurations (data above the 'just assimilated' condition only)	101
Table 2A.1	Data for determination of Bollard Friction	142
Table 2A.2	Frictional data for kinetic test on the 305 mm diameter vessel and impeller diameter of 110 mm at 300 rpm	144
Table 2B.1	Frictional Data (650 mm Vessel)	149
Table 2B.2	Frictional Data (1200 mm Vessel)	149

CHAPTER ONE

INTRODUCTION

1.1 OVERVIEW

Today, the preferred route for the extraction of gold from cyanide solutions and pulps is by means of adsorption onto activated carbon. This route is more economical and efficient than the conventional filtration and zinc precipitation process route.

This study involves the development of a scale-up procedure for a key parameter used in the quantitative description of the adsorption of gold onto activated carbon. Such a procedure is needed because the agitation intensities in laboratory and full scale CIP vessels are significantly different (1,2). Any parameter that is influenced by agitation intensity will therefore have different values at the two different scales. It is usually more convenient to measure the values of parameters at a laboratory scale than at full industrial scale. In order for such information to be useful, however, it is essential to develop a reliable relationship between the values at laboratory and full scale conditions.

As an introduction to the study, an overview will be given of the most important carbon based extraction system - the CIP process - and of the method used to describe the process quantitatively. This will provide the background needed to explain the objective and relevance of this work.

1.2 A BRIEF HISTORY OF THE CIP PROCESS

It was first recorded in 1847 that activated carbon could adsorb gold and in 1880 W.N. Davis patented the use of wood charcoal for the recovery of gold from chloride leached solutions(3). W.D. Johnston in 1894 patented the use of wood charcoal as an adsorbent of gold from cyanide solution(4,5). In 1916, Yuanmi mine in Western Australia recovered gold from cyanide solution by pumping the pregnant solution through three successive filters containing carbon. The loaded carbon was incinerated and the resultant ash smelted to recover the gold. At that time there was no known procedure to elute the gold from the carbon(3,5). The loadings of gold on the early charcoal were very low because the quality of the charcoal that was available was not good. The technique was not developed further for many years because of the efficiency and predictability of an alternative extraction route, namely the precipitation of gold using zinc dust.

Chapman(4,5) in 1939, patented the use of fine carbon for gold recovery from cyanide pulp with the loaded carbon recovered by flotation using diesel oil and a frother. The gold loaded-carbon (flotation concentrate) was smelted to recover the gold. Bufflesfontein Gold Mine used a similar process and added fine carbon to pyrite flotation after cyanidation and filtration and recovered extra gold in the pyrite concentrate(4,6).

The U S Bureau of Mines pioneered the research and development of the modern carbon-based extraction procedure for gold. They used activated carbon manufactured from coconut shells, which they found to be a very good adsorbent of gold from cyanide solution. Such a carbon has a high abrasive resistance and is physically durable in agitated slurries.

Getchell Mine in Nevada followed the Chapman method and smelted the carbon to recover the adsorbed gold(5). Later, this mine used the elution process developed by U.S. Bureau of Mines that employed hot caustic soda solution to strip the gold from the loaded carbon. The gold was electrowon from the eluate. Getchell Mine recycled the stripped carbon for between 10 to 15 cycles before replacing it, but they never gave it any regenerative treatment(5).

In 1961, Carlton Mill at Cripple Creek in Colorado, built a CIP circuit in which the carbon moved counter-current to the flow of the cyanided pulp. Airlifts moved the carbon pulp continuously onto external vibrating screens that separated the pulp from the carbon in each stage. The loaded carbon was eluted using hot caustic cyanide and reactivated thermally. This was done prior to recycling, by heating the eluted carbon in a steam atmosphere in a kiln externally heated to 600°C. The gold in the eluate was recovered by electrowinning in the so-called Zadra cell. The Carlton flowsheet of 1961 has undergone little change in subsequent CIP circuits(5).

Homestake Gold Mine in South Dakota, USA, established the first large-scale CIP circuit in 1973 to treat about 2250 tons of slimes per day(5). This scale of production initiated a world-wide interest in the CIP process.

Research on the amenability of extracting gold from South African gold ores and gold containing materials (for example, fine calcines, finely ground concentrates and tailings) using this process went on and the following improvements have evolved(5):

- a batch elution procedure incorporating a hot caustic cyanide soak followed by a wash with hot water, - (patented by Anglo-American Research

- Laboratories);
- an acid treatment of eluted carbon in dilute hydrochloric acid to remove scale formed by calcium carbonate and calcium sulphate precipitates from the pulp;
 - the use of internal screens to retain the activated carbon for circulation counter-current to the pulp in the CIP circuit;
 - the use of the CIP process to reclaim gold from dumps and slime dams;
 - the introduction of higher reactivation temperatures for effective regeneration of the carbon after fouling by organic substances in the pulp; and
 - the design and development of the Anglo-American Corporation (AAC) pump cell which is a novel contactor for CIP and resin-in-pulp (RIP) applications. It combines the functions of pumping, screening and agitation in a single drive unit operating with a modular high capacity cell (7).

1.3 A TYPICAL MODERN CIP PLANT

A typical CIP adsorption circuit today comprises a number of well stirred contactors (vessels) in series. Leached pulp - after it has been pre-screened at 0.6 mm (4) to remove any large particles or woodchips that might block the interstage screens - is fed to the first contactor. After undergoing agitation in that contactor it gravitates through the series to the last contactor. In each vessel interstage screens retain the activated carbon and prevent the carbon particles from moving cocurrent with the slurry. Activated carbon (fresh and/or regenerated) is added periodically to the last vessel in the series, and periodically is moved up through the CIP train to the first vessel. Thus the carbon moves countercurrent to the flow of the leached pulp.

The countercurrent movement of the carbon is achieved by pumping or air-lifting the carbon and the pulp from one contactor to the preceding contactor in the adsorption train. This process is illustrated in Figure 1.1. Not all of the carbon and pulp in a contactor is transferred to the preceding stage. As a result the gold loading on the carbon depends on the length of time a particle has stayed in the adsorption system.

The loaded carbon from the first contactor is sent to the elution circuit where the gold (and the silver) are stripped from the carbon in an elution column using hot caustic cyanide solution. The eluate containing the gold (and silver) is then fed to an electrowinning cell containing a stainless steel anode and a permeable cathode made of steel wool. The barren electrolyte is returned to the elution circuit as an eluant, so the elution and electrowinning units form a closed circuit. The gold and the silver values are finally recovered by smelting the steel wool to bullion.

1.4 THE MODELLING OF ADSORPTION

Stange(8), Bailey(9,10) and Woollacott, Stange and King(11), after considering the number of variables and the complexity of their interactions in CIP adsorption systems, concluded that simulation techniques are the most cost-effective means of conducting an extensive and in-depth examination of design and operational alternatives.

Simulation (as outlined by Stange(8), Ford and King(12), King(13) and Lynch(14)) has become indispensable in the modern mineral processing industry for the following reasons:

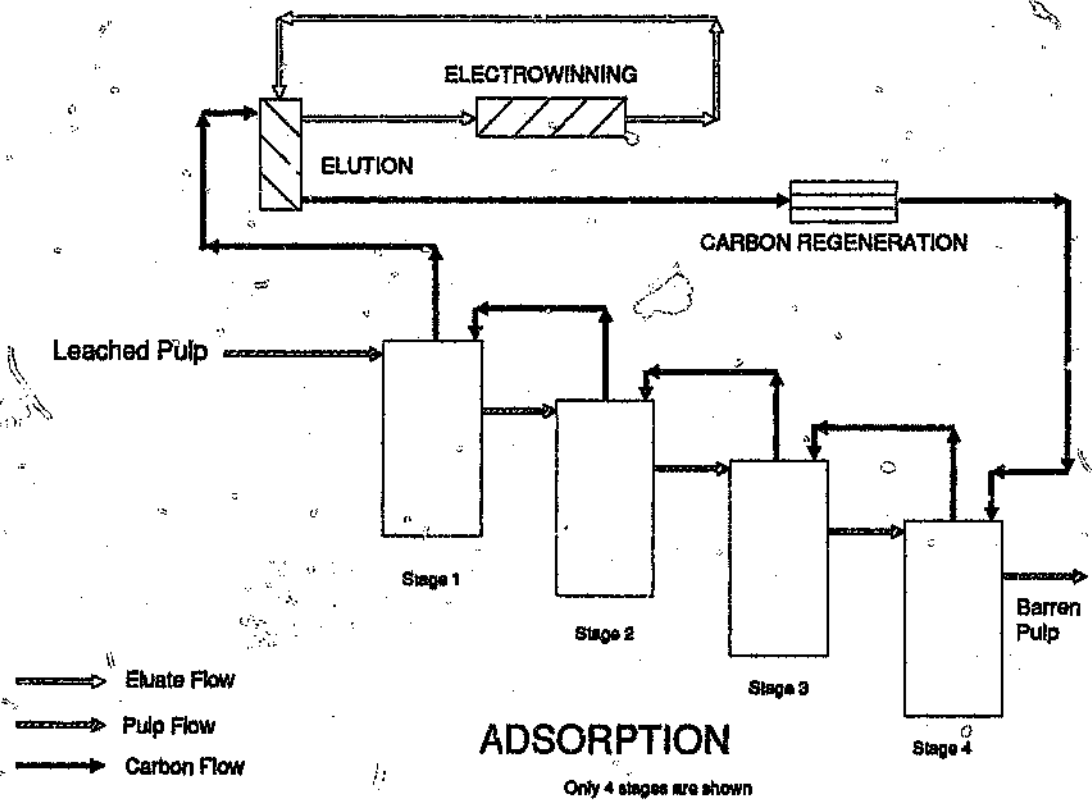


Figure 1.1: Schematic diagram of a typical CIP circuit

- Flowsheet alternatives for existing plants as well as for new plants can be evaluated at minimum cost;
- The financial implications for different processing alternatives can be determined at minimum cost and with minimum data;
- The complex interactions between the various units in a flowsheet can be studied, perhaps leading to an increased knowledge of the processes taking place;
- Interactive simulations make good training and educational tools; and
- Equipment scale-up and off-line optimization can be done at minimum cost.

In the simulation of the CIP process attention must be focused on the the kinetics of adsorption. This is because the adsorption of gold from cyanide solutions onto activated carbon does not reach equilibrium within the time allowed in industrial extraction circuits(2,4,19). To simulate adsorption therefore requires a quantification of the kinetics of adsorption. The rate of adsorption is modelled either empirically or mechanistically.

1.4.1 Empirical Rate Models

Empirical rate models for the adsorption of aurocyanide from solutions onto activated carbon have been reviewed by among others van Deventer(4), Le Roux(2), Le Roux et al(19) and Woollacott et al(11). The common ones are listed below, as discussed by Woollacott et al(11):

Simple First Order Rate model

This model has been used to describe the initial rate of adsorption of aurocyanide onto activated carbon. It has the form (3,11):

$$R = k_1 C \quad 1.1$$

Dixon Model (developed by Dixon et al (15) and used by among others William and Glasser (16)). It is given by:

$$R = k_2 (C[y^* - y] - k_3 y) \quad 1.2$$

The kn model (developed by Fleming et al (17)). It is given by:

$$y - y_0 = k_4 C_{ss} t^n \quad 1.3$$

Nicol's Model (developed by Nicol et al (18)). It has the form:

$$R = k_5 (KC - y) \quad 1.4$$

where R is the rate of adsorption of gold per unit mass of carbon. y is the concentration of gold on carbon and C the gold concentration in solution at time t. y_0 is the initial concentration of gold on carbon and C_{ss} the steady-state concentration of gold in solution.

k and n are constants for a particular plant.

k_1 to k_5 are rate constants, and K and y^* are equilibrium parameters.

As usual with empirical models, these models are limited either as far as adequacy of fit is concerned or in terms of the time span over which they accurately describe the residual concentration of gold in solution. Predictions outside the ranges investigated, therefore, cannot be done reliably.

1.4.2 Mechanistic Rate Models

Mechanistic rate models used to describe the adsorption

of aurocyanide from solution onto activated carbon attempt to describe one or more of the following transport mechanisms (2,19,20):

1. Film diffusion: the diffusion of the adsorbate (in this case aurocyanide) from the bulk liquid phase through an assumed hydrodynamically stagnant layer or liquid film surrounding the adsorbent (activated carbon in this case);
2. Pore diffusion: diffusion of the adsorbate within the pores of the particles of carbon;
3. Surface diffusion: diffusion of adsorbate along the pore wall of the adsorbent; and
4. Adsorption onto the internal surface of the carbon.

Each of the four steps potentially constitutes a resistance to the transport mechanism of the adsorbate (19,20), and have been considered in different ways by different workers (2,20).

The Classical Film diffusion model

This has the form (2,4):

$$R = A_s k_f (C - C^*) \quad 1.5$$

where A_s is the film area per unit mass of carbon, k_f is film mass transfer coefficient, C^* is the gold concentration in solution at equilibrium with a carbon loading of y .

C^* can be determined from an appropriate isotherm equation. A number of these are applicable to CIP adsorption systems.

1.4.3 More Complex Rate Models

As indicated by Woollacott et al (11), a number of adsorption models have been developed that consider other

rate controlling mechanisms in addition to film diffusion control. Dixon, Cho and Pitt considered a pore diffusion model while Brinkmann and King considered film diffusion, pore diffusion and reaction kinetics as the rate controlling mechanisms (11). Johns introduced a factor to represent the degree of control exerted by intraparticle diffusion in the kinetic term in his film diffusion model (11).

Le Roux(2) and Young(20) used the Homogenous surface diffusion model developed by Crittenden. This approach assumed that only film diffusion and surface diffusion are rate controlling. They were able to make good predictions of the experimental data using this approach.

Van Deventer(4) - who based his model on Peel's branched pore model - assumed that carbon consists of macropores in which rapid initial adsorption of gold from solution takes place, and micropores, in which restricted diffusion occurs. He was also able to make good predictions of the experimental data using this approach. His model, however, is mathematically complex and in practice it is difficult to use.

The need to consider at least two rate-controlling mechanisms in describing adsorption kinetics has been recognised for some time. In those models that attempt to do this, account is taken of film diffusion and at least one of the intraparticle diffusion mechanisms.

Film diffusion is described in terms of the Classical Film diffusion mechanism that was employed in the development of Equation 1.5. The key parameter needed to do this is the film mass transfer coefficient, k_f . Intraparticle diffusion is described in various ways - but all of these require the definition of an intraparticle mass transfer coefficient of some kind, k_i .

For the modelling approaches to be successful in their attempt to describe the adsorption process the values of these mass transfer coefficients must be estimated experimentally.

1.5 THE SCALE-UP PROBLEM

It would be most convenient if all the parameters needed in the adsorption models could be estimated in the laboratory. For many of the parameters this can be done because they are not scale dependent. For example, the equilibrium condition that drives adsorption is influenced by the chemical environment and the nature of pulp and carbon. This influence is not affected by the scale of the adsorption system. The parameters in the equilibrium model can therefore be measured at laboratory scale provided the test conditions are the same as those anticipated in the plant.

The same is true of the intraparticle mass transfer coefficient, k_1 . Its magnitude depends on the chemistry of the leached solution, the nature of the pulp and the nature and state of the carbon. These conditions can be accurately reproduced in the laboratory and so the values of the parameters can be estimated at that scale.

In the case of the film mass transfer coefficient, however, the situation is different. The nature of the film surrounding the carbon particles is very dependent on the intensity of the agitation in the adsorption system, as well as on other factors such as the size of the carbon particles, the pulp density and the chemical conditions of the solution and carbon. All of these factors except that of agitation intensity are not influenced by the scale of the adsorption system.

An increase in the intensity of agitation in adsorption

systems leads to:

- a reduction of the thickness of the diffusion film at the surface of the carbon particles,
- improved dispersion of the solid throughout the adsorption vessel,
- improved redistribution of the solution so that as soon as the gold is adsorbed onto carbon from the solution adjacent to a particle it is mixed with the bulk of the solution leading to the attainment of a uniform residual solution concentration in a short time.

Since all these three consequences of increased agitation intensity favour adsorption, k_f increases with agitation intensity.

As k_f is affected by agitation intensity, it is not correct to use values of k_f measured at a laboratory scale directly to describe plant adsorption at large scale. The agitation intensity at large scale is invariably much lower than it is in laboratory scale experiments. Consequently for simulation of full scale operations using laboratory scale data, it is necessary to develop a relationship of some sort between the values of k_f at different scales. This relationship is referred to as a scale-up model. Such a model should have reasonably good extrapolation and interpolation characteristics. Its immediate usefulness is that the behaviour of adsorption processes at any scale can be simulated at very little cost on a computer in contrast to time consuming and expensive experimentation in large scale equipment.

1.6 OBJECTIVES AND SCOPE AND OF THIS RESEARCH

In the development of CIP technology, a major difficulty has been the deficiencies in the equipment design to implement the process (7). One specific problem has been the lack of understanding of the way in which the geometrical configuration of the contactors and the mixing conditions in them affect the kinetics of adsorption.

It must be emphasised that though the absence of scale-up information does not prohibit the construction and operation of full scale plants, it does increase both the risk and capital costs involved.

1.6.1 Objective

The objective of this research, therefore, is to establish a scale-up procedure for the film mass transfer coefficient in CIP adsorption systems.

1.6.2 Scope

The scope of this project is as follows:

- to review the literature and in particular mass transfer correlations that are relevant to CIP systems;
- to obtain kinetic and torque data at different scales;
- to find the most appropriate scale-up model for the film mass transfer coefficient.
- to develop a scale-up procedure that is practical to use and as reliable as possible.

CHAPTER TWO

MIXING AND AGITATION THEORY

2.1 INTRODUCTION

Mixing involves many different kinds of operations. The principal applications of mixing equipment in the process industry are (21):

- Blending of solid powders and pastes,
- Suspensions of solids in liquids,
- Dispersion or emulsification of immiscible liquids,
- Dissolution of solids, liquids or gases, and
- Promotion of chemical reactions.

Since mixing is an operation dependent upon fluid motion, it is necessary to evaluate mixing in terms of fluid mechanics. The fluid flow pattern in a mixer is complex and is influenced largely by the geometry of the system and the speed of rotation of the agitator (22,23).

In this project, the system under consideration is the mixing of activated carbon with a gold leach slurry for the purpose of transferring the gold from solution onto the activated carbon.

The mass transfer of gold from the solution phase onto the carbon is enhanced by forced convection through agitation (22). This can be accomplished with compressed air or by using mechanical agitators. Mechanically agitated vessels are superseding the older compressed air-stirred pachucas or Brown tanks because they use less power (24-26). Other problems experienced with air-stirred CIP systems include:

- uneven carbon distribution,

- clogging of the interstage screens due to the violent wave action, and
- difficulties in getting the carbon to re-suspend after a period of air shut down(24-26).

2.1.1 Degree of Agitation

The degree of agitation that is needed in a mixer depends on the application. In some situations, for example the preparation of a two-phase feed for a chemical reactor, it is important that the suspension is maintained in a fairly homogeneous condition. However, in CIP adsorption vessels, all that is required is to ensure that all the carbon particles are fully assimilated in the slurry(24,26). They should neither settle on the bottom of the contactor if the density of the slurry is lower than that of the carbon nor float on the surface of the slurry if the density of the slurry is higher than that of the carbon. Consequently, an important criterion in the design of a CIP contactor is the power required to just assimilate the carbon particles.

Any increase in the speed of the agitator above that required to just assimilate the particles leads to an increase in the rate of transfer of gold(25,26), but indications are that the increase is only slight(26). There appears to be little benefit in a small increase in transfer rate especially when compared to the cost of extra power that must be applied(25) and the increased abrasion of the carbon particles and equipment that results(24-26).

2.2 CONTACTOR GEOMETRY AND POWER FOR AGITATION

2.2.1 The Vessel

Cylindrical flat bottom tanks have been most widely used for CIP adsorption vessels(28), though some problems occur with the accumulation of unsuspended solids in the centre of the bottom of the tank and at the joints between the bottom of the tank and the wall(29).

Baffles are necessary in the vessels to eliminate the formation of a single vortex. If vortices are allowed during the agitation, unreliable adsorption patterns result due to inefficient agitation of the contents of the vessel(30). Scale-up relationships developed from data obtained under such conditions may be unreliable(29). The presence of baffles leads to an increase in power consumption of the agitator but it also promotes mass transfer operations as their presence gives rise to significant velocity fluctuations in the vessel(31).

Baffles are normally arranged off the bottom and the wall of the vessel to avoid the accumulation of solids behind them(32).

2.2.2 Power and Flow Numbers of Impellers

The power drawn by impellers depends on the speed, diameter and the design of the impeller, and the following mixing environmental factors(33):

- physical properties of the fluid (slurry) medium,
- vessel size and geometry,
- impeller location relative to the vessel and slurry,
- slurry boundaries relative to other impellers or obstructions in the vessel,

- the inclusion, design and location of baffles.

The theoretical power, P_H , drawn by a hydraulic mixer is given by (26, 33):

$$P_H = \rho N^3 D^5 \quad 2.1$$

where D is the diameter of the impeller (m),

N is the rotational speed of the impeller (s^{-1}),

ρ is the density of the suspension ($kg\ m^{-3}$).

The actual hydrodynamic power, P , drawn by the impeller of a mixer is invariably different from P_H . The ratio P/P_H is termed the power number, N_p . Consequently the actual power drawn by an impeller is given by (26, 33):

$$P = N_p \rho N^3 D^5 \quad 2.2$$

The power number of an agitation system provides an indication of the margin between the power that is applied and the power that is theoretically required to turn the impeller.

Power is not the only criterion that is important in mixing. The volume of the liquid or slurry moved per unit time by the impeller is also important because clearly it is the rate of movement of the liquid or slurry that will determine the degree of mixing. The rate of movement of the liquid is termed the pumping capacity of the impeller, Q_d , and it is defined as the volume of liquid (slurry) discharged through the impeller per unit time. This is proportional to the product of the tip speed of the agitator and its discharge area, the proportionality constant being termed the discharge flow number, N_d . The discharge flow number is therefore defined as (33, 39):

$$N_d = \frac{Q_d}{ND^3}$$

2.3

2.2.3 Circulation and Types of Impellers

In the study of the suspension of solids in liquids, by mechanical agitation, impellers may be classed as either radially or axially discharging. Radial flow impellers discharge slurry (fluid) from the impeller perpendicular to its axis of rotation. For axial flow impellers the slurry enters the impeller and discharges from it parallel to its axis.

The criterion used when classifying an impeller as being either radial or axial flow type is the magnitude of the ratio of the power number to the flow number, N_p/N_d . This ratio is also an indicator of pumping efficiency of the impeller in a given geometry.

An impeller may be considered to be an inefficient pump (33). Its pumping efficiency is defined as the ratio of the discharge flow number to the power number, N_d/N_p . The larger the ratio N_d/N_p , the higher the pumping efficiency.

Impellers with low pumping efficiencies are called shear type impellers and most radially discharging impellers belong to this group. Impellers with high pumping efficiencies are called circulation or flow impellers, and axially discharging propellers and inclined (pitched) blade turbines belong to this group. Thus axial flow impellers have higher pumping capacity than radial flow impellers. The actions of radial and axial flow impellers are shown schematically in Figures 2.1 and 2.2.

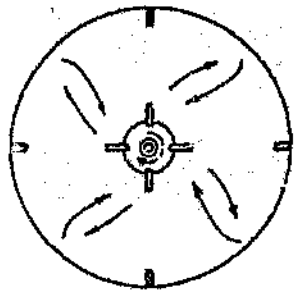
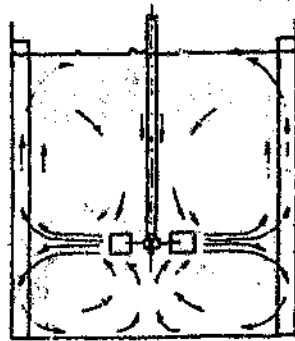


Figure 2.1: Schematic diagram of radial flow pattern

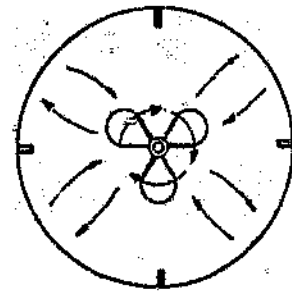
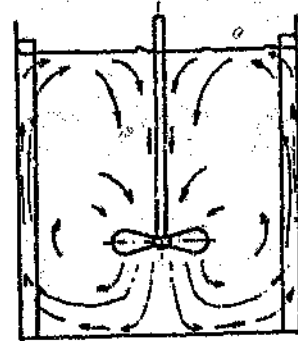


Figure 2.2: Schematic diagram of axial flow pattern

respectively. Chudacek(34) reported that for complete off-bottom suspension of solids, axially discharging impellers are more efficient than radially discharging impellers. Coetzee and Cloete(26) confirmed this conclusion.

2.3 SUSPENSION CRITERION AND MODELLING

For an efficient mixing tank geometry, the factors controlling the solid suspension should be identified. Chudacek(34) has shown that scale-up parameters for mixing are not constant, but are dependent upon the mechanism of suspension. Two types of criterion of suspension in agitated vessels can be defined as:

- complete suspension criteria - in which the behaviour of the last fraction of unsuspended solids at the bottom of the vessel is used as the determinant of suspension speed, and
- homogenous suspension criteria - which use the attainment of certain degrees of suspension homogeneity in the vessels as a determinant of suspension speed.

2.3.1 Complete Suspension Criteria

The first suspension criterion that will be used was initially proposed by Zwietering(27,34) in 1958. It is known as the complete-off-bottom suspension (CBS) criterion. By this criterion, the critical suspension speed, N_{js} , is defined as the minimum impeller speed necessary to ensure that no solids remain stationary on the bottom of the tank for longer than 1-2 seconds.

Despite much research on suspension of solids in liquids,

the best overall correlation is still the one proposed by Zwietering (27, 33, 35, 36), and the critical speed is given by:

$$N_{js} = S v^{0.1} d^{0.2} \left(\frac{g \Delta \rho}{\rho_L} \right)^{0.45} X^{0.13} D^{-0.85} \quad 2.4$$

where S is a dimensionless particle suspension parameter. Data for S are available in graphical form for a variety of impeller types, impeller clearances and impeller-vessel diameter ratios.

v is the kinematic viscosity,
d is the particle diameter,
X is percent weight of solids,
D is the impeller diameter,
g is the gravitational constant,

$$\Delta \rho = \rho_s - \rho_L,$$

where

ρ_s is the specific gravity of solids being suspended and ρ_L is the specific gravity of the liquid.

The exponents of the parameters in the Zwietering's Equation were found to be independent of impeller type, vessel size, impeller clearance and impeller to vessel diameter ratio. The dimensionless constant, S, accounted for the variations in the system geometry (27, 36, 39).

Bohnet and Neismak reported a CBS criterion reproducibility of 2-5% but cautioned that if suspension speed is determined only by observation of the tank bottom, this completely neglects the behaviour of the remainder of the tank and that exact measurement of the CBS becomes difficult at higher solid concentrations (34). Other researchers proposed various fractions of solid

suspension, for example Standinger and Moser proposed 100% suspension from the bottom of the tank over a short period, and Hirsekorn and Miller termed this condition complete suspension in their work(34). Chudacek(34) proposed 98% suspension, which he claimed overcame the difficulty of dis-proportionately increased energy expenditure when suspending the last amount of unsuspended solids in a baffled flat bottom tank.

2.3.2 Homogenous Suspension Criteria

This suspension criterion considers the agitation speed required to achieve a given degree of suspension homogeneity. A truly homogenous particle distribution in an agitated tank is, however, nearly impossible to achieve in most solid-liquid systems(34). The determination of suspension speed by the homogenous criterion requires a number of concentration measurements at different locations in the vessel. Particle degradation and interference of the flow pattern by the sampling vessel during sample withdrawal often pose difficulties in obtaining a truly representative sample and hence this measurement of concentration distribution in a stirred vessel can be extremely tedious. Since attainment of a homogenous distribution of the solids in CIP adsorption vessels(25,26) is not necessary, the homogenous suspension criteria will not be considered further.

2.3.3 Assimilation of Floating Solid Particles

For the situation where the solid particles are less dense than the liquid/slurry in which they are to be mixed, the particles tend to float. In such a case, an equivalent criterion to N_{js} in the Zwietering's Equation

may be referred to as the speed to just assimilate the solids. This is defined as the speed required to ensure that particles float on the surface of the liquid/slurry for a period of time not longer than 1 to 2 seconds.

Nienow(37) said that this process is actually more energy intensive than solid suspension. He indicated that the determination of the energy and speed may be complicated by fine solids entrapping large amounts of air leading to a reduction in the effective density of the solids.

Though the problem has not been studied extensively Joosten et al(37), using a four-bladed 45° pitch impeller for vessels of 0.27 to 1.8 m diameter, got the following relationship for the minimum speed, N_{ja} to disperse the floating solids:

$$N_{ja} = (0.036 \left(\frac{D}{T}\right)^{-3.65} \left(\frac{\Delta\rho}{\rho_L}\right)^{0.42} \left(\frac{g}{D}\right)^{0.5})^{2.5}$$

where T is diameter of the vessel.

This equation was derived for solids in the particle size range of 2 to 10 mm. They found that large D/T (D/T = 0.6) gave the minimum power. It was noted that particles which are not easily wetted give more problems in the determination of the speed and energy required to disperse floating solids. Taking note of this observation, precautions were taken in this investigation to wet the carbon particles properly. They were soaked in water at least twenty four hours before use to dislodge air entrapped in the particles.

2.3.4 Suspension Modelling

The extensive range of geometries and materials examined by Zwietering, coupled with the advantage of being able to estimate N_{ja} from Equation 2.4, for a wide range of

conditions has resulted in this equation being the one recommended for design(36) of agitation equipment. At first sight, the purely empirical approach adopted precludes any insight being gained into the mechanisms responsible for suspension. However, the fact that all the parameters specifying the liquid and particle properties have the same exponents independent of the agitation geometry at least suggests that the same mechanism applies to all geometries investigated. Several attempts have been made at modelling suspension mechanisms with varied degrees of success.

Kneule, Kolar, Einkenkel and Mersmann, and Musil and Vlk(34) presented models of suspension where the suspension speed was determined from the postulated theoretical power required for solid suspension. They assumed that the power consumed was used only for suspension of solid and that the stirred tank was hydrodynamically homogeneous. Their models were based on incomplete energy balances, since the energy losses occurring in the recirculating liquid due to internal friction and slurry/wall friction were excluded. This omission constitutes a significant flaw in their models.

If suspension models based on energy balances are to succeed, the balance must take into account the following (34,36):

- the energy required to suspend the solids in the ascending stream in the tank periphery,
- energy consumed in slurry/wall friction losses,
- energy consumed in frictional losses in the slurry along the recirculation path from impeller discharge to impeller intake, and
- energy gained by the recirculation stream from falling solids descending toward the impeller.

The energy balance models would therefore have little chance of success since not all of the above mentioned energy terms can be satisfactorily quantified.

Nienow and Miles(38) developed a model for particle suspension in slurries. This model depends on convective flow near the base of the vessel. Assuming u_{base} is the minimum average velocity independent of direction, u_{base} is required to achieve complete suspension. The velocity at any level, u , in the agitated vessel based on many experimental studies is given by(38):

$$\bar{u} = A \frac{(ND^2)}{(T^2H)^{1/3}} \quad 2.6$$

where A is a dimensionless coefficient of proportionality which decreases rapidly with increasing distance from the impeller and H is the height of the slurry in the vessel. This expression (Equation 2.6) implies that the impeller clearance from the base must be low in order to obtain u_{base} with the lowest agitator speed for a particular vessel-impeller configuration.

If E is the mean power per unit mass ($= P/\rho V$), where V is the volume of slurry, and ρ is the density of the slurry, then using Equation 2.2 in Equation 2.6, gives:

$$u \propto u_{base} \propto E^{1/3} D^{1/3} \quad 2.7$$

Equation 2.7 suggests two things, viz:

- u_{base} is attained at lower specific energy by using a large diameter impeller. Alternatively, a larger slower impeller should enable particle suspension to be achieved at lower values of E; and
- a lower energy dissipation rate is required in large scale systems compared to geometrically similar smaller scale systems.

CHAPTER THREE

MASS TRANSFER AND SCALE-UP MODELS

3.1 THE FILM MASS TRANSFER COEFFICIENT

In Chapter 1, the mechanisms influencing the mass transfer of gold from solution onto activated carbon were discussed. In that discussion, it was pointed out that diffusion through the 'stagnant' film around the carbon particles may influence the overall kinetics of adsorption. From the perspective of the classical film diffusion model, the degree of agitation influences the thickness of this film and hence the rate of mass transfer through it.

3.1.1 Definition

In a continuum, if the concentration of a given species is different at different points and the species is mobile then a mass flux, Ψ , will be set up that will tend to eliminate the concentration difference.

The mass flux will be proportional to the concentration difference, the proportionality constant being referred to as the mass transfer coefficient. In the case of the transfer of a species from a bulk fluid - where its concentration is C - onto the surface of a solid - where its concentration is C_s - the species is transferred through a film of liquid adjacent to the surface. In this case the coefficient is termed the film mass transfer coefficient, k_f , and is defined as follows:-

$$k_f = \frac{\Psi}{C - C_s} \quad 3.1$$

3.1.2 Classical Film Diffusion Theory

This theory postulates a linear concentration gradient across the film and diffusion of the species in a direction perpendicular to the surface on which the species adsorb. Diffusion through the film can be described by Ficks first law:

$$\Psi = - D_c \frac{dC(r)}{dr} \quad 3.2$$

where D_c is the diffusion coefficient, $C(r)$ is the concentration of the species at r which is the distance from the surface into the liquid.

Assuming the carbon particles used are all spherical and the flux of the diffusing species, Ψ , is constant, and integrating Equation 3.2 over the radial film of thickness, δ , we obtain:

$$\Psi = \frac{D_c}{\delta} (C - C_s) \quad 3.3$$

In this equation C is now the concentration in the bulk liquid as previously defined. From the definition of the film mass coefficient, k_f , and Equation 3.3, it can be seen that according to the classical film diffusion theory, $k_f = D_c/\delta$.

3.1.3 Estimation of the Film Mass Transfer Coefficient

The classical film mass transfer theory (2,19,20) assumes equilibrium between C_s and the average adsorbent loading or solid phase concentration, y , of the adsorbent species. The mass balance for a batch reactor of volume, V , containing a mass M of adsorbent, is given by:

$$-V \frac{dC}{dt} = M \frac{dy}{dt} \quad 3.4$$

The rate at which the species are adsorbed onto the adsorbent is determined by the flux through the film. Therefore:

$$M \frac{dy}{dt} = \Psi A = Ak_f(C - C_s) \quad 3.5$$

where A is the film area which is equal to the surface area of the adsorbent particles. For spherical particles of diameter, d:

$$A = 6 \frac{M}{\rho_c d} \quad 3.6$$

where ρ_c is the dry density of the adsorbent in air.

Hence:

$$\frac{dC}{dt} = -\beta k_f(C - C_s) \quad 3.7$$

where

$$\beta = 6 \frac{M}{V \rho_c d} \quad 3.8$$

Equation 3.7 may be developed in two ways, viz:

- the linear film transfer model where the adsorbate concentration at the particle surface C_s is assumed negligible as compared to the bulk liquid concentration C , at the initial moments of adsorption, and
- the non-linear film transfer model in which the liquid phase concentration at the particle-liquid surface is not negligible but assumed to be in equilibrium with the solid adsorbate concentration at the interphase. The equilibrium relationship can be expressed using an appropriate isotherm model. This

model is used to extend the range of the film mass transfer model over a longer period of time than is possible with the simple linear film mass transfer model (19).

Le Roux et al (19) compared the estimates of the mass transfer coefficient, k_f for the adsorption of aurocyanide onto activated carbon from experiments using a wide range of initial solution concentrations of gold. The data was fitted using both the linear and non-linear film mass transfer models. They found that there was little to choose between the two models and concluded that there was no justification to use the more sophisticated non-linear film transfer model. This approach has been adopted by many workers (4,6,20).

Integrating Equation 3.7 with C_s being equal to zero, yields:

$$\ln\left(\frac{C}{C_0}\right)\bigg|_{t=0} = -k_f \beta t \quad 3.9$$

where C_0 is the initial concentration of gold in solution. The film mass coefficient, k_f , can therefore be determined from the initial slope of the plot of $\ln C/C_0$ against time.

3.1.4 Problems of Intraparticle Mass Transfer

Because there are potentially more than one rate controlling mechanism in the adsorption of gold onto carbon, Equation 3.9 is valid only if film diffusion is rate controlling. Le Roux has studied this question in some detail. He developed a two-mechanism model in which film diffusion and intraparticle surface diffusion were assumed to be rate controlling. He showed that in batch adsorption experiments over long periods of time both mechanisms needed to be taken into account and that

intraparticle diffusion was more important. During the initial period of adsorption, film diffusion was rate controlling, but the intraparticle mechanism rapidly started to influence the adsorption rate as the concentration of gold on the carbon built up (2,6,19). The transition from film to intraparticle diffusion control extended to longer adsorption periods the lower the initial gold tenor of the solution (2,19). From his data as shown in Figures 3.1 and 3.2, it can be seen that at an initial gold tenor of 8.73 ppm gold or lower, film diffusion is the only rate controlling mechanism and that it is rate controlling over a fairly extended period of time (about 60 minutes). The important consequence of this is that any experiment to determine the film transfer coefficient must be done with low initial gold tenors and over adsorption periods significantly shorter than one hour.

3.2 THE FILM MASS TRANSFER COEFFICIENT AND DIMENSIONLESS MASS TRANSFER CORRELATIONS

The impact of agitation intensity on mass transfer is commonly described through the influence of the hydrodynamics of the system on the mass transfer coefficient. This influence is commonly described by means of correlations between relevant dimensionless numbers.

The dimensionless numbers that are most widely used in these correlations are the Sherwood number, the Reynolds number and the Schmidt number.

The Sherwood number, Sh , represents the ratio of total mass transfer to mass transfer by molecular diffusion. It is defined as (30):

where D , the coefficient of molecular diffusion and L is

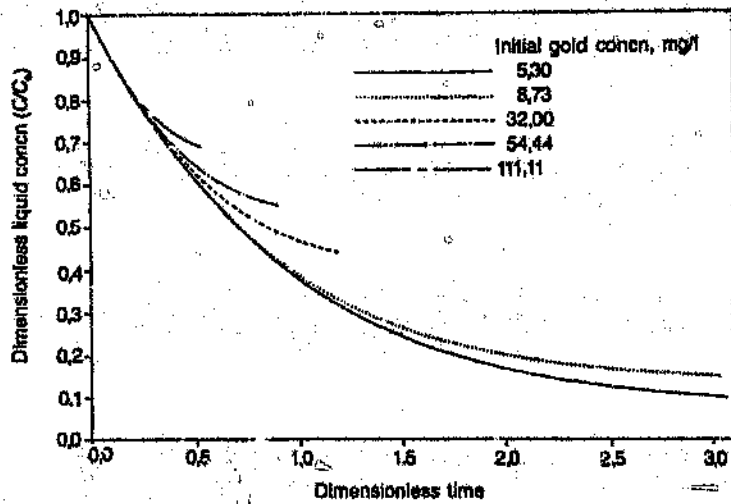


Figure 3.1: Non-linear film diffusion model: Dimensionless time-concentration profiles for different initial gold concentrations (After Le Roux et al (19))

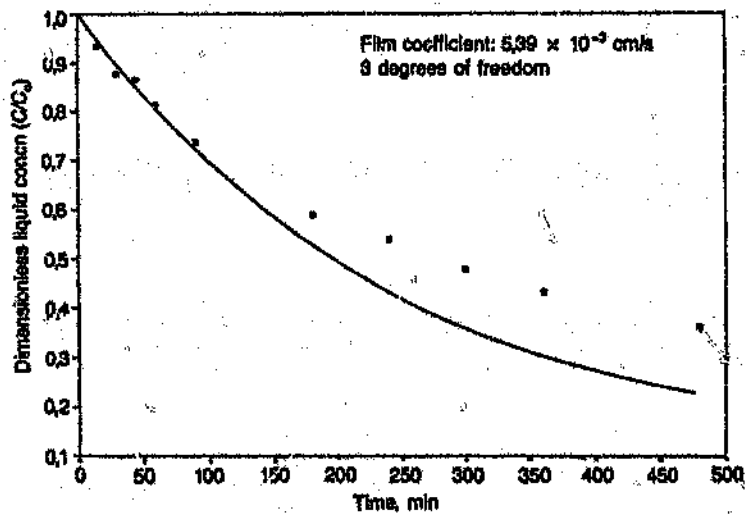


Figure 3.2: Non-linear film diffusion model for an initial gold concentration of 8.73 mg/dm³ (After Le Roux et al (19))

$$Sh = \frac{k_r L}{D_s} \quad 3.10$$

the characteristic dimension of the system. In agitation systems, it is usually taken to be the diameter of the impeller, D (30).

The Reynolds number, Re , of the system is used to characterize the velocity profile, and it is given by (30):

$$Re = \frac{u p L}{\mu} \quad 3.11$$

where u is the particle-fluid slip velocity and μ and ρ are the viscosity and density respectively, of the liquid.

The Schmidt number, Sc , which represents the ratio of the kinematic viscosity to the molecular diffusion coefficient, D_s , is given by (30):

$$Sc = \frac{\mu}{\rho D_s} \quad 3.12$$

The most commonly used forms of the correlations between these dimensionless numbers are those shown in Equations 3.13 and 3.14 (30):

$$Sh = K Re^r \cdot Sc^s \quad 3.13$$

and

$$Sh = A + B Re^m \cdot Sc^n \quad 3.14$$

where A , B , K , m , n , r , s are constants.

A commonly used form of Equation 3.14 is the Froessling expression as stated in Equation 3.15:

$$Sh = 2 + 0.72 Re^{1/2} Sc^{1/3} \quad 3.15$$

The Froessling Equation, though originally derived for laminar bulk flow of fluid around a single particle, has been found to be capable of empirical modification to fit data from a wide range of configurations and turbulent bulk flows(39). Examples of the correlation equations that have been developed for stirred reactors are presented in Table 3.1.

In principle, the film mass transfer coefficient for a CIP system could be estimated using one of these mass transfer correlations discussed above. The main difficulty of this approach is the decision on which of the many mass transfer equations (as stated in Table 3.1) to use and what particle-fluid slip velocity in the Reynolds number should be used. These choices are difficult to make because the hydrodynamics of the slurry-stirred contactors in CIP adsorption systems are complex. Additional difficulties arise because:

- the molecular diffusion coefficient of aurocyanide is not known. Johns(6) assumed a value of $10^{-9} \text{ m}^2\text{s}^{-1}$. Woollacott et al(11) suggested that it would be no greater than $1.8 \times 10^{-9} \text{ m}^2\text{s}^{-1}$.
- the viscosity term is also not known, though a number of empirical equations exist that could be used to estimate it.
- the conditions under which most of these correlation equations were established either cannot be exactly duplicated or do not apply. Variables that may influence these correlations but are not fully considered in the correlations include the size distribution of the solids, impeller size, power and flow numbers, tank geometry, viscosity, pulp density, impeller speed, and adsorption properties of the adsorbent.
- the correlations are difficult to test because the experiments are difficult to conduct with sufficient

Table 3.1: Dimensionless Mass Transfer Relationships Reported for Stirred Reactors

Investigator	Ref.	Relationship	Impeller type	Reynolds no. range	System studied	Characteristic length, L
Hixson & Baum	30	$Sh=0.16Re^{0.62} Sc^{0.5}$	Turbine at 45°	$\geq 6.7 \times 10^4$	Dissolution	vessel diameter
Hixson & Baum	30	$Sh=2.7 \times 10^{-5} Re^{1.4} Sc^{0.5}$	Turbine at 45°	$\leq 6.7 \times 10^5$	Dissolution	vessel diameter
Kafarov	30	$Sh=1.96 \times 10^{-5} Re^{1.4} Sc^{0.5}$	Turbine at 45°	$3.3 \times 10^2 - 7.7 \times 10^3$	Dissolution	impeller diameter
Kafarov	30	$Sh=0.625 Re^{0.62} Sc^{0.5}$	Turbine at 45°	$7.5 \times 10^3 - 6.7 \times 10^5$	Dissolution	impeller diameter
Kafarov	30	$Sh=1.22 \times 10^{-3} Re Sc^{0.5}$	3-blade propeller	-	Dissolution	impeller diameter
Johnson & Cheng Y. Haung	30	$Sh=0.0924 Re Sc^{0.5}$	6-blade turbine	-	Dissolution	vd in Sh# id in Re#
Baker & Treybal	30	$Sh=0.052 Re^{0.83} Sc^{0.5}$	6-bladed turbine	-	Dissolution	vd in Re id in Sh
Humphrey & van Ness	30	$Sh=0.0034 Re^{0.87} Sc^{0.5}$	turbine	-	Dissolution	vessel diameter
Humphrey & van Ness	30	$Sh=0.13 Re^{0.58} Sc^{0.5}$	propeller	-	Dissolution	vessel diameter
Akselrud	6	$Sh=c Re^{0.5} Sc^{0.33}$	-	-	Dissolution	-
Latterman et al	40	$Sh=0.77 Re^{0.159} Sc^{1/3}$	plate turbine	-	Adsorption	particle diameter

vd and id refer to vessel and impeller diameter respectively.

degree of accuracy.

The above difficulties make the determination of the film mass transfer coefficient from the dimensionless correlations impractical and unreliable. The usefulness of these correlations in the current study lies in their claim to be able to describe mass transfer in systems that are geometrically similar but of different scales. How this claim may be exploited to develop scale-up models is discussed in the next section.

3.3 DEVELOPMENT OF A SCALE-UP MODEL

3.3.1 Basis

In Section 1.5, the nature of the scale up problem was discussed in broad terms. It is now necessary to consider the problem in detail.

At the root of the scale-up problem is the desire to measure the film mass transfer coefficient under well controlled conditions in a laboratory environment. To be able to use the values so measured in order to predict the value of the transfer coefficient in larger vessels it is necessary to understand how the differences in the two situations will affect the transfer coefficient. Such an understanding is quantified in the form of a scale-up model.

In order to develop such a model, it is first necessary to identify the key factors that are different in the two scales. It is not difficult to arrange that the chemistry of the solution and the carbon used in the laboratory experiments are the same as will exist at the larger scale. In addition the size and physical nature of the solids - both ore and carbon particles - can be

the same at the two scales. Thus the variables μ , D , ρ (in the dimensionless mass transfer correlations) will be the same at the two scales.

What will be different will be the nature of the film through which mass transfer is taking place. The hydrodynamics of the system as manifested in such things as the carbon-solution slip velocity and the size and nature of eddies in the slurry affect the nature of the film profoundly. The factors that influence these are the size and rotational speed of the impeller and the geometry of the impeller and the mixing system. These factors have been discussed already in Chapter 2. The difficulty in developing a scale-up model arises from the difficulty of quantifying the influence of these factors on the hydrodynamics in the first instance and ultimately on the transfer coefficient itself.

The mass transfer correlations described in the previous section attempt to do this by means of dimensionless parameters that have physical significance. The differences in the hydrodynamics are accounted for by the Reynolds number and the differences in scale by the characteristic length, L .

In defining the Reynolds number, the usual assumption made is that the particle-fluid slip velocity, u , is proportional to the notional velocity (26,30,39), as stated in Equation 3.16.

$$u = \pi ND \quad 3.16$$

where N is the rotational speed of the impeller in revolutions per second. Substituting Equation 3.16 in Equation 3.15, for the same vessel geometry and scale,

$$k_f \propto N^{1/2} \quad 3.17$$

As the power is proportional to the speed to the third power, (Equation 2.2), it follows from Equation 3.17 that the mass transfer coefficient should be proportional to power to the exponent 1/6. Most workers who used the theoretical dimensionless equations (Harriott, Sanger and Deckwer, Glasbury, Oyama and Sindoh, and Coetzee and Cloete(26)), found the mass transfer coefficient to be proportional to power input to the exponent of between 0.1 and 0.3 for various mixer geometries. This is consistent with the value of 1/6 stated above.

Nienow(39) used the same approach when considering the effect of different geometries. He used the more general correlation - Equation 3.17 to obtain:

$$k_f \propto N^{x_1} \quad 3.18$$

He found that x_1 generally lies between 0.4 and 0.6 for efficient suspension geometries and between 0.65 and 0.9 for inefficient geometries. When these values are substituted into Equation 2.2, it yields:

$$k_f \propto P^{x_2} \quad 3.19$$

with x_2 lying between 0.13 and 0.2 for efficient geometries, and 0.21 and 0.3 for inefficient geometries. These values apply to systems in which the adsorbent was fully suspended in the liquid.

Latterman et al(40) investigating the adsorption of phenol from water onto activated carbon got a relationship for k_f to be proportional to the specific power input to the exponent of 0.149. They used only one impeller-vessel configuration but varied the particle size of the activated carbon.

The success of the mass transfer correlations in providing a workable basis for explaining the influence of hydrodynamics on the mass transfer coefficient is

encouraging and the use of these correlations in developing a scale-up model will now be considered.

3.3.2 Derivation of Scale-up Equations from Mass Transfer Correlations

The correlation equation that is most amenable to the development of scale-up procedures is Equation 3.13. If this is expanded, the following relationship is obtained:

$$\frac{k_L L}{D_s} = K \left(\frac{NL^2 \rho}{\mu} \right)^x \left(\frac{\mu}{\rho D_s} \right)^y \quad 3.20$$

As already mentioned the terms D_s , μ , ρ will be the same at the different scales and may be collected in a proportionality constant, J , as:

$$J = KD_s \left(\frac{\rho}{\mu} \right)^x \left(\frac{\mu}{\rho D_s} \right)^y \quad 3.21$$

Equation 3.20 may be developed in different ways, depending on whether D or T are used for the characteristic length. The rotational speed, N in the these correlation may be replaced using either the power input, P , or the specific power input, E .

To do this, Equations 3.22 and 3.23 are used.

$$P \propto N^3 D^5 \quad 3.22$$

and

$$E \propto \frac{P}{T^3} \quad 3.23$$

On this basis, the following scale-up models can be developed.

i. L in both Sh and Re is represented by D:

$$k_f \propto JN^2 D^{2r-1} \propto N^a D^b \quad 3.24$$

and

$$k_f \propto D^{b-5a/3} (E^{1/3} T)^a \propto D^c (E^{1/3} T)^d \quad 3.25$$

ii. L in both Sh and Re is represented by T:

Equations 3.26 and 3.27 are obtained:

$$k_f \propto N^a T^a \quad 3.26$$

and

$$k_f \propto T^a (ED^{-5})^a \quad 3.27$$

iii. L in the Sh and in the Re is represented by T and D respectively.

Equations 3.28 and 3.29 are obtained:

$$k_f \propto N^a D^a T^a \quad 3.28$$

and

$$k_f \propto D^a T^a E^a \quad 3.29$$

iv. L in the Sh and Re is represented by D and T respectively.

Though this option has been tried by some previous workers as shown in Table 3.1, it does not explain the real situation in a mixer. The Re takes care of the

hydrodynamics of the mixer and this depends more on the impeller used than on the vessel. In this light, option ii is also questionable.

The various constants in these relationships a , b , c , m , v_1 , v_2 , w , z_1 , z_2 , and z_3 , may be estimated using multiple regression analysis.

3.3.3 Other Approaches for the Development of a Scale-Up Model

The relationship between k_f and the speed of agitation developed by Nienow(39) - Equation 3.18 may be derived from the mass transfer correlations, when the only variable being changed is the impeller speed. Several workers, however, have ignored the assumptions on which this relationship was developed and have suggested that the k_f may correlate only against the speed, power or specific power at different scales.

These approaches are entirely empirical and do not have even the weak theoretical basis that the mass transfer correlations enjoy. This approach yields the following relationships - (Equations 3.30 to 3.32):

$$k_f \propto N^n \quad 3.30$$

$$k_f \propto P^m \quad 3.31$$

and

$$k_f \propto E^x \quad 3.32$$

It is known that the T/D ratio influences the impeller speed at which particles are suspended. It is probable therefore that the T/D ratio will influence the mass

transfer coefficient. Three further empirical relationships (Equations 3.33 to 3.35) may be considered:

$$k_f \propto N^{0.5} (D/T)^{0.5} \quad 3.33$$

$$k_f \propto P^{0.5} (D/T)^{0.5} \quad 3.34$$

and

$$k_f \propto E^{0.5} (D/T)^{0.5} \quad 3.35$$

3.3.4 Summary

In the discussions so far, a number of potential scale-up models have been developed. These are Equations 3.24 to 3.35. In Chapter 5 the usefulness of these models will be tested using the experimental data described in Chapter 4.

3.4 DETERMINATION OF THE POWER TO JUST ASSIMILATE THE CARBON

Nienow(39), and Coetzee and Cloete(26) reported the effect of conducting mass transfer experiments at speeds above and below that required to ensure that all particles are fully mixed in the slurry. They reported that as the speed increases the film transfer coefficient increases rapidly up to the point where the adsorbent particles are fully incorporated into the solution. Thereafter its value increases at a much slower rate as the impeller speed increases. The phenomenon is easily explained in terms of the increase in the total effective film area as more adsorbent particles are incorporated into the slurry as the impeller speed increases. Once all the particles have been incorporated, the value of

the transfer coefficient increases only as a result of the increasing intensity of agitation.

Nienow(39) suggested that no matter what mixer geometry is being used the hydrodynamics of a given adsorption system should be very similar at the point at which all the adsorbent particles have just been assimilated. The film transfer coefficient at this point - defined as $k_{f,ja}$ should therefore have the same value for all mixing geometries. This effect has found significant support from several investigators- Nienow and Miles(38), and Coetzee and Cloete(26).

Clearly the possibility that $k_{f,ja}$ may be scale independent is most significant. The measurement of $k_{f,ja}$ and the associated speed, N_{ja} , power, P_{ja} and specific power, E_{ja} , was therefore investigated in this work. This was done by plotting k_f against speed or power on logarithmic scale. This results in two sets of straight lines that intercept at the speed required to just assimilate the carbon particles, N_{ja} (39). The slope of the line for the speeds in excess of N_{ja} is lower than that of the line for speeds below N_{ja} .

The procedure adopted in this work will now be described. In order to estimate the value of $k_{f,ja}$, N_{ja} and P_{ja} , the relationship between k_f and speed or power above and below the 'just-assimilated' point needs to be established. As will be seen in Chapter 5, these relationships manifest as straight lines when the logarithm of k_f is plotted against the logarithm of N or P . Representing logarithm k_f as Y and logarithm P or logarithm N as X , the following two relationships therefore apply:

$$\begin{aligned} y &= \alpha + \beta x & \text{for } x < x_c \\ &= \delta + \gamma x & \text{for } x > x_c \end{aligned} \quad 3.36$$

where x_c represents the N_{j_a} or P_{j_a} or e_{j_a} . α and δ are the intercepts on the ordinate axis, and β and γ are the slopes of the lines below and above x_c .

In order to obtain accurate values, a Fortran program based on Least Squares Minimization of the errors between the model and experimental points was written. The program is able to estimate the intercepts with the k_e axis (thus the values of α and δ), the two slopes (the values of β and γ) and the point of intersection of the two lines, (x_c, k_{e,j_a}) . The statistical theory developed and the program are outlined in Appendices 3A and 3B, respectively.

Although the 'best' values of the parameters in a model may be obtained, this is not a guarantee that the model represents the data. It would therefore be useful if the models developed could be tested statistically for adequacy. Hence for exhaustive treatment of the process of estimation of parameters, the process must follow the following steps (42, 43):

- estimate the values of the parameters,
- test statistically the degree to which the model fits the experimental data, and
- estimate the errors in the parameters (ie the confidence intervals for the parameters).

The analyses that were conducted are discussed in Chapter 5.

CHAPTER FOUR

EXPERIMENTAL

4.1 INTRODUCTION

The experimental work is needed to measure the dependence of the mass transfer coefficient on the mixer geometry and agitation intensity. In designing the experimental program, three aspects required attention. Firstly, a standard adsorption system needed to be designed so that the physico-chemical environment would be the same in every test. Any changes in the mass transfer coefficient would therefore be the result of differences in geometry and agitation intensity. Secondly, careful consideration of which geometries should be tested was necessary. Finally, the agitation systems themselves and the power measurement procedures needed to be set up and tested.

4.2 THE DESIGN OF THE ADSORPTION CHEMISTRY

In the design of the adsorption chemistry, consideration was given to the selection of the initial gold concentration, designing the same solution chemistry, and selecting the type of carbon and inert solids for the slurry.

4.2.1 Initial Gold Concentration

Most CIP plants operate with initial gold concentration between 1 and 14 ppm. However, plants that process leached calcines have much higher gold concentration. As discussed in Chapter 3, the gold concentration of the initial solution should be below 8 ppm in order to minimise the influence of intraparticle diffusion on the

adsorption rate.

4.2.2 Solution Chemistry

To ensure that the solution chemistry was the same in all tests and that the solutions were relevant to plant practice, synthetic solutions were prepared according to the AARL recipe (2,19), namely:

- Boric acid (H_3BO_3) at 3.1 g/l,
- Calcium Chloride ($CaCl_2 \cdot H_2O$) at 3.2 g/l,
- Sodium cyanide (NaCN) at 200 mg/l, and
- Sodium Hydroxide (NaOH) at 1.75 g/l to achieve a solution pH of about 10. (A Knick pH-Meter 761 Calimatic was used for all pH measurements).

The reagents were all of analytical grade. The gold was added as potassium aurocyanide, ($KAu(CN)_2$), a pure crystalline salt with about 68% gold. An appropriate quantity was dissolved in the buffer solution to make its gold concentration to between 3 and 5 ppm.

Distilled water was used in the preparation of the solutions for the small scale tests. However, due to large volumes required to fill the large scale vessels, tap water was used in making up the solutions for these tests. The solution was prepared at least a day before use to ensure adequate formation of the aurocyanide complex (2,19).

4.2.3 Carbon

It was desirable to use an activated carbon that is used commercially. A large sample of coconut - based activated carbon was obtained from Western Deep Levels Gold Plant 1. It was sieved to between 2.36 and 1.00 mm. It was washed thoroughly with water and in 5%

hydrochloric acid solution to remove all fines and then rinsed generously with water and dried at 110 ° C. One day prior to each test the required amount of the dried carbon was taken and soaked in distilled water to remove entrapped air in the particles. The quantity of carbon used was the amount needed to achieve a carbon concentration of 5 g/l of slurry.

An attempt was made to determine the density of the carbon using a pycnometer but failed. Because of the adsorptive properties of the carbon particles it was not possible to get stable readings from the pycnometer. The density of the dried, activated carbon was, therefore, estimated by assuming that the particles were spherical - the assumption made in the derivation of Equation 3.9. The mass of a quantity of dried activated carbon was measured, and the number of particles was counted (4). From this, the density, ρ_c of was estimated using Equation 4.1.

$$\text{Density, } \rho_c = \frac{M_c}{N_c \pi d^3 / 6} \quad 4.1$$

where M_c is the mass of the carbon,
 N_c is the number of particles of carbon and
 d is the mean diameter of these particles.

The average density of the carbon estimated in this way was 762.9 kgm⁻³. Van Deventer(4), Le Roux et al(19) and Van der Merwe(46) reported 900, 818 and 838.8 kgm⁻³, respectively. The value obtained in this work is slightly lower than these values. However, the error is not important because it is consistent. All values of k_f reported in this thesis are offset by an amount determined by the magnitude of the error in the density of the carbon. However, it was considered preferable to use these values for the mass transfer coefficient, rather than to avoid the error by reporting values of the

product of the mass transfer coefficient and the specific film area. The scale-up procedure in both cases would be the same.

4.2.4 Inert Solids

It was necessary to use slurry instead of solution because of the significant effect that solid particles have on the film mass transfer coefficient, k_f (47). In addition this was necessary because the scale-up procedure to be developed must be applicable to normal plant practice. Therefore, the solids used were the same for all tests and typical of plant conditions. A synthetic sand (pure silica, SiO_2) was considered but rejected because it was too fine and it was not really a typical plant sand. Instead, filter plant residue from Western Deep Levels Gold Plant 2 was used. The impact of any residual gold in this residue was considered insignificant compared to errors that could arise from using synthetic solids and/or wrongly sized sand. The filter residue was dried, mixed, sampled and stored in plastic bags. The density of the dried sand was 2725 kgm^{-3} and its particle size distribution was as given in Table 4.1. The slurry density used in all kinetic tests was 1.45 kgl^{-1} , which is typical for operating plants (9,10).

Table 4.1: Particle size distribution of the solids used for the slurry.

sieve size (micrometre)	% mass retained	% cumulative passing
+ 150	2.5	97.5
+ 90	17.9	79.6
+ 75	7.4	72.2
+ 0	72.2	

4.3 GEOMETRICAL CONSIDERATIONS

Baffled flat bottomed open cylindrical vessels are the most widely employed in South African C/P plants. This type of vessel was selected for this investigation.

The diameters of the vessels used were 185, 305, 330, 690 and 1200 mm. The volume of the smallest vessel - 185 mm diameter - was approximately 5 litres which is the volume of beakers that are often used in laboratory studies. The volume of the biggest vessel used was about 1360 litres. Facilities were not available to conduct tests in vessels larger than this.

The baffle design that was selected is given in Table 4.2. Due to the limitations of time and cost, the ratios of the height of the slurry and the height of the impeller from the bottom of the vessel to the diameter of the vessel were held fixed at 1 and 0.25 respectively. These configurations are typical of South African practice and no variations on them were studied in this work.

Hydrofoil impellers have been found to consume less power



than pitched blade turbines in keeping ore particles in suspension(10). Consequently this has been the preferred type in many South African CIP installations. No other type was investigated in this study.

Hydrofoil impellers of diameters 110, 130, 142, 275 and 480 mm were obtained from Kemix (Pty) Ltd. All of these had blade angles of 20° and the same nominal power number 0.35 and flow number 0.6. The 142 and 480 mm diameter impellers were rubber lined.

Table 4.2: Baffle Design for the vessels used.

No. of baffles	4
Width of baffles	$0.10T^*$
Height of baffles	T
Clearance above vessel base	$0.075T$
Clearance from vessel wall	$0.02T$

* T is the diameter of the vessel.

4.4 THE MEASUREMENT OF SPEED AND POWER

The rotational speed of the impeller was measured using a variable range hand tachometer (accurate to 10 rpm in the speed range of 160 to 2000 rpm and accurate to 1 rpm in the speed range of 16 to 200 rpm).

Power was calculated by measuring the torque exerted on the slurry due to the rotation of the impeller. In order to be able to measure this torque, either the drive arrangement or the vessel was mounted in such a way that it was free to rotate. The force required to restrain this motion when the slurry was agitated was then measured. The force was measured using a Route Optelec

Model 338 load cell. This had a maximum range of 2000 g accurate to 0.1 g.

The load cell was calibrated using loads of known masses. The calibration curve and its equation are given in Figure 4.1.

Two difficulties occurred in the measurement of the power input for agitation, namely friction and fluctuations in the force readings. These were overcome as follows:

4.4.1 Dealing with Friction

An estimate of the static frictional torque, τ_{fri} , was obtained for the different agitation systems as described in Appendices 2A and 2B. The dynamic frictional torque would be less than τ_{fri} . In the calculation of the power, however, it was assumed to be equal to τ_{fri} .

Friction was accounted for, using the following procedure:

The torque exerted on the load cell, τ_{lc} , is given by:

$$\tau_{lc} = F \cdot l_1 \quad 4.2$$

where l_1 is the perpendicular distance from the axis of the agitator to the point at which the force, F , is applied to the load cell.

From a torque balance, the total torque, τ , applied to the agitator is given by:

$$\tau = \tau_{lc} + \tau_{fric} \quad 4.3$$

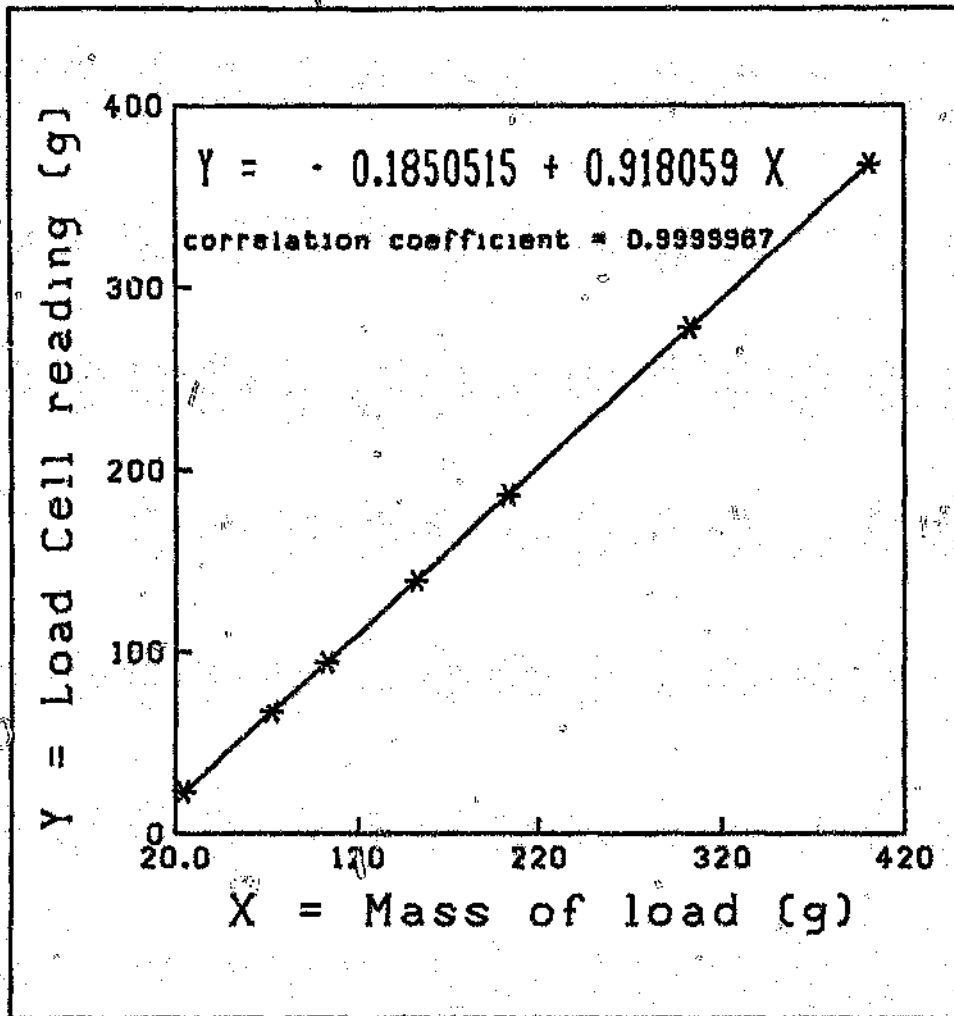


Figure 4.1 Calibration curve for the load cell

The corresponding applied power is given by:

$$\text{Power for agitation, (W)} = 1.2\pi \frac{N}{60} \quad 4.4$$

where N is the speed of agitation in revolutions per minute, and the units of torque are Newton metres.

4.4.2 Dealing with Fluctuations

Due to the turbulent nature of the slurry in the mixing vessel, the force exerted on the load cell fluctuated considerably. Two measures were adopted in order to obtain a satisfactory measure of the mean force exerted. Firstly, the signal from the load cell was dampened electronically. The circuit that was found most suitable to do this is shown in Figure 4.2. This arrangement was sufficient to dampen the fluctuations in the tests conducted in the small vessels (185, 305 and 330 mm diameter vessels). In the two large vessels (690 and 1200 mm diameter vessels), mechanical dampening was also necessary. The systems used to do this are described in the next section.

4.5 THE AGITATION SYSTEMS USED

For each geometry needed to measure the film mass transfer coefficient, at least six tests are required to estimate the parameters in Equation 3.36.

4.5.1 185, 305 and 330 mm diameter vessels

With these vessels, the torque required to restrain the motion of the vessel was measured. The vessels were mounted on a torque table, the movement of which was restrained through a plate that rested against the load

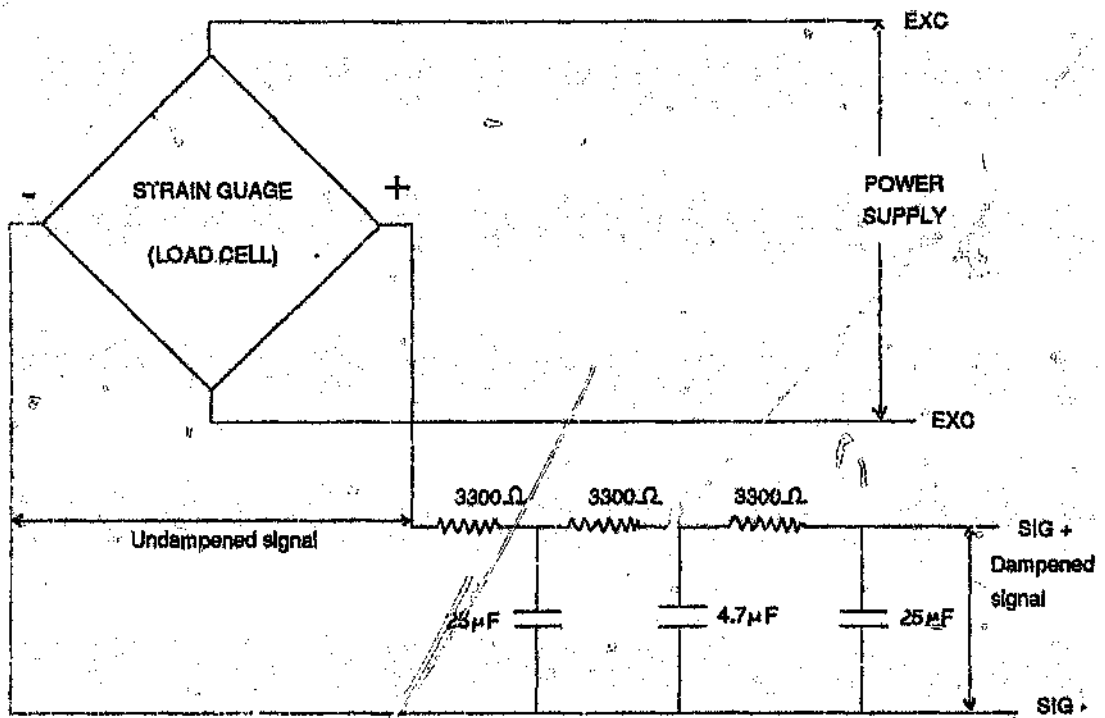


Figure 4.2: Schematic diagram of the modification to the load cell circuit

cell. The schematic diagram of this arrangement is shown in Figure 4.3.

The friction in the table bearing was determined by putting a string around the turntable while the impeller was stopped and hanging different loads at the end of the string over a small stationary bar. The friction on this small bar was also estimated. The procedure is outlined in Appendix 2A.

4.5.2 690 and 1200 mm diameter vessels

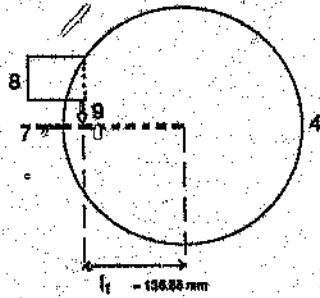
The mechanical arrangements of these two mixing systems are shown in Figures 4.4 and 4.5. In both cases, the drive was mounted on a thrust bearing so that it was free to rotate. This rotation was restrained through the torque arm which was tethered to the load cell.

Due to the higher level of power input in these vessels, the fluctuations in the load cell readings were not satisfactorily dampened using the electronic means alone. It was necessary to employ mechanical dampening as well. This was achieved using a spring and a dash pot system as indicated in Figures 4.4 and 4.5.

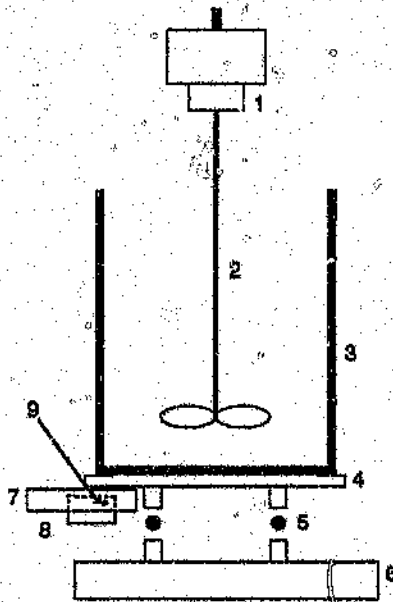
The static friction in the system was estimated by attaching a nylon string to the impeller and taking it over a small bar and attaching loads of known masses to its end. The details of the measurement are outlined in Appendix 2B.

4.6 KINETIC TESTS

For each agitation system, the kinetic experiment proceeded along similar lines. The required volume of



TOP VIEW OF TORQUE TABLE (VESSEL REMOVED)

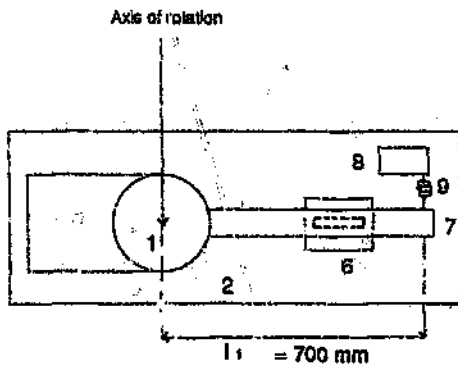


LEGEND

- 1 Chuck
- 2 Impeller
- 3 Vessel
- 4 Torque Table
- 5 Ball bearings
- 6 Base plate
- 7 Torque plate
- 8 Load cell
- 9 Load cell tip

ELEVATION

Figure 4.3: Schematic diagram of the agitation system for the 185, 305 and 330 mm diameter vessels

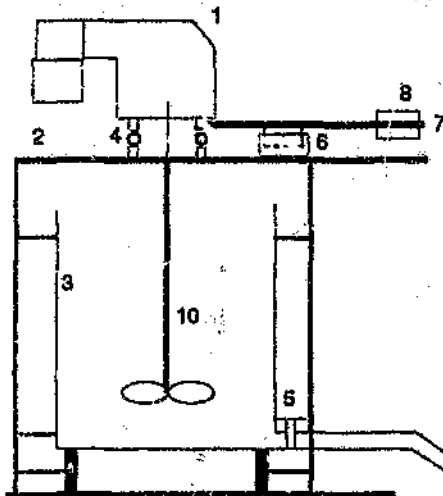


TOP VIEW OF AGITATION SYSTEM
(VESSEL EXCLUDED)

LEGEND

Agitation System

- 1 Motor & Gear box
- 2 Support
- 3 Vessel (690 mm dia.)
- 4 Support bearings
- 5 Drain valve
- 6 Dash pot
- 7 Torque arm
- 8 Load cell
- 9 Spring attached to Load cell
- 10 Impeller (275 mm dia.)



ELEVATION

Receiving Vessel

- 11 Motor & Gear box
- 12 Impeller
- 13 Discharge vessel
- 14 500 micron sieve
- 15 Compressed air
- 16 Valve

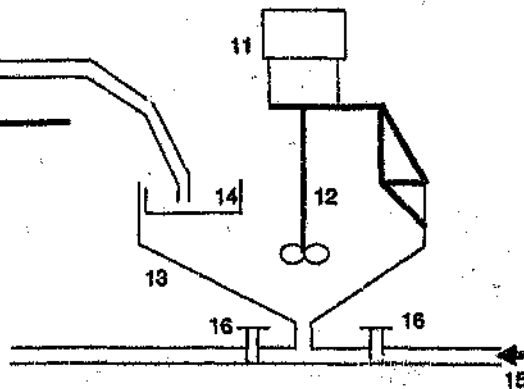
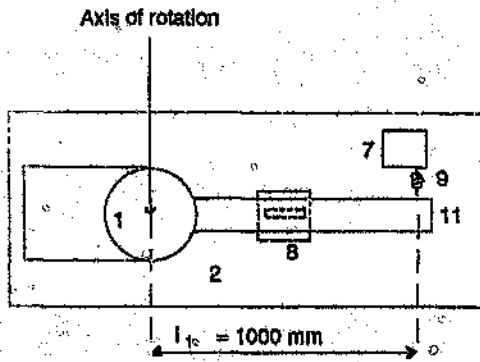


Figure 4.4: Schematic diagram of the agitation system for the 690 mm diameter vessel

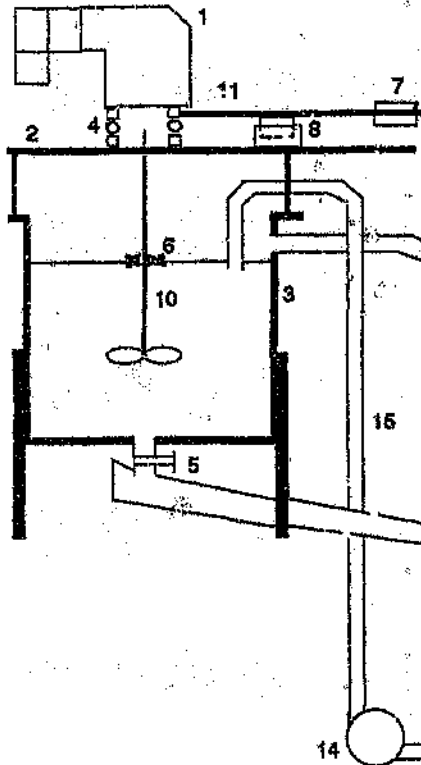


TOP VIEW OF AGITATION SYSTEM
(VESSEL EXCLUDED)

LEGEND

Agitation System

- 1 Motor & Gear box
- 2 Support
- 3 Vessel (1200 mm dia.)
- 4 Support bearing
- 5 Drain valve
- 6 Stabilising bearing
- 7 Load cell
- 8 Dash pot
- 9 Spring attached to Load cell
- 10 Impeller (480 mm dia.)
- 11 Torque arm



ELEVATION

Receiving Vessel

- 12 Motor & Gear box
- 13 500 micron sieve
- 14 Return pump
- 15 Flexible hose
- 16 Receiving vessel
- 17 Impeller
- 18 Valve
- 19 Compressed air

Figure 4.5: Schematic diagram of the agitation system for the 1200 mm diameter vessel

synthetic gold-bearing solution was made up. The required amount of the dry mine residue was charged to this. The speed of the impeller was adjusted to the desired value. The temperature of the slurry was taken. An initial sample of the slurry was taken. The pre-soaked carbon was then poured into the slurry as quickly as possible and the time was noted. Samples were taken every other minute for the first ten minutes. Each sample was immediately passed through a 500 micron sieve to remove carbon particles after which the sample was filtered. The gold concentrations of the samples were later determined using Atomic Absorption Spectrometer (AAS).

When conducting tests in the two larger systems additional measures had to be adopted at the end of each kinetic test. Because of large quantities of materials involved, some measures were taken to conserve the residual gold. The slurry was drained rapidly through a 500 micron sieve to remove the carbon from it. The physical arrangements are shown in Figures 4.4 and 4.5. In the case of the 1200 mm diameter vessel some tests were conducted using the residual slurry from the previous tests. In such cases the gold concentration of the slurry was increased to around the desired value before the next kinetic test was started. This was done by adding potassium aurocyanide solution.

The film mass transfer coefficient was determined from this data as described in Section 3.1.3.

4.7 REPRODUCIBILITY TESTS

Before embarking on the experimental program, the reproducibility of the experimental procedure described in the previous section was investigated. The tests were

conducted in the 305 mm diameter vessel using the 130 mm diameter impeller. The film mass transfer coefficients were determined four times at each of three agitation speeds namely, 200, 400 and 600 rpm. Mine dump sand was used for the inert solids needed to make up the slurry. This sand was different from the one used in the rest of the test-work. It was coarser and had a different particle size distribution. In all other respects, for example the chemistry of the solution, the test procedure employed was as described above.

The results of the reproducibility tests are recorded in Table 4.3. The percent relative standard deviations of the k_f values for the 600, 400 and 200 rpm value are 3.2, 5.2 and 33.2 respectively. The results show satisfactory reproducibility in the determination of k_f at 400 and 600 rpm. As shown in the table, the relative standard deviations were 3.3 and 5.2 per cent respectively. The relatively higher variance value of k_f at 200 rpm, can be attributed to the agitation intensity being insufficient to fully assimilate the carbon. Assimilation of carbon will therefore be variable and so inconsistent results would be expected.

Table 4.3: Reproducibility in the estimation of mass transfer coefficient (130 mm diameter impeller in the 305 mm diameter vessel)

Agitation Speed (rpm)	600	400	200
Test No.	$k_f \times 10^5$	$k_f \times 10^5$	$k_f \times 10^5$
1	3.91	3.09	2.22
2	4.12	3.00	1.70
3	3.81	2.92	1.21
4	3.95	3.29	1.09
mean k_f	3.95	3.07	1.55
std. dev.	0.13	0.16	0.52
% rel. std. dev.	3.3	5.2	33.2
95% C. I.	3.95 ± 0.21	3.09 ± 0.25	1.55 ± 0.83

95% C.I. is the 95% confidence interval.

The reproducibility of the power input data is shown in Table 4.4. It can be seen that least variation was experienced in the power measurements at 200 rpm. This is expected because the mixing conditions are less intense at lower agitation speeds. As can be seen acceptable levels of variation between the different tests were obtained - the relative standard deviations ranging from 1.8 to 3.9 per cent.

Table 4.4: Reproducibility in the estimation of power input (130 mm diameter impeller in the 305 mm diameter vessel)

Agitation Speed (rpm)	600	400	200
Test No.	P (W)	P (W)	P (W)
1	19.46	8.45	2.31
2	19.59	8.43	2.15
3	20.12	8.47	2.16
4	19.83	9.01	2.12
Mean Power	19.83	8.59	2.19
std. dev.	0.37	0.28	0.085
% relative std. dev.	1.80	3.27	3.89
95% C. I.	19.83±0.57	8.59±0.45	2.19±0.14

95% C.I. is the 95% confidence interval.

4.8. RESULTS

The power data as calculated according to the procedure given in Section 4.5 are presented in Appendix 1A and summarized in Table 4.5.

The data from the various kinetic tests conducted are presented in Appendix 1B and in Figures 4.6 to 4.14. The film mass transfer coefficients calculated from the data according to the procedure given in Section 4.6 are presented in Table 4.6.

Table 4.5: The power data for the various impeller-vessel configurations

Impeller+vessel diameter (mm)	Speed (rpm)	Power (W)	Speed (rpm)	Power (W)
110 + 185	200	1.59	400	5.38
	250	2.14	500	7.74
	270	2.64	550	9.98
	300	3.33	600	12.23
110 + 305	300	2.75	500	7.94
	400	5.25	600	13.13
	450	6.92	700	22.92
130 + 305	200	2.64	500	12.43
	300	5.20	600	19.31
	350	6.52	650	27.96
	400	8.27		
142 + 305	200	3.03	400	11.31
	230	4.14	500	21.65
	300	5.25	600	39.64
110 + 330	300	2.45	600	15.08
	400	4.76	650	17.61
	500	9.99	700	20.79
	550	12.88	800	34.79
130 + 330	250	2.43	500	14.66
	300	4.89	550	19.29
	350	7.58	600	24.35
	390	10.95	650	30.65
142 + 330	200	2.16	400	15.25
	250	3.88	500	21.86
	300	6.20	550	30.22
	350	9.33	640	44.95
275 + 690	149	35.04	261	95.01
	171	43.62	283	113.98
	200	59.19	309	140.31
480 + 1200	110	260.02	140	350.29
	125	297.44	150	421.02
	131	326.81	162	467.09

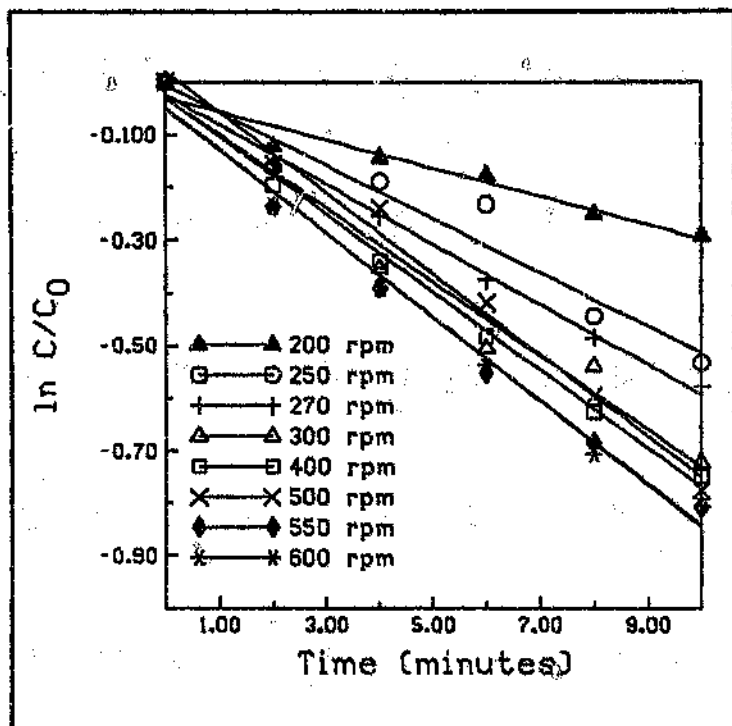


Figure 4.6: Kinetic tests for 185 mm diameter vessel: impeller diameter = 110 mm

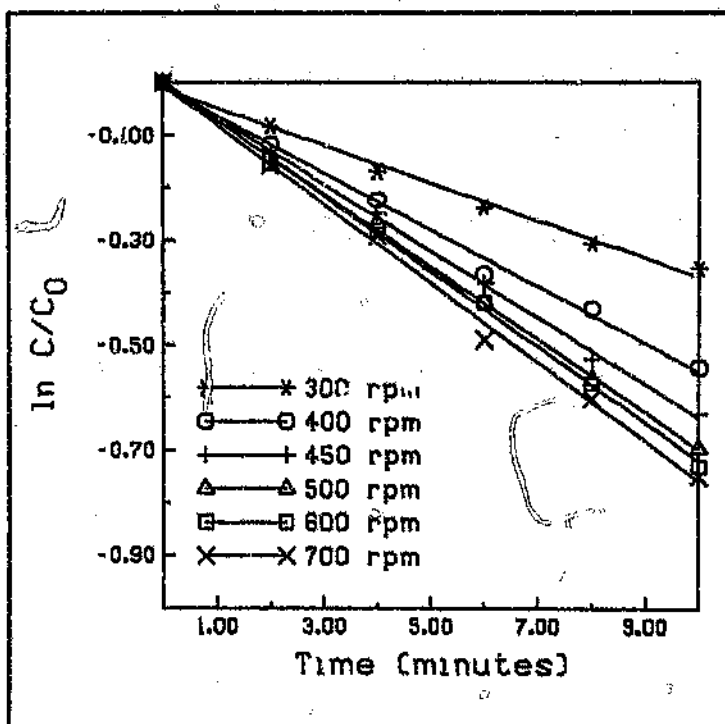


Figure 4.7: Kinetic tests for 305 mm diameter vessel: impeller diameter = 110 mm.

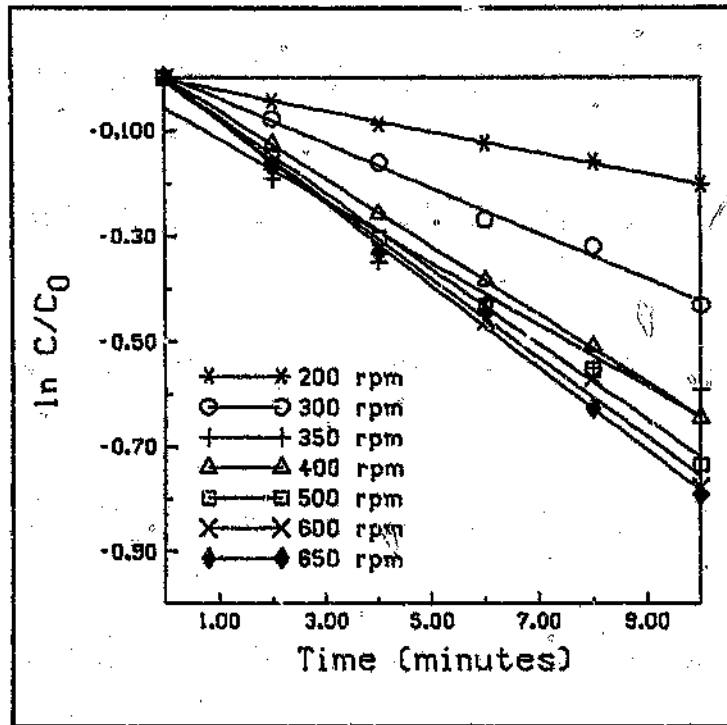


Figure 4.8: Kinetic tests for 305 mm diameter vessel: impeller diameter = 130 mm.

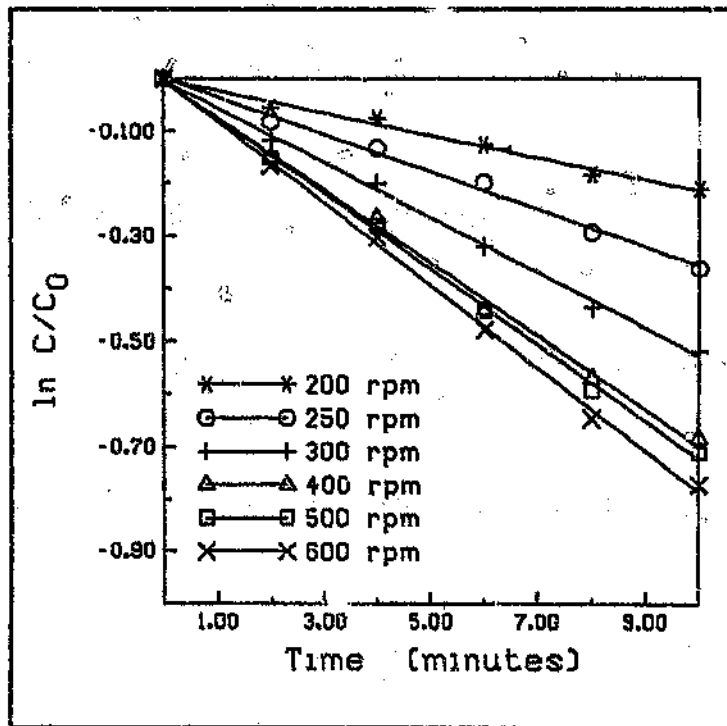


Figure 4.9: Kinetic tests for 305 mm diameter vessel: impeller diameter = 142 mm.

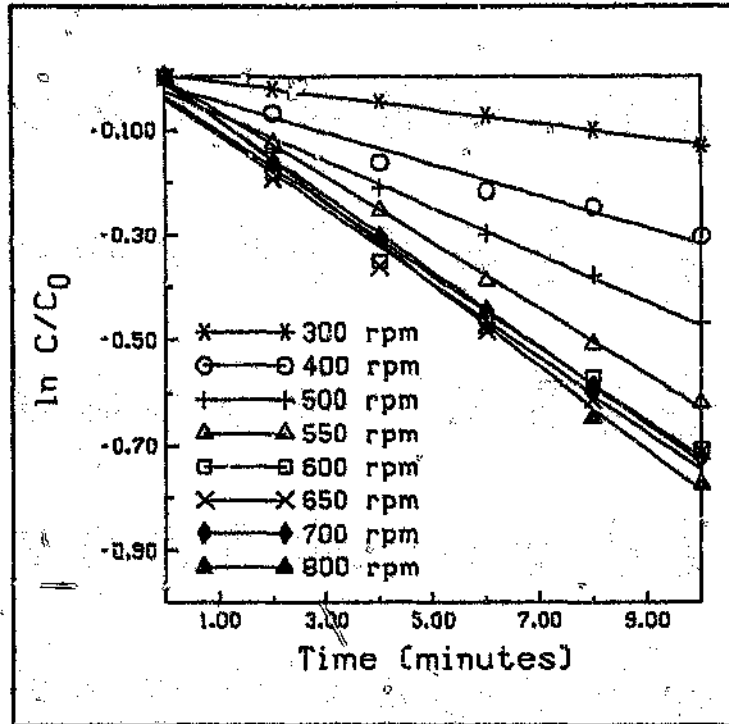


Figure 4.10: Kinetic tests for 330 mm diameter vessel: impeller diameter = 110 mm.

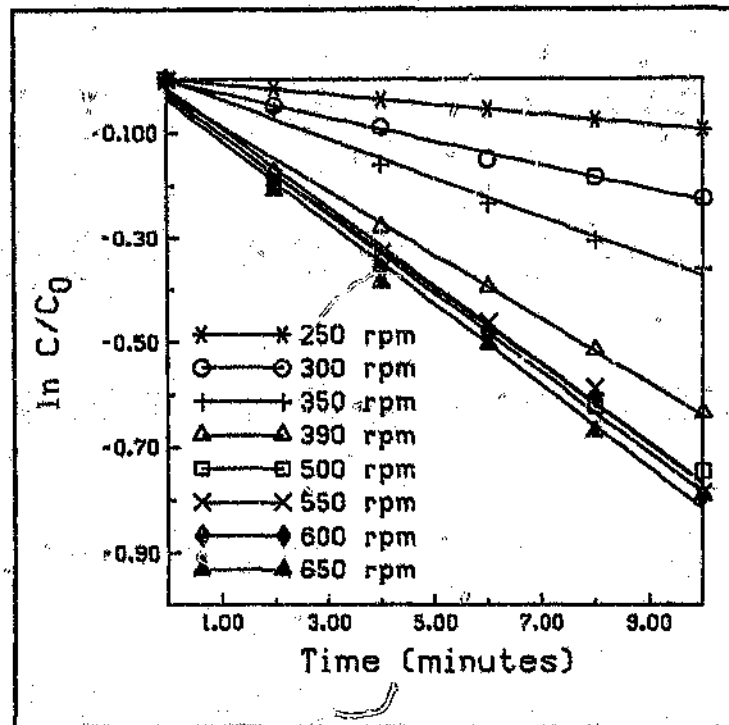


Figure 4.11: Kinetic tests for 330 mm diameter vessel: impeller diameter = 130 mm)

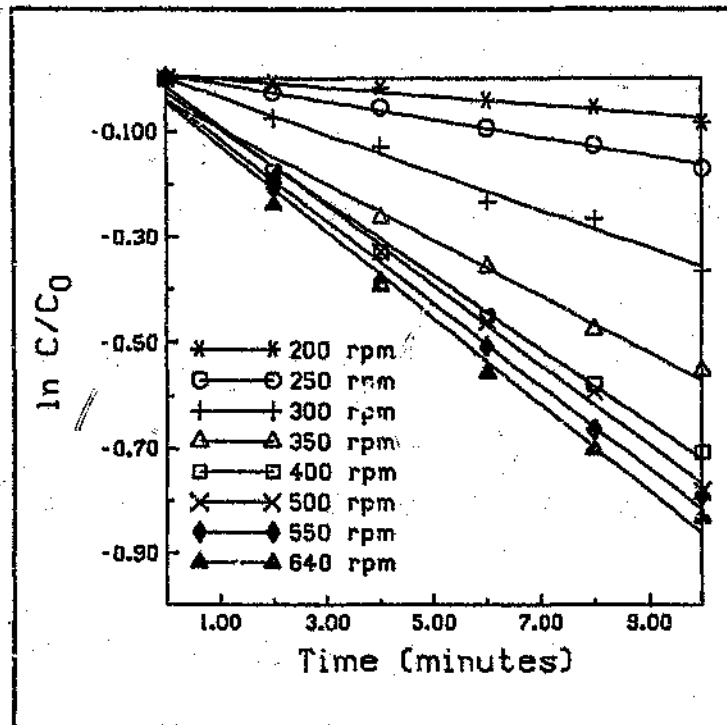


Figure 4.12: Kinetic tests for 330 mm diameter vessel: impeller diameter = 142 mm.

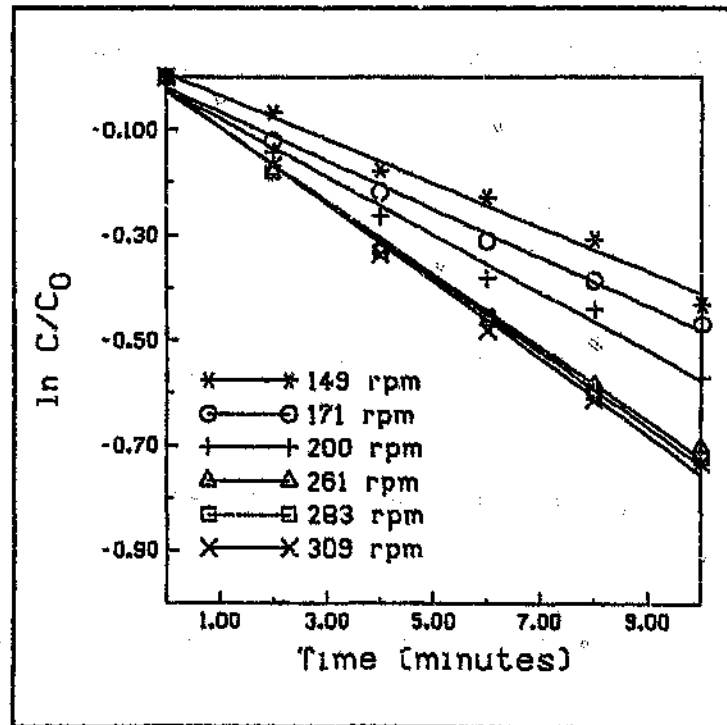


Figure 4.13: Kinetic tests for 690 mm diameter vessel: impeller diameter = 275 mm.

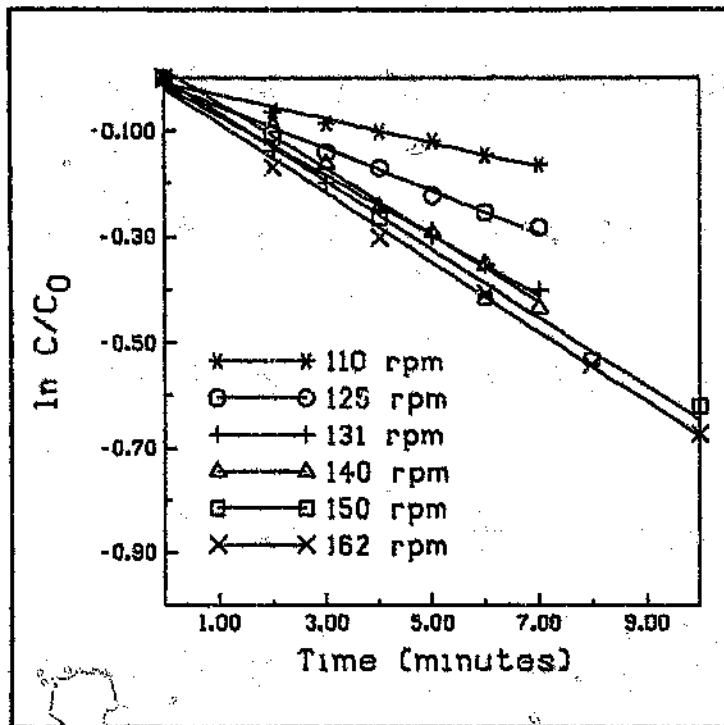


Figure 4.14: Kinetic tests for 1200 mm diameter vessel: impeller diameter = 480 mm.

Table 4.6: The film mass transfer coefficient obtained for the various impeller-vessel configurations

Impeller+vessel diameters (mm)	Speed (rpm)	$k_f \times 10^{-5}$ (ms^{-1})	Speed (rpm)	$k_f \times 10^{-5}$ (ms^{-1})
110 + 185	200	0.43	400	3.90
	250	2.67	500	4.05
	270	3.00	550	4.17
	300	3.69	600	4.20
110 + 305	300	1.89	500	3.66
	400	2.86	600	3.80
	450	3.36	700	3.97
130 + 305	200	1.088	500	3.771
	300	2.253	600	3.954
	350	3.902	650	4.108
	400	3.389		
142 + 305	200	1.135	400	3.654
	250	1.896	500	3.797
	300	2.777	600	4.129
110 + 330	300	0.70	600	3.62
	400	1.59	650	3.72
	500	2.36	700	3.86
	550	3.30	800	4.13
130 + 330	250	0.51	500	3.88
	300	1.20	550	3.97
	350	1.98	600	4.00
	390	3.25	650	4.11
142 + 330	200	0.43	400	3.66
	250	0.89	500	3.96
	300	1.88	550	4.10
	350	2.79	640	4.30
275 + 690	149	2.21	261	3.67
	171	2.44	283	3.76
	200	2.92	309	3.87
480 + 1200	110	1.19	140	3.30
	125	2.10	150	3.39
	131	2.97	162	3.46

CHAPTER FIVE

DISCUSSIONS OF THE RESULTS

In this chapter, the results obtained in the investigation are discussed and compared with available information.

5.1 KINETIC DATA

Figures 4.6 to 4.14 show clearly that the concentration-time data represented by the simple film diffusion model (Equation 3.9) represents the initial adsorption data well. Of the sixty three kinetic tests conducted, only five gave results that were not fitted well by Equation 3.9. The correlation coefficient for each line is given in Appendix 1B.

As expected, the data shows that the greater the speed of agitation, the greater the magnitude of the slopes of the plots.

5.2 THE INFLUENCE OF AGITATION SPEED AND POWER ON THE MASS TRANSFER COEFFICIENTS

Figures 5.1 to 5.10 show how the film mass transfer coefficient, k_f , varies with the speed or power input in the different agitation systems tested. As can be seen, when the data for a given system is plotted using logarithmic scales, two straight lines are obtained. As explained in Section 3.4, the line with the steeper slope describes the effect of increasing agitation when not all the carbon is fully assimilated into the slurry. The line with the shallower slope describes the effect of agitation when the carbon is fully assimilated. The data was analyzed as described in Section 3.4, by fitting a

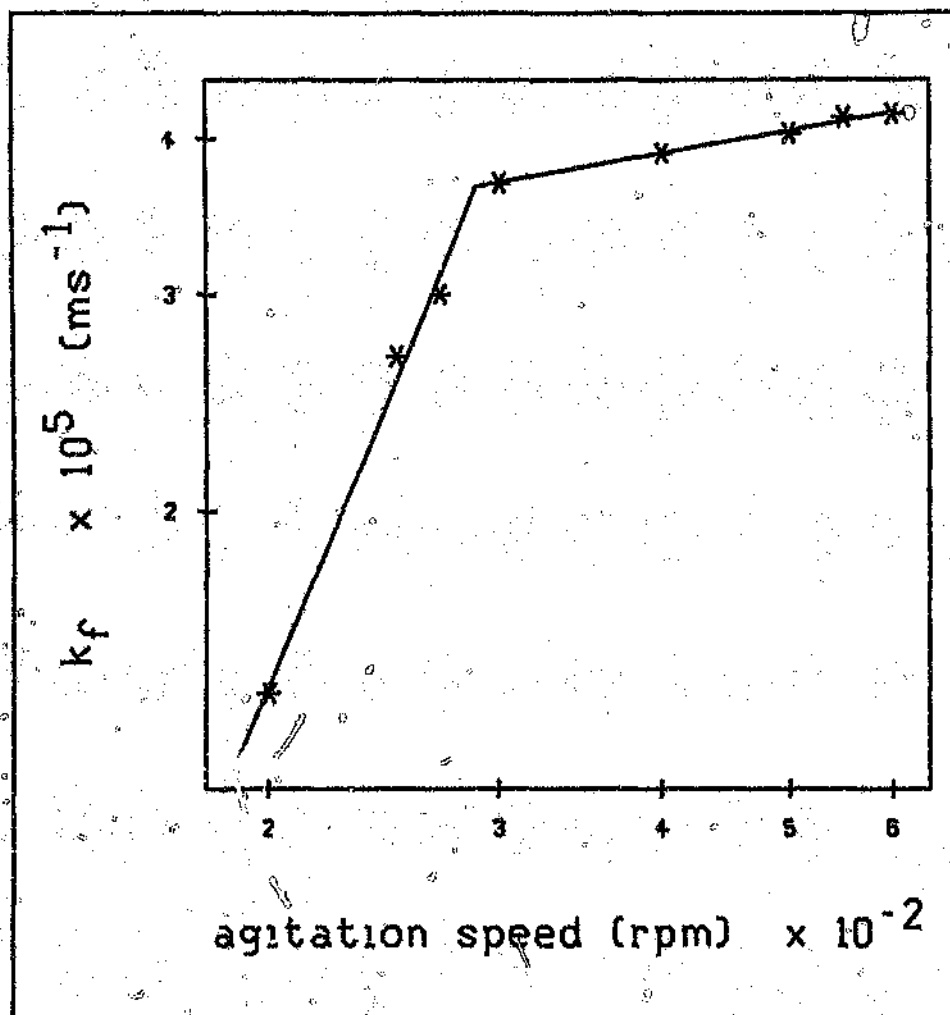


Figure 5.1: The effect of speed of agitation on the film mass transfer coefficient (impeller diameter = 110 mm, vessel diameter = 185 mm)

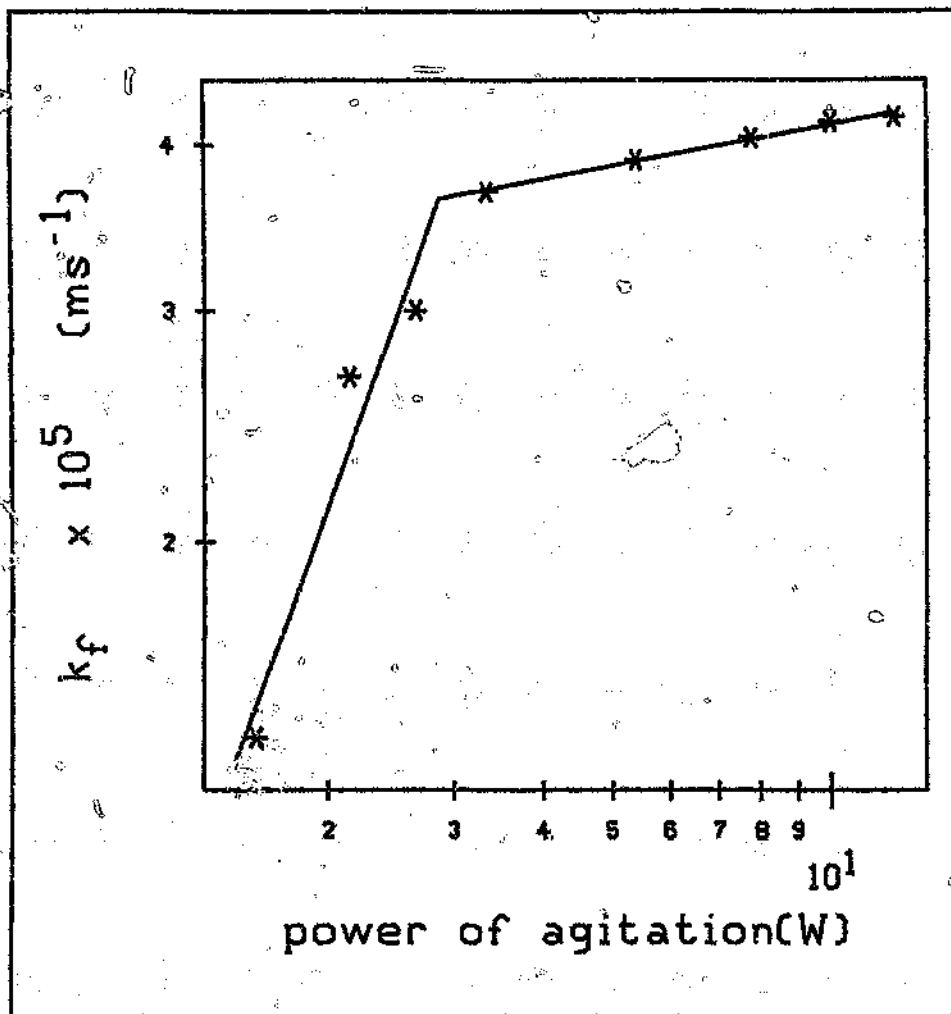


Figure 5.2: The effect of power of agitation on the film mass transfer coefficient (impeller diameter = 110 mm, vessel diameter = 185 mm)

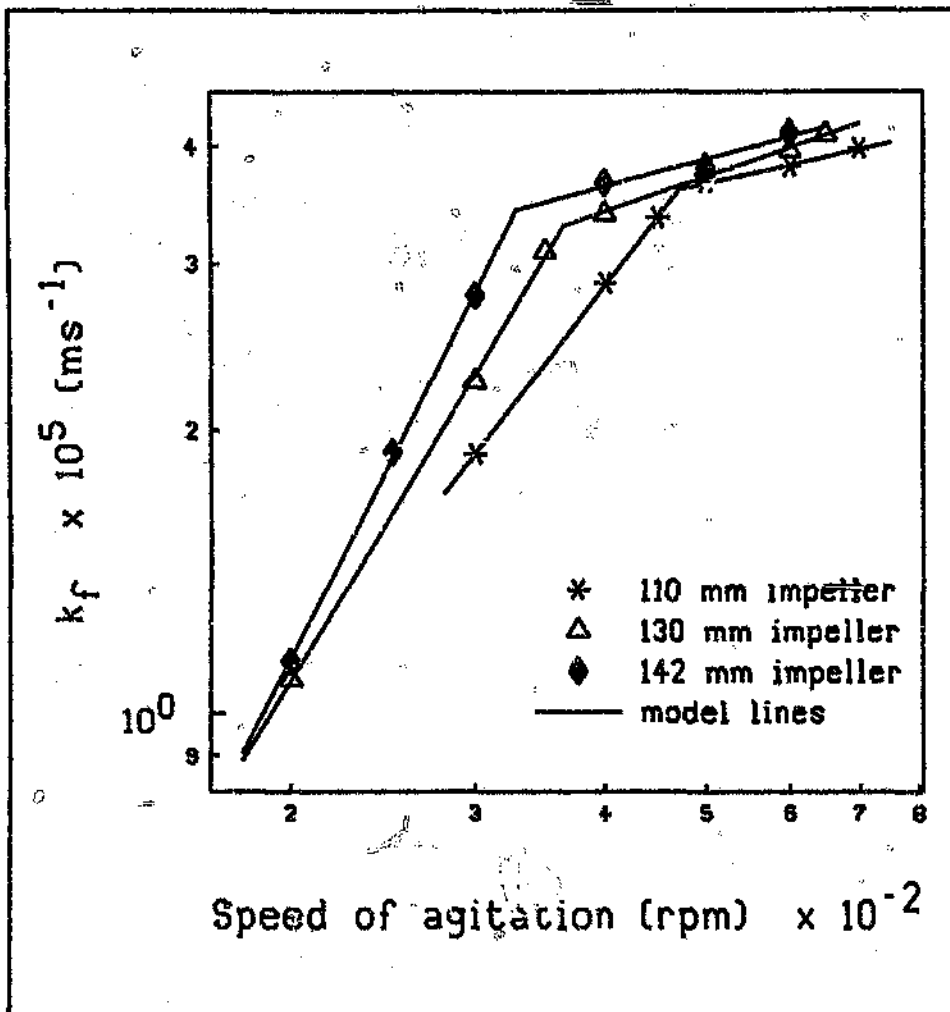


Figure 5.3: The effect of speed of agitation on the film mass transfer coefficient (vessel diameter = 305 mm)

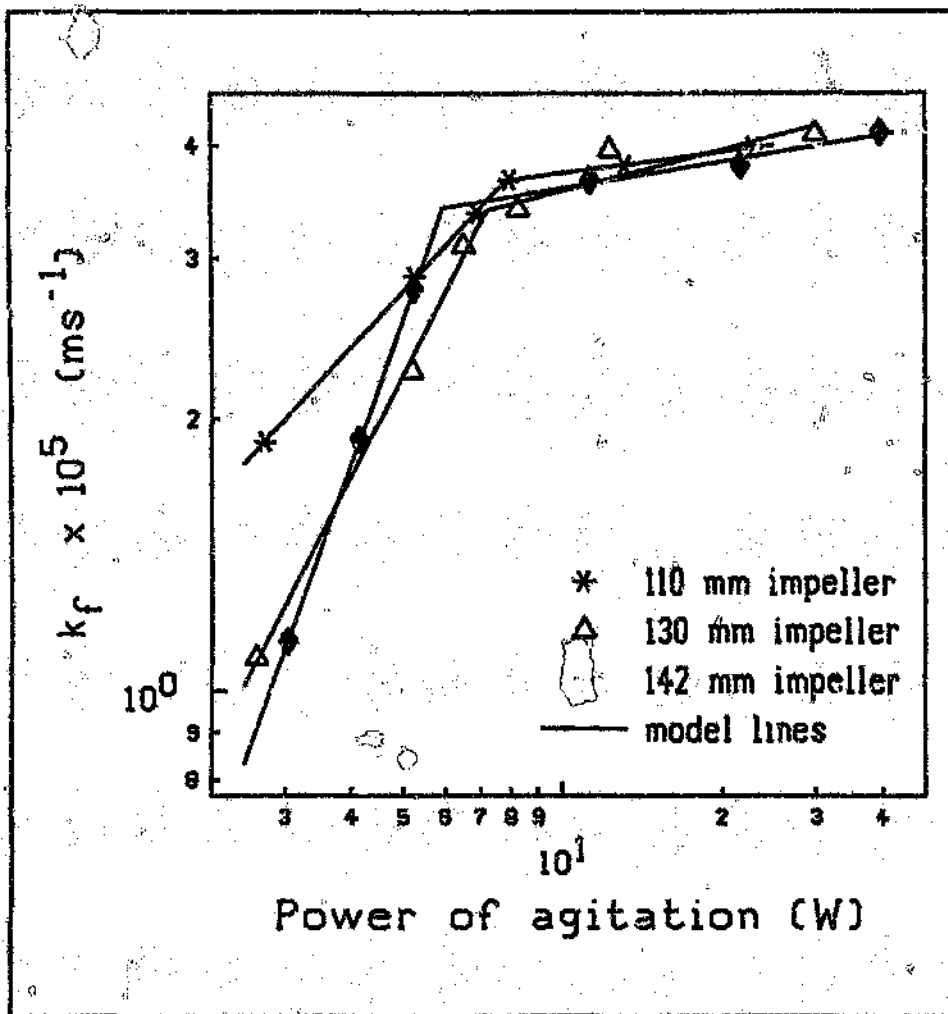


Figure 5.4: The effect of power of agitation on the film mass transfer coefficient (vessel diameter = 305 mm)

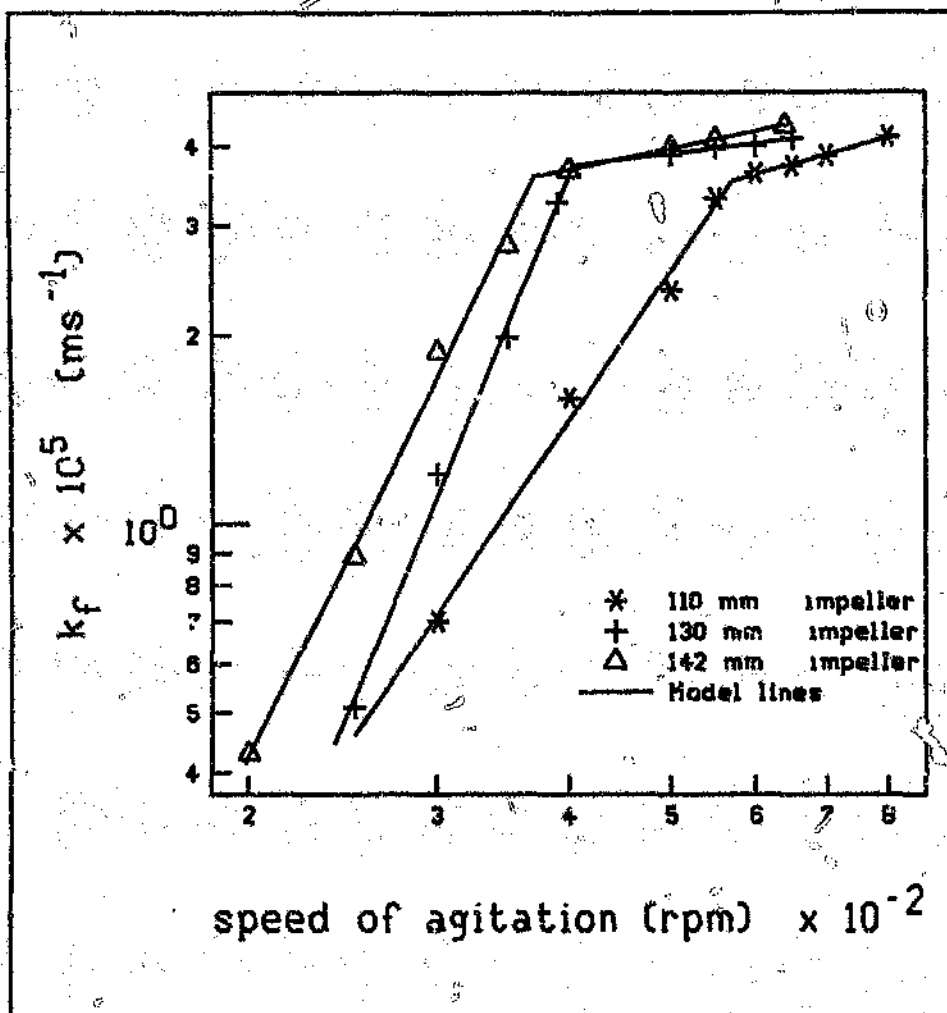


Figure 5.5: The effect of speed of agitation on the film mass transfer coefficient (vessel diameter = 330 mm)

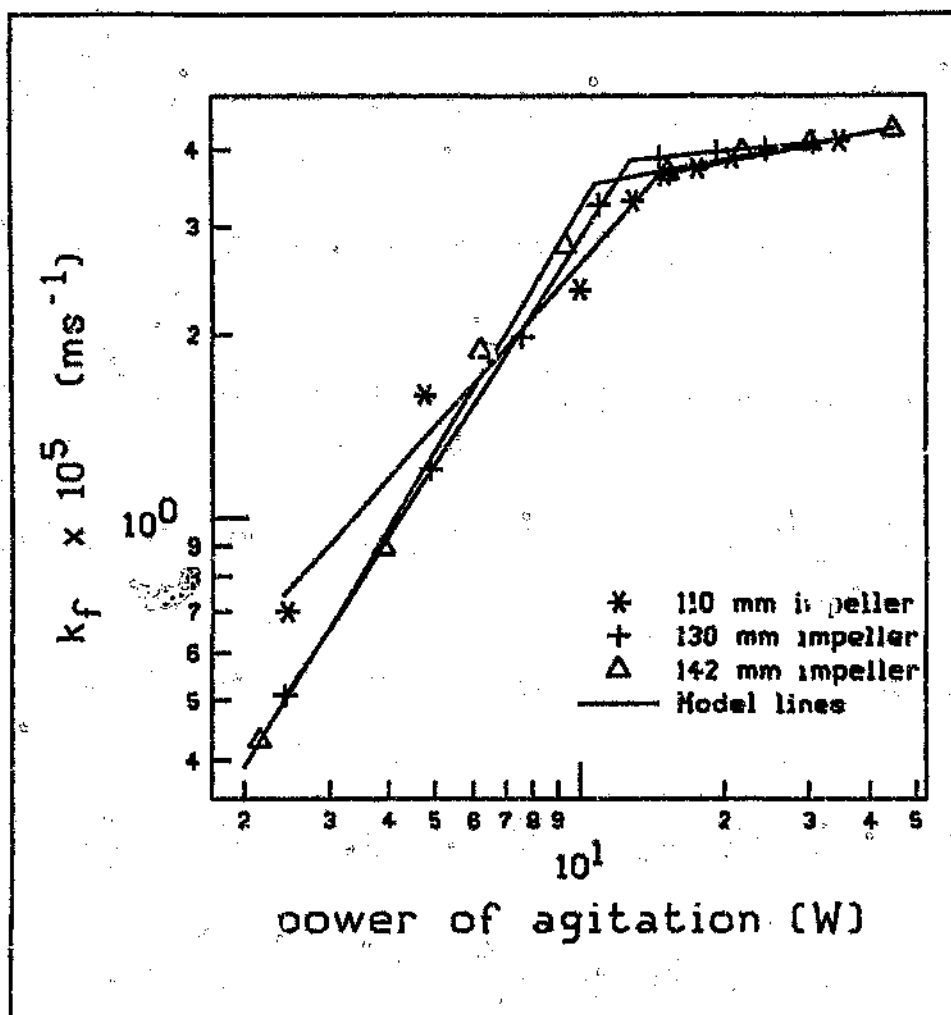


Figure 5.6: The effect of power of agitation on the film mass transfer coefficient (vessel diameter = 330 mm)

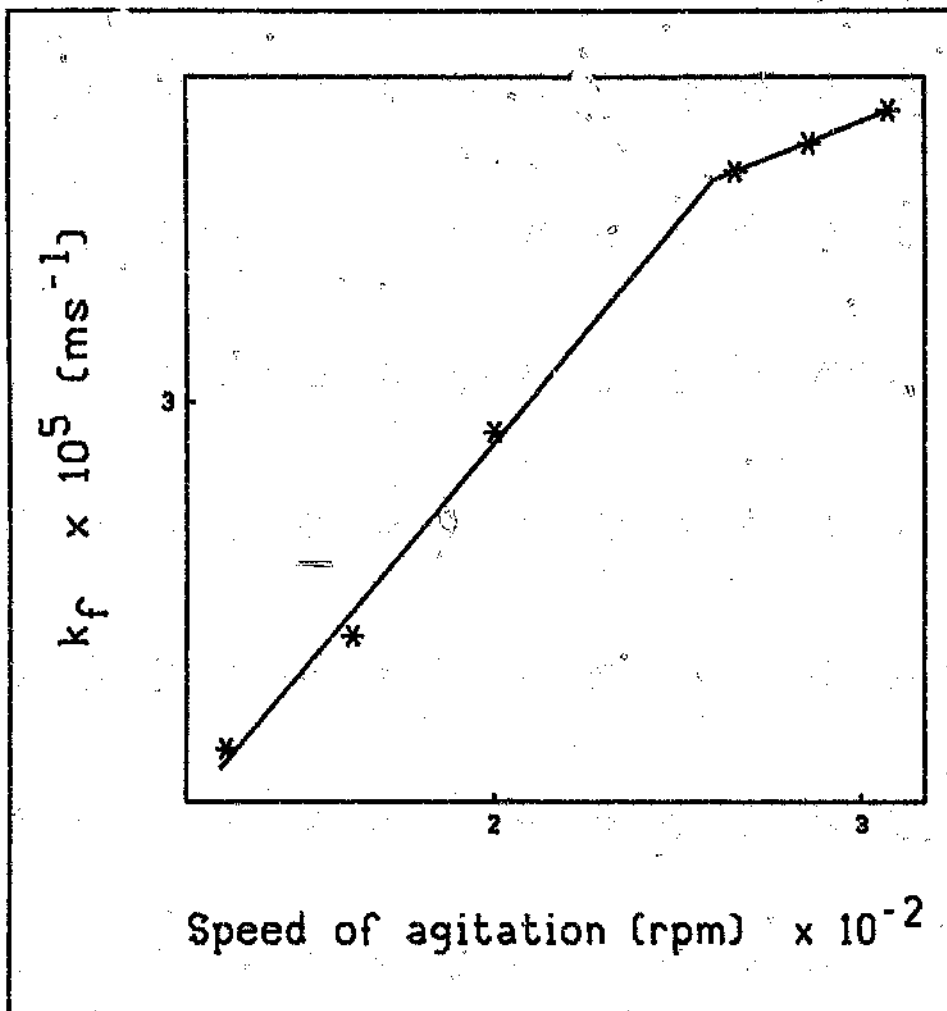


Figure 5.7: The effect of speed of agitation on the film mass transfer coefficient (impeller diameter = 275 mm, vessel diameter = 690 mm)

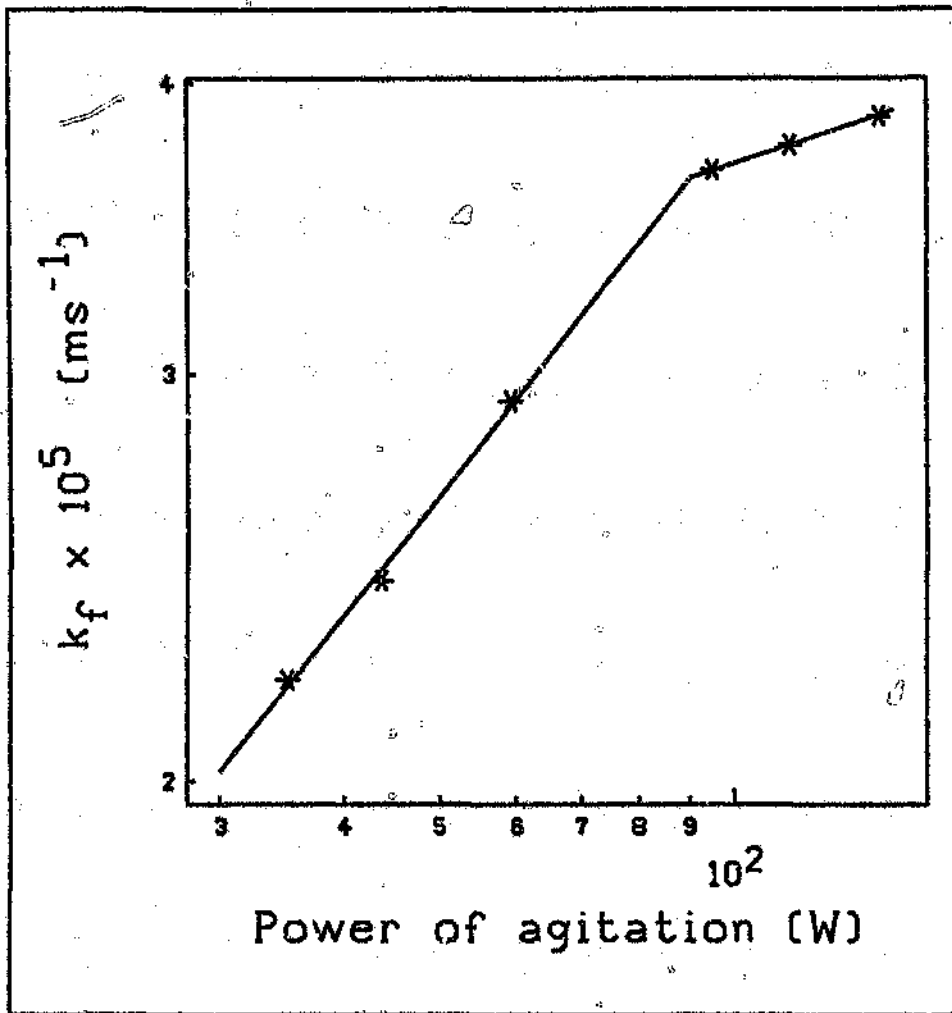


Figure 5.8: The effect of power of agitation on the mass transfer coefficient (impeller diameter = 275 mm, vessel diameter = 690 mm)

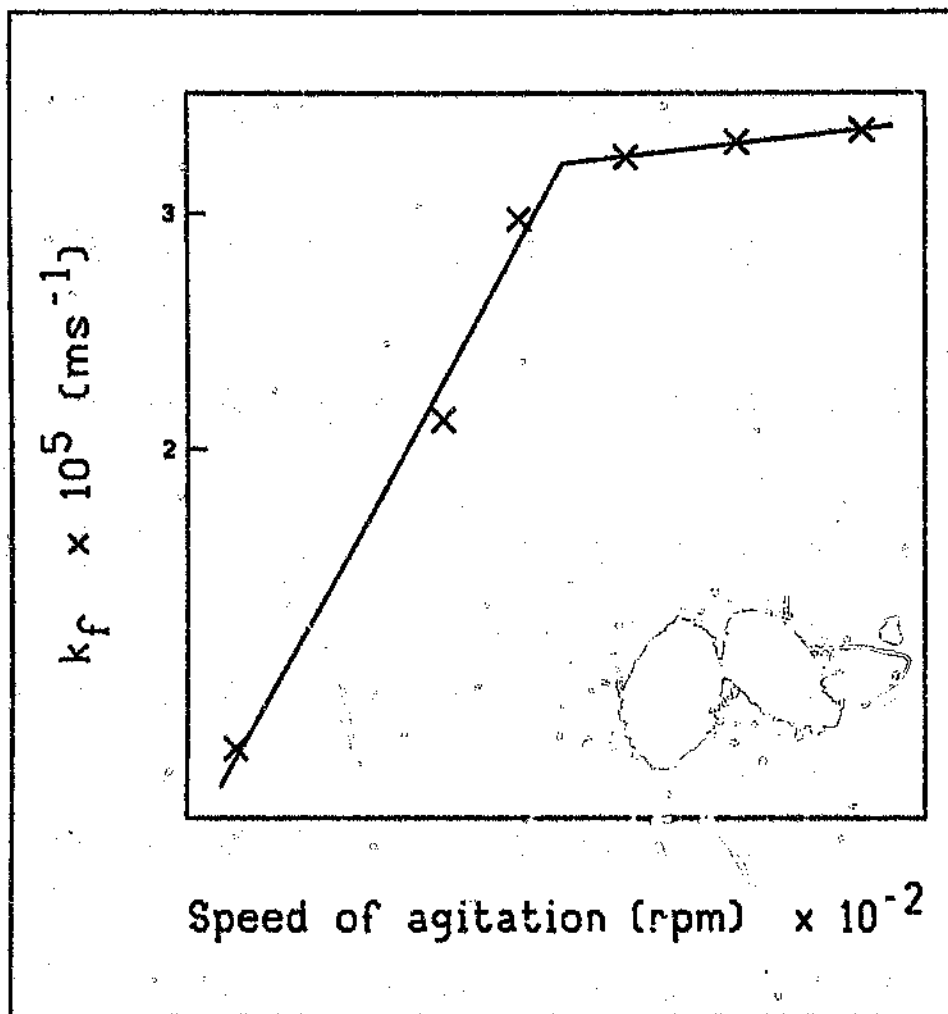


Figure 5.9: The effect of speed of agitation on the film mass transfer coefficient (impeller diameter = 480 mm, vessel diameter = 1200 mm)

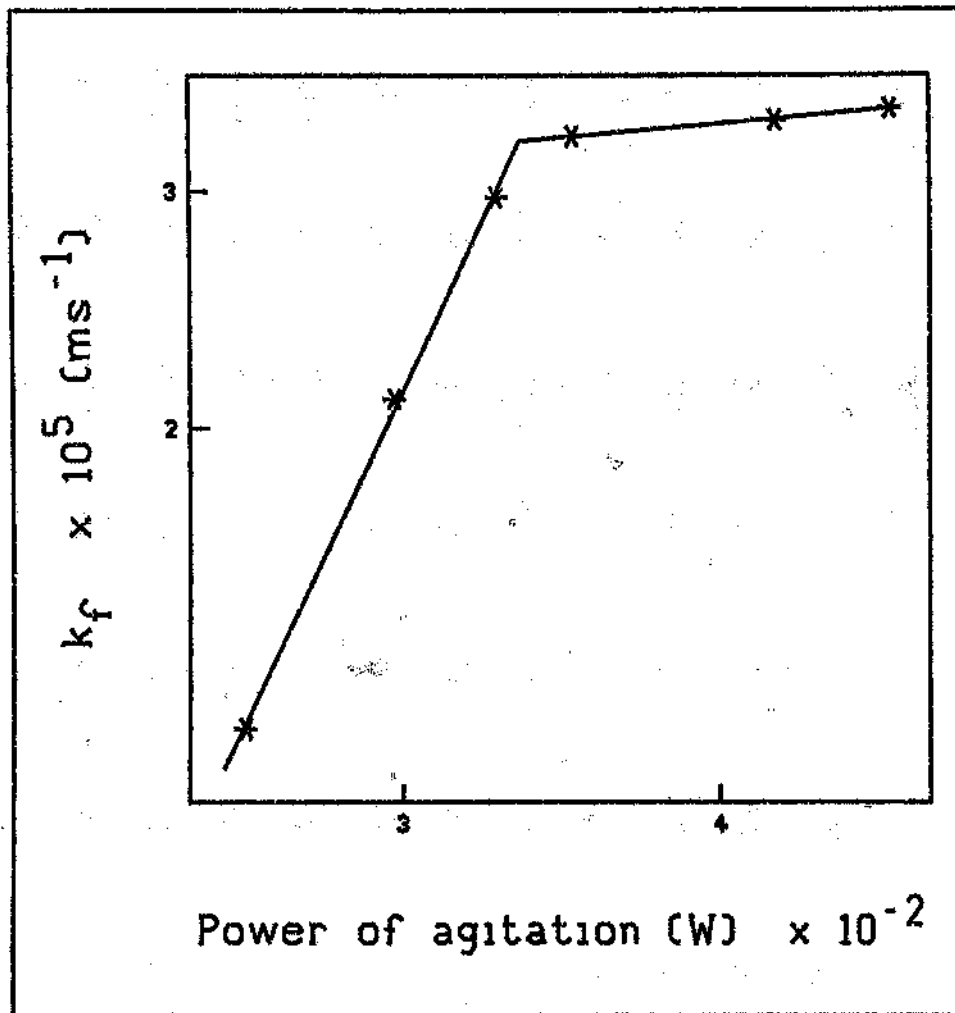


Figure 5.10: The effect of power of agitation on the film mass transfer coefficient (impeller diameter = 480 mm, vessel diameter = 1200 mm)

bi-linear model (Equation 3.36) to the data.

Since repeat measurements were not conducted, no formal test for lack of fit of the model (44) can be done. However, the regression correlation coefficient does give both quantitative and qualitative information on the goodness of fit of the model to the experimental data (44). A program used to determine the correlation coefficient of the model to the data is given in Appendix 4B. As shown in Table 5.1, it is clear that the model fits the data well.

Figure 5.1: Fitting the Bi-linear Model

impeller + vessel diameter (mm)	Corr. Coeff. from Speed data #	Corr. Coeff. from Power data *
110 + 185	0.9981	0.9870
110 + 305	0.9999	0.9999
130 + 305	0.9997	0.9988
142 + 305	0.9996	0.9998
110 + 330	0.9974	0.9922
130 + 330	0.9988	0.9998
142 + 330	0.9989	0.9987
275 + 690	0.9988	0.9996
480 + 1200	0.9964	0.9999

for Figures 5.1, 5.3, 5.5, 5.7 and 5.9

* for Figures 5.2, 5.4, 5.6, 5.8 and 5.10

Three important types of information may be obtained by fitting this model to the mass transfer and speed/power data. The first concerns the speed or power which is required to just assimilate all the carbon into the slurry. The second concerns the value of the mass transfer coefficient at the just assimilated point. Finally, and most importantly, the relationship between the mass transfer coefficient and speed or power may be quantified. Each of these will be discussed in detail.

5.3 QUANTIFYING THE INFLUENCE OF AGITATION ON THE MASS TRANSFER COEFFICIENT

As shown in Section 5.2, it is expected that for a given agitation system the mass transfer coefficient and the speed or power will have simple power relationship. This is born out in Figures 5.1 to 5.10. What is important for scale-up is the value of the exponent on power (or speed) in the relationship. Only the data above the just assimilated point is relevant to this discussion.

As can be seen from Table 5.2, the exponents on power, P , or the specific power, E , (in Equations 3.31 and 3.32) vary from 0.0736 to 0.1619. The mean value is 0.1225 with a standard deviation of 0.035. The values found are quite close to the range predicted by Nienow(39) (Equations 3.18 and 3.19) - that is 0.12 to 0.2. Values found by other workers are as follows. Coetzee and Cloete (26), in two sets of experiments, used prochem impellers and inclined blade turbines to adsorb sodium onto resins and silver cyanide onto activated carbon from clear water and slurry. The values of the exponents that they obtained were 0.167, 0.203 and 0.265, respectively. Latterman et al(40), adsorbing phenol from clear water onto activated carbon using a plate turbine got k_f to be proportional to the specific power to the exponent of 0.149.

The values found in the current work are generally lower than the values found in the literature. This could be ascribed to the fact that the presence of fine solids increases the power requirement for agitation and at the same time tends to inhibit adsorption. The systems used by the authors mentioned were also quite different from the one used for the present data, and as would be seen later, this can lead to significant variations in the results. For example, the adsorbent particle size used

by them was smaller than the one used in this investigation, and hence higher rates of adsorption would be expected in their studies.

The values of the exponents for the different agitation systems are compared in Figure 5.11. The values are rather scattered and appear to have no dependence on vessel size. This observation corroborates the suggestions of Coetzee and Cloete(26), and Nienow and Miles(38) that the exponent of the power in the k_f - power relation above the 'just assimilated' condition is constant and independent of scale and geometry.

Table 5.2: Values of the exponents of E and N for the various impeller/vessel geometries- ($N > N_{ja}$ - Equation 3.30 and $E > E_{ja}$ - Equation 3.32)

Vessel diameter (mm)	Impeller diameter (mm)	Exponent, x_1 on N	Exponent, x_2 on E
185	110	0.1909	0.1026
305	110	0.2406	0.0768
	130	0.3830	0.1529
	142	0.2966	0.0970
330	110	0.4654	0.1564
	130	0.2054	0.0736
	142	0.3447	0.1450
690	275	0.3145	0.1362
1200	480	0.3234	0.1619

Plotting on one diagram all the data generated in this work as shown in Figure 5.12, further supports such a contention.

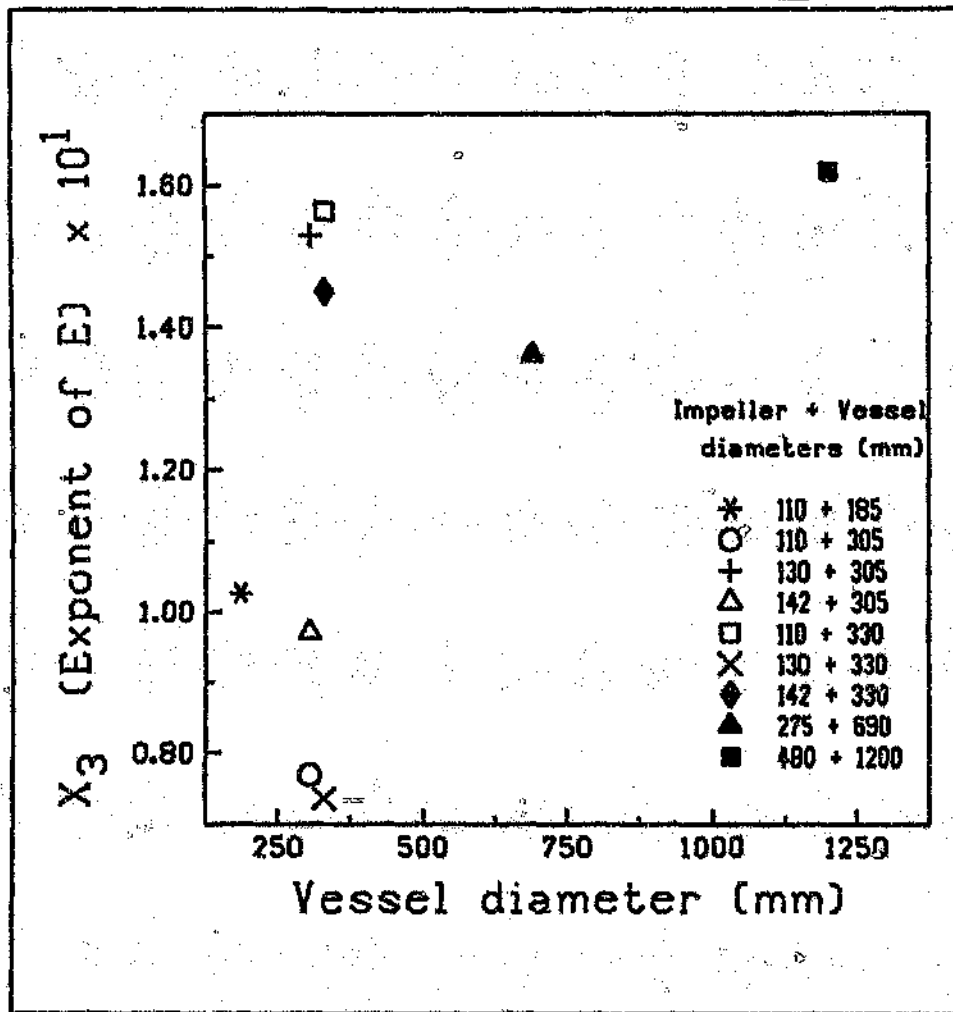


Figure 5.11: The exponent X_3 , (Equation 3.32) of E vrs vessel diameter.

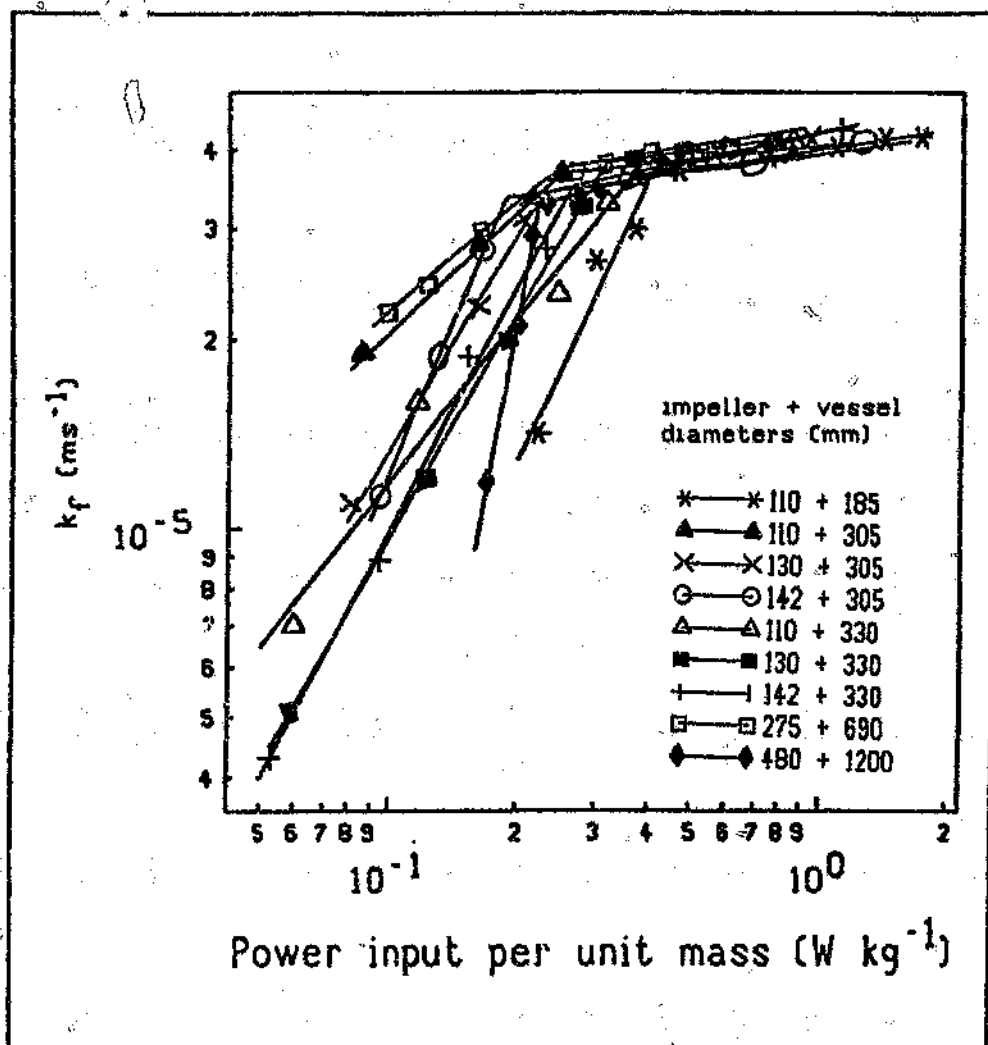


Figure 5.12: The effect of specific power input on the film mass transfer coefficient for the various impeller-vessel configurations

5.4 TESTING THE POTENTIAL SCALE-UP MODELS

In the last section the relationship between the mass transfer coefficient and the power was studied using data from a given agitation system. The concluding remarks and Figure 5.12 suggest that the simple relationship between k_f and specific power that applies for one agitation system may apply to a different system. This lends support to the scale-up model described previously in Equation 3.32. In this section, this equation as well as the other scale-up models (developed in Sections 3.3.2 and 3.3.3) need to be tested more rigorously.

This is done by conducting a regression analysis on all the acquired data above the 'just assimilated' point. The scale-up models to be tested are Equations 3.24 to 3.35. The four parameter models (Equations 3.28 and 3.29), however, were not tested because the available data was considered too few to make the estimated values generally valid.

In the comparative analysis to choose the best model from among the potential scale-up models, the sum of the squares of the relative errors between the predicted and actual values at each data point were determined to ensure equal weighting to each point. The multiple correlation coefficient of the regression analysis, r , for each model was also determined. The best parameter values for these models as well as the relevant regression statistics are presented in 5.3.

From the table, it is clear that Equations 5.1 and 5.2 represent the data best. It is not immediately obvious whether or not Equation 5.1 is better than Equation 5.2 because although the correlation coefficients are fairly similar, the former has three parameters while the latter has only two. Both models have different degrees of

Table 5.3: Testing of the Scale-up models

Model No.	Expression $\times 10^5$	Equation No.	r	Mean of Sum of Squares of R.E.	Std. Dev. of Mean of SSRE
3.35	$k_f = 2.854 E^{0.217} (T/D)^{0.083}$	5.1	0.930	5.848×10^{-4}	5.576×10^{-4}
3.32	$k_f = 4.124 E^{0.185}$	5.2	0.907	7.617×10^{-4}	1.146×10^{-4}
3.33	$k_f = 2.14 N^{0.115} (T/D)^{-0.136}$	5.3	0.821	1.438×10^{-3}	2.544×10^{-3}
3.24	$k_f = 1.012 N^{0.167} D^{0.662}$	5.4	0.773	1.760×10^{-3}	2.381×10^{-3}
3.26	$k_f = 2.05 N^{0.1} T^{-0.011}$	5.5	0.753	1.870×10^{-3}	2.93×10^{-3}
3.30	$k_f = 1.94 N^{0.11}$	5.6	0.748	1.948×10^{-3}	2.90×10^{-3}
3.25	$k_f = 3.106 D^{-0.242} (E^{1/3} T)^{0.194}$	5.7	0.753	1.906×10^{-3}	2.475×10^{-3}
3.27	$k_f = 3.121 T^{0.093} (ED^{-3})^{0.035}$	5.8	0.722	2.110×10^{-3}	2.940×10^{-3}
3.34	$k_f = 4.24 P^{-0.015} (T/D)^{-0.058}$	5.9	0.356	3.838×10^{-3}	4.964×10^{-3}

R.E. is the relative errors

SSRE is sum of squares of relative errors

freedom - and this can lead to misleading conclusions.

A statistical test used by Moys and King(48) for comparing models addresses this problem. The method assumes that models A and B exist and have m_A and m_B number of parameters respectively. If m_B is less than m_A then a statistic λ_{AB} is defined by:

$$\lambda_{AB} = \frac{(S_B - S_A) / (m_A - m_B)}{S_A / (N - m_A)} \quad 5.10$$

where S_A is the sum of squares of the residuals due to model A, S_B is the sum of squares of the residuals due to model B. N is the number of experimental points involved. The statistic λ_{AB} may be used as a means of testing whether or not model A is better than model B. If λ_{AB} is less than the $F_{(m_A - m_B), (N - m_A)}$ statistic at a given level of confidence, then model B is statistically better than model A.

The values of the relevant variables with Equation 5.1 being model A and Equation 5.2 being model B, are:

$$S_A = 2.7554 \times 10^{-11}, \quad S_B = 3.6515 \times 10^{-11}, \quad N = 33, \quad m_A = 3, \\ m_B = 2 \text{ and } \lambda_{AB} = 9.756.$$

From Statistical tables $F_{1,30} = 4.17$ (at 95% confidence level) and $= 7.56$ (at 99% confidence level). Since λ_{AB} is significantly greater than $F_{1,30}$ at both 95 and 99 % confidence levels, model A (the three parameter model is statistically better than model B (the two parameter model). The usefulness of Equation 5.1 is demonstrated in Figure 5.13 by the fact that the data points all lie within a 5% error band.

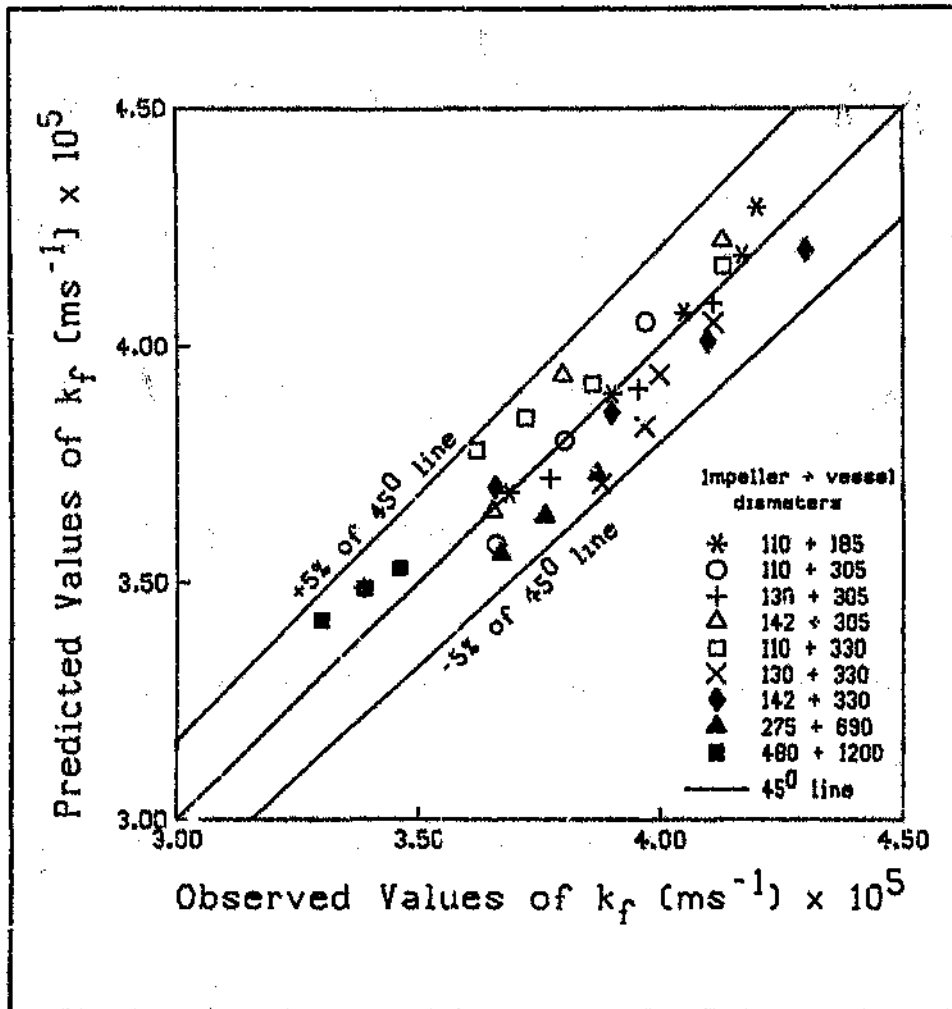


Figure 5.13: Observed and Predicted values of k_f using scale-up Equation 5.1

5.5 THE FILM MASS TRANSFER COEFFICIENT AT THE 'JUST ASSIMILATED' CONDITION

The values of the film mass transfer coefficient at the 'just assimilated' point, k_{f,j_a} , have been estimated using the bi-linear model. These values are presented in Table 5.4. In Figures 5.14 and 5.15, they have been plotted against the speed, N_{j_a} and specific power, E_{j_a} that are required to just assimilate the carbon particles into the slurry. It is clear that the values of k_{f,j_a} are very similar despite the widely different speeds and power inputs at which the 'just assimilated' conditions occurred for the various impeller-vessel configurations. Nienow and Miles (38) came to a similar conclusion when they plotted k_{f,j_a} against the power per unit mass of slurry for forty different impeller-vessel configurations.

Table 5.4: k_{f,j_a} values obtained from the speed and power data for the various impeller/vessel geometries.

Impeller and Vessel diameter (mm)	$k_{f,j_a} \times 10^5$	
	From Speed data	From Power data
110 + 185	3.66	3.65
110 + 305	3.60	3.66
130 + 305	3.29	3.38
142 + 305	3.42	3.41
110 + 330	3.52	3.62
130 + 330	3.71	3.84
142 + 330	3.57	2.52
275 + 690	3.64	3.64
480 + 1200	3.26	3.27

This observation is important because it suggests that k_{f,j_a} is scale independent - a fact that could be

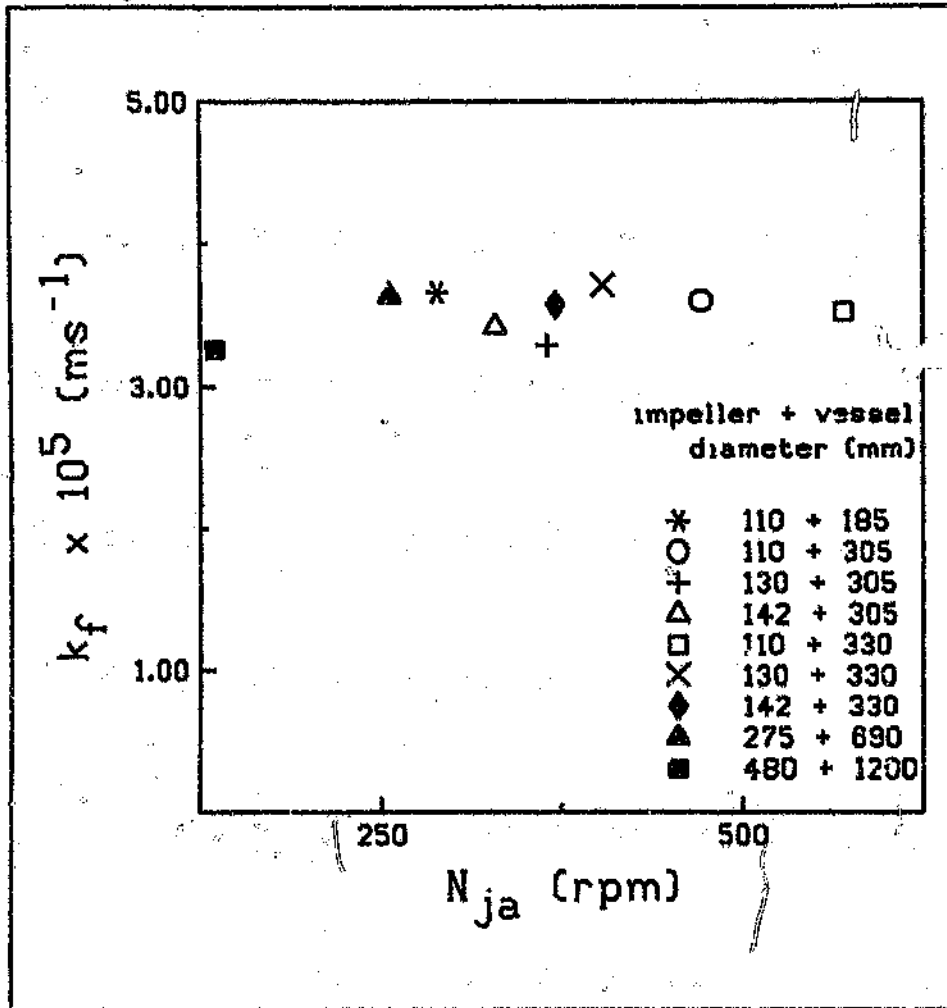


Figure 5.14: The film mass transfer coefficient vrs speed of agitation at the 'just assimilated' condition for the different impeller-vessel configurations

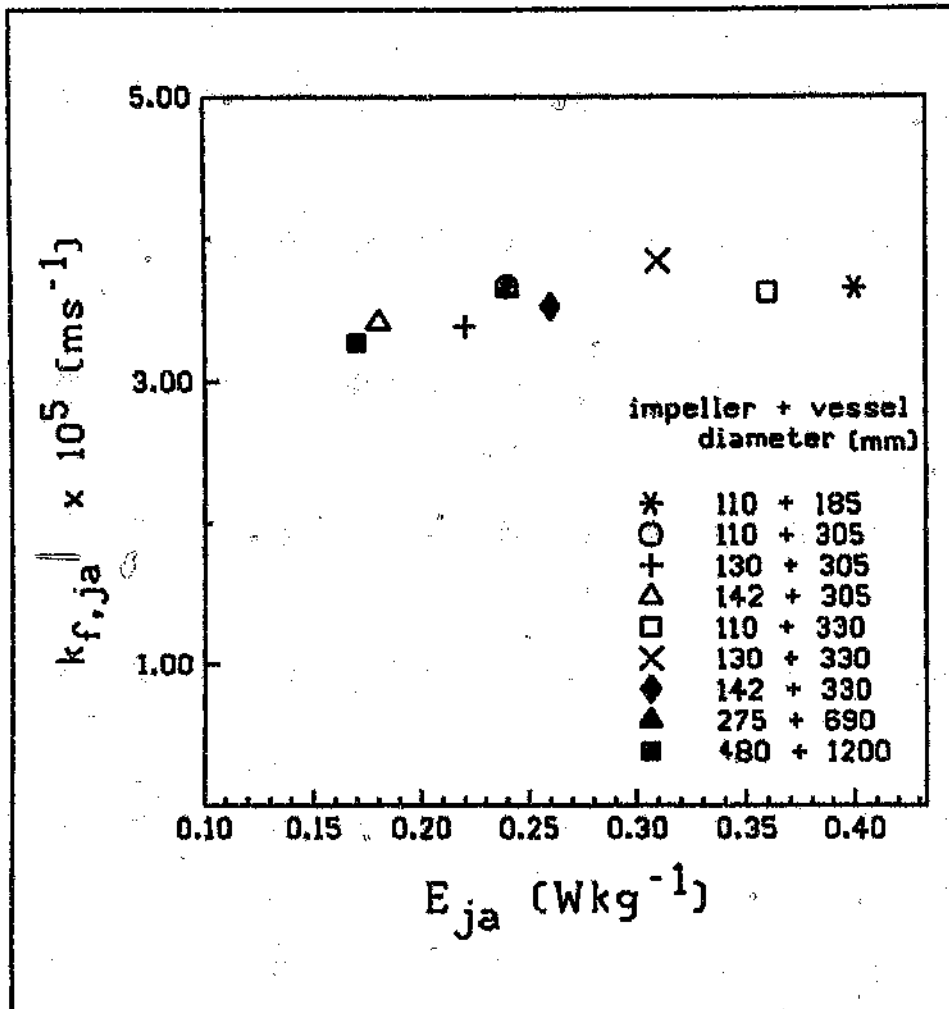


Figure 5.15: The film mass transfer coefficient vrs the specific power input for agitation for different impeller-vessel configurations

exploited in developing a useful scale-up procedure. To test this hypothesis, the mean value of $k_{f,ja}$ as determined from the speed data and from the specific power data were calculated. These with the associated standard deviations are as follows:

- using the speed data, the mean $k_{f,ja} = 3.52 \times 10^{-5} \text{ ms}^{-1}$ with relative standard deviation of 4.62%.
- using the specific power data, the mean $k_{f,ja} = 3.55 \times 10^{-5} \text{ ms}^{-1}$ with relative standard deviation of 4.94%.
- using both speed and specific power data, the mean $k_{f,ja} = 3.54 \times 10^{-5} \text{ ms}^{-1}$ with relative standard deviation of 4.66%.

The standard deviation associated with the measurement of the film transfer coefficient was shown in Section 4.7 to be in the range 3.3 to 5.2%. The standard deviations of the estimates of the value of $k_{f,ja}$ are in the same range. Clearly there is, therefore, no discernible difference between the different estimates of $k_{f,ja}$. Nienow's contention that $k_{f,ja}$ may be scale independent appears to be valid.

Before leaving this topic, a further question needs to be addressed. This concerns whether or not there is difference between the values of $k_{f,ja}$ estimated from the speed data and the values estimated using the power data. This question was considered by conducting a pairing comparison. This assumes that the differences between the values of related data constitute a random sample from a normal population, $N(\delta, \sigma_p)$. The pairs (X_i, Y_i) (for $i = 1, 2, \dots, 9$) are independent, but X_i and Y_i within the pair are usually dependent. Let X_i represent $k_{f,ja}$ values from the speed data and Y_i the $k_{f,ja}$ values from the power data (in Table 5.4). The paired difference d_i is then defined as:

$$d_i = X_i - Y_i$$

5.11

The mean, $\bar{\delta}$, and standard deviation, σ_d , of the set of d_i values are respectively -0.0356 and 0.061. The 95% confidence interval for the mean, $\bar{\delta}$, can then be determined. Using the t-Tables the value of $t_{0.025, 8}$ at 8 degrees of freedom is 2.306. Hence the 95% confidence interval for the mean paired difference should be:

$$-0.0356 \pm 2.306 \frac{0.061}{\sqrt{9}} \quad 5.12$$

which is -0.0825 to 0.0113.

If there is no difference between the X and Y data then the mean value for the paired differences should be zero. To test the significance of the difference between the X and Y data at a 95% confidence level ($\alpha = 0.05$) the one sided rejection region that requires t to have a value greater than $t_{0.05} = 1.860$, where

$$t = \left| \frac{\bar{\delta}}{\sigma_d/n^{0.5}} \right| = \left| \frac{-0.0356}{0.061/\sqrt{9}} \right| = 1.75 \quad 5.13$$

This is less than $t_{0.05} = 1.860$ and hence with 95% confidence, it can be stated that no significant difference exists between the two methods of estimating the $k_{c, 1a}$. This implies that $k_{c, 1a}$ can be estimated from either speed or power data without a significant error.

5.6 THE SPEED/POWER TO JUST ASSIMILATE THE CARBON

It is clear from Figures 5.1 to 5.10 that it is most important that the degree of agitation is sufficiently great that all the carbon is fully assimilated in the slurry. If this condition is not satisfied then low adsorption rates are likely. In plant practice, the situation could be worse than is suggested in these figures, because the carbon may settle and become locked

in a sediment at the bottom of the tank. In the tests conducted in this work the carbon floated when agitation was not sufficiently intense.

The bi-linear model allows an estimate to be made of the speed and the power required to just assimilate the carbon into the slurry. Although this information is not directly relevant to the scale-up model, it is nevertheless useful to know and so it will be discussed in some detail. The relevant data is shown in Table 5.5.

Table 5.5: Speed and Power to just assimilate the carbon in the slurry

impeller + vessel diameter (mm)	T/D	Speed N_{j_s} (rpm)	Power P_{j_s} (W)	Power per unit mass E_{j_s} (Wkg^{-1})
110 + 185	1.682	288	2.86	0.40
110 + 305	2.773	472	7.86	0.24
130 + 305	2.346	365	7.22	0.22
142 + 305	2.148	329	5.95	0.18
110 + 330	3.000	570	14.60	0.36
130 + 330	2.538	404	12.74	0.31
142 + 330	2.324	371	10.72	0.26
275 + 690	2.509	255	90.37	0.24
480 + 1200	2.500	135	333.82	0.17

As can be seen in Table 5.5, for impellers of the same design, the larger the diameter, the smaller the power per unit mass of slurry required to assimilate the carbon particles. This is in agreement with the predictions of suspension theory as outlined in Chapter 2, (Equations 2.4, 2.5 and 2.7).

Chapman et al(36) on analyzing Zwietering's data for propellers of different diameters in the same vessel, found N_{j_s} to be proportional to impeller diameter to the power of -1.67. From their own data, they found it to

be proportional to the diameter to the power of -1.5. In this work, using the data for the three impeller diameters of 110, 130 and 142 mm in the 305 and 330 mm vessels, the following results were obtained:

For the 305 mm vessel:

$$N_{ja} \propto D^{-1.45} \quad 5.14$$

and for the 330 mm vessel:

$$N_{ja} \propto D^{-1.73} \quad 5.15$$

Looking at the data for the specific power input, the following relationships were obtained:

For the 305 mm vessel:

$$E_{ja} \propto D^{-1.048} \quad 5.16$$

and for the 330 mm vessel:

$$E_{ja} \propto D^{-1.225} \quad 5.17$$

Although the exponents of D found in this work (from Equations 5.14 and 5.15) are similar to those reported by Chapman it should be noted that the mixing situations are different. Chapman's findings relate to the suspension of solids that settle out of the fluid. The findings in this work relate to the assimilation of particles that tend to float.

As Nienow(37) has indicated the subject of the assimilation of floating particles has not been studied adequately. The most relevant work that has been reported is that due to Joosten et al(37) - Equation 2.5. The values of N_{ja} predicted using this equation are compared with measured values in Table 5.6. (The predicted values were calculated assuming that the

density of the carbon was 762.9 kgm^{-3} (as explained in Section 4.2.3)). As can be seen, the predictions are generally different from the measured values.

Table 5.6: Predicted and measured values for N_{j_a}

Impeller + Vessel diameter (mm)	Joosten's Equation	N_{j_a} from Exptal. work
110 + 185	234	288
110 + 305	584	472
130 + 305	398	365
142 + 305	323	329
110 + 330	675	570
130 + 330	458	404
142 + 330	366	371
275 + 690	308	255
480 + 1200	232	135

To investigate the influence of vessel diameter the data from three agitation system was considered. These were systems in which the T/D ratio was similar. The values for E_{j_a} and N_{j_a} for these systems are shown in Table 5.7. As can be seen from Figure 5.16, E_{j_a} and N_{j_a} are strongly dependent on the vessel diameter.

Table 5.7: The values of E_{j_a} and N_{j_a} for systems with similar T/D ratios

Vessel diameter T , (mm)	Impeller diameter D , (mm)	T/D	N_{j_a} (rpm)	E_{j_a} (Wkg^{-1})
330	130	2.538	404	0.311
690	375	2.509	255	0.240
1200	480	2.500	135	0.170

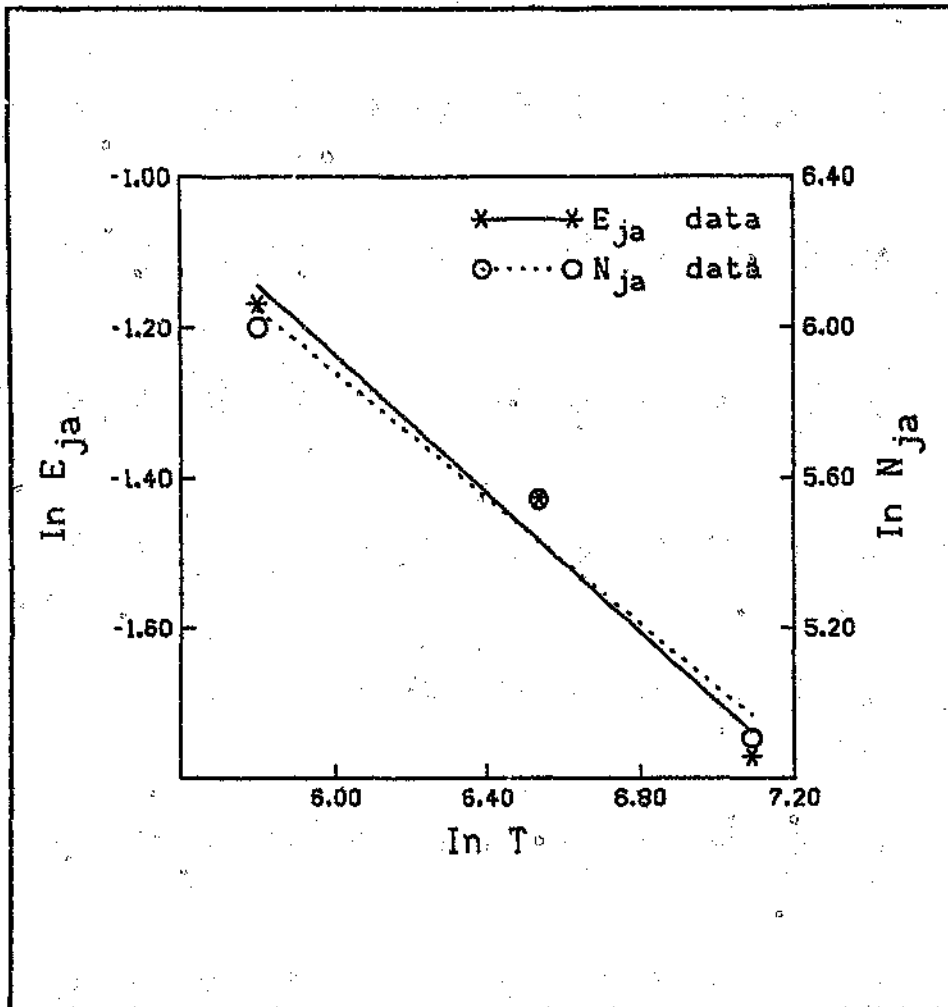


Figure 5.16: The effect of scale (vessel diameter) on E_{ja} and N_{ja} for systems with similar T/D ratios

The correlation relationships were found to be

$$E_{j_s} \propto T^{-0.4615} \quad 5.18$$

and

$$N_{j_s} \propto T^{-0.8369} \quad 5.19$$

for which the correlation coefficients were -0.987 and -0.985 respectively. Chapman et al(36) obtained a relationship similar to Equation 5.18 in which the exponent was -0.28. Their work, however, involved the suspension of settled solids as opposed to the current work in which floating solids were assimilated. However, they cautioned that minor differences in geometry could cause deviations from this value.

The data that has been generated may be used to develop a correlation similar to the Joosten Equation (Equation 2.5). Taking the form of that equation, correlation Equations 5.20 and 5.21 were obtained. Their respective correlation coefficients were 0.987 and 0.624.

$$N_{j_s} \propto \left(\frac{T}{D}\right)^{1.09} D^{-0.770} \quad 5.20$$

and

$$E_{j_s} \propto \left(\frac{T}{D}\right)^{-0.150} D^{-0.351} \quad 5.21$$

As can be seen only Equation 5.20 shows a good correlation with the data.

5.7 SOURCES OF ERROR IN THIS INVESTIGATION

Errors in the measurement of torque: In this work, the static and dynamic friction in the bearings holding the impeller shaft (or under the torque table) were assumed equal. The problems associated with accounting for friction have already been discussed.

Errors arising from geometrical inconsistencies:

Strict geometrical similarity is an essential prerequisite for accurate scale-up study. For example the thickness of the impeller is not frequently reported but it has been shown by Chudacek(45) to influence the power number. He said even minute variations in blade angle that cannot be visually distinguished can be a source of error. For instance, he reported the results of experiments with two identical blades of equal diameters. One had its blades set at exactly 45° and the other at $43-44^{\circ}$ due to a manufacturing error. The erroneous turbine gave a 4.6% lower value in the power numbers that could not be otherwise explained. This highlights the importance of precision of manufacturing of impellers used in these tests.

Similar small geometrical inconsistencies in vessels of different scales may be a contributing factor to the lack of agreement between the scale-up relationships reported by different authors. In this regard, it must be remembered that the 142 and 480 mm diameter impellers used in this investigation were rubber lined and all the others were not.

Differences in power numbers: All the impellers used in this work were manufactured to the same specifications in regards to their geometric configuration. In principle this should lead to systems in which the power and flow numbers are similar. The flow numbers were not measured in this work. However, the power numbers could be estimated for each test conducted. This data is presented in Table 5.8. The maximum and minimum values are 0.36 and 1.14. As can be seen, all the power numbers are greater than the nominal value of 0.35 as given by the manufacturer.

Chudacek(45) indicated that power and flow numbers are

dependent on impeller clearance, impeller diameter, vessel height, shape of the bottom of the vessel and impeller blade geometry. The causes of the variations seen in the measured power numbers have not been investigated.

Changes in cyanide concentration: In the kinetic experiments conducted in the 1200 mm diameter vessel, the slurry from one test was used in two subsequent tests (after aurocyanide had been added). On several occasions the lengthy periods of agitation that were necessary between tests resulted in excessive destruction of cyanide. This resulted in an improvement in the adsorption rates due to the change in solution chemistry. In larger scale tests the cyanide levels were not always the same. The results from those in which excessive destruction had occurred were discarded.

Table 5.8: Power numbers determined for the various mixing configurations (data above the 'just assimilated' condition only)

Impeller+Vessel diameter (mm)	Speed (rpm)	Power Input (W)	Power Number (dimensionless)
110 + 165	300	3.33	1.14
	400	5.38	0.78
	500	7.74	0.57
	550	9.98	0.55
	600	12.23	0.52
110 + 305	500	7.94	0.59
	600	13.13	0.56
	700	22.92	0.62
130 + 305	400	8.27	0.52
	500	12.43	0.40
	600	19.31	0.36
	650	27.96	0.41
142 + 305	400	11.31	0.46
	500	21.65	0.44
	600	39.64	0.47
110 + 330	600	15.08	0.65
	650	17.61	0.59
	700	20.79	0.56
	800	34.79	0.63
130 + 330	500	14.66	0.47
	550	19.29	0.47
	600	24.35	0.45
	650	30.65	0.45
142 + 330	400	15.25	0.61
	500	21.86	0.45
	550	30.22	0.49
	640	44.95	0.44
275 + 690	261	95.01	0.51
	283	113.98	0.48
	309	140.31	0.45
480 + 1200	140	350.29	0.75
	150	421.02	0.73
	162	467.09	0.64

CHAPTER SIX

CONCLUSIONS AND SCALE-UP PROCEDURE

6.1 CONCLUSIONS

The following conclusions may be drawn from the work reported:

- The classical film mass transfer diffusion model was found adequate to represent the rate data of adsorption of aurocyanide onto activated carbon during the initial periods of the kinetic tests.
- An increase in the power input for agitation leads to an increase in the mass transfer rate. This will also lead to an increase in the loss of carbon due to attrition. (This effect was not investigated in this work). In selecting the power to be applied for agitation, one consideration is that a maximum rate of mass transfer to carbon and a minimum loss of carbon due to attrition should be obtained. Hence the power selected should be at least that required to just assimilate the carbon particles. At lower power inputs, the mass transfer coefficient drops off rapidly. At higher power inputs, only a small increase in adsorption rates will occur at the expense of an increase in the carbon attrition rate and power costs.
- The film mass transfer coefficient at the 'just assimilated' condition, $k_{f,ja}$ is constant and is independent of impeller-vessel geometry. It may be estimated from kinetic tests in which either speed or power are measured.
- For impellers of the same design, the larger the diameter, the smaller the specific power input required to suspend the solids. Thus an impeller-vessel configuration that is efficient for

suspension is also efficient for the adsorption process. The results show that what is required is a large low-speed impeller. Such a system will also minimize carbon attrition.

- For approximately equal vessel-impeller diameter ratios, it was found that the specific power required to just assimilate the carbon particles is proportional to the vessel diameter to the exponent of -0.4615.
- A scale-up procedure has been developed from the current investigation and is presented below.

6.2 SCALE-UP PROCEDURE

From the results and discussions of this investigation, the recommended scale-up procedure for the film mass transfer coefficient in CIP adsorption systems is as outlined below:

1. Run kinetic tests at laboratory scale using slurry and activated carbons that correspond as closely as possible to the slurries and carbons that occur or will occur at full scale. The vessel and impeller designs must be geometrically similar for the laboratory and full scale equipment.
2. Run kinetic experiments at a laboratory scale at different speeds of agitation and determine the corresponding values of the specific power input for agitation. In the determination of the applied power, frictional forces must be taken into account. From the kinetic data, determine the film mass transfer coefficient at each speed investigated.
3. Consider only the data derived from tests in which the carbon was fully assimilated into the slurry. Which points these are may be determined by referring to a logarithmic plot of k_f against speed or specific

power. Fit these data to Equation 3.35 to obtain values for K_0 , t_s , and t_c . From this work the values for t_s and t_c were 0.117 and 0.089 respectively.

$$k_f = K_0 E^{t_s} (T/D)^{t_c} \quad 3.35$$

4. Use these values of K_0 , t_s , and t_c to predict the values of k_f at a larger scale (as indicated by D and T) at the level of specific power input, E that is to be installed.
5. The installed specific power, E , should be greater than E_{j_s} - the specific power required to assimilate all the carbon into the slurry. The value of E_{j_s} should be obtained from mixer supplies or can be estimated using Equations 5.20 and 6.1:

$$N_{j_s} \propto \left(\frac{T}{D}\right)^{1.09} D^{-0.771} \quad 5.20$$

$$E_{j_s} = \frac{N_p N_{j_s}^3 D^5}{T^3} \quad 6.1$$

(Note: Equation 5.20 applies to the situation where the carbon tends to float. If the carbon tends to settle, less power is required (37)).

6. The k_f obtained from step 4 can be substituted into an appropriate kinetic model so that the performance at the full scale CIP plant can be simulated.

6.3 LIMITATIONS OF THE SCALE-UP MODEL

The model that has been developed is empirical and therefore it may be valid only in the range of conditions that has been investigated.

The scale-up model has been developed for a specific geometric configuration, namely:

Impeller configuration:

- hydrofoil impellers with a blade angle of 20° ,
- some were rubber lined and others were not.

Mixer configuration:

- flat bottomed cylindrical vessels,
- slurry depth to vessel diameter ratio was 1,
- the ratio of impeller height off the bottom to vessel diameter was 0.25,
- vessel diameters varied from 185 to 1200 mm.

Baffle configuration:

- four vertical baffles used,
- width of baffles was $0.1T$, where T is the diameter of the vessel.

The scale-up model that has been developed may be applicable to other configurations but these have not been tested.

6.4 RECOMMENDATIONS FOR FUTURE WORK

This investigation is an initial attempt to model the scale-up of typical CIP systems. It is obvious that much more research is required in this area. The following areas in particular require attention:

- Since the current work was conducted with hydrofoil impellers of the same nominal power and flow numbers and angle, it would be desirable to conduct similar work with other kinds of impellers. The scale-up model that has been developed may then be tested for different configurations.
- Tests should be conducted in systems with the same geometry as employed in this work but at very much larger scales.
- Work should be done to determine the extent to which carbon attrition increases with increased agitation

speeds. This will help to decide how far above the 'just assimilated' point it will be economical to operate.

- Regenerated carbon, which is commonly used in the industry, should be used. Since the particle shape and surface roughness are different from those of virgin carbon, the scale-up parameters may vary from those found in this work.

REFERENCES

1. Stange W., The Modelling and Simulation of In-Pulp Adsorption Processes in Recent Developments in In-Pulp Technology, School, Mintek, Randburg 7 - 8 October 1991
2. Le Roux J.D., Modelling of the effect of organic fouling on the adsorption of gold cyanide by activated carbon in a Batch Reactor.
MSc Thesis Univ. of the Witwatersrand, 1989
3. McDougal G.J. and Fleming C.A., Extraction of Precious metals on Activated Carbon, in Ion Exchange and Sorption Processes in Hydrometallurgy; eds. Streat M. and Naden D
4. van Deventer J.S.J., Kinetic Models for the Adsorption of Metal Cyanides onto Activated Carbon.
PhD Thesis, University of Stellenbosch, 1984
5. Laxen P.A., General Introduction, Lecture 1
Carbon School SAIMM Johannesburg 1985
6. Johns M.W., The Simulation of gold Adsorption using a film Diffusion Model
MSc Thesis Univ. of the Witwatersrand 1985
7. Whyte R.M, Dampsey P. and Stange W., The AAC Pump-cell - A novel Approach to the Design and Operation of CIP Gold Recovery Circuits. Presented at the Randol Conference on Innovations in Gold and Silver Recovery Phase IV, Randol Sacramento, 1989 pp 174-183
8. Stange W., Towards more effective Simulation of Mineral Processing Systems, MSc Dissertation

University of the Witwatersrand, 1989.

9. Bailey P.R., Lecture 6, Carbon School, SAIMM, Johannesburg, 1985
10. Bailey P.R., Application of Activated Carbon to the Recovery; Chapter 9 in Extractive Metallurgy of Gold in South Africa ed. G.G Stanley, Monograph M7 Johannesburg, 1987.
11. Woollacott L.C., Stange W.W. and King R.P., Towards More Effective Simulation of CIP-CIL processes: Part 1 : The modelling of Adsorption and Leaching. J. S. Afr. Inst. Min. Metall. vol. 90, no. 10. 1990 pp257 - 273
12. Ford M.A. and King R.P., The Simulation of Ore-Dressing Plants; International Journal of Mineral Processing; vol.12 1984; pp285 - 304.
13. King R.P., Application of Computer Simulation Techniques in the Ore Dressing Plant Design and Operation; SAIMM Colloquium: Control and Simulation in the Mineral Industry; Johannesburg, 1984
14. Lynch J.A., Computer in Mineral Processing, The First Twenty-Five Years, 18th Int. APCOM Symposium, IMM, London, 1984
15. Dixon S., Cho E.H. and Pitt C.H., The interaction between gold cyanide, silver cyanide and high surface area charcoal. AIChE Symposium Series 74, vol. 74 no. 173 pp 75-83, 1978.
16. Williams D.F. and Glasser D., The Modelling and Simulation of Processes for the adsorption of Gold by

activated charcoal.

J. S. Afr. Inst. Min. Metall. vol 85 no.8 1985

17. Fleming C.E., Nicol M.J. and Nicol D.I., The Optimisation of a carbon-in-pulp adsorption circuit based on the kinetics of extraction of cyanide by activated carbon. Presented at Mintek meeting 'Ion Exchange and Solvent Extraction in Mineral Processing'. Mintek, Randburg, Feb. 1980.
18. Nicol M.J., Fleming C.A. and Cromberge G., The adsorption of Gold cyanide on to activated carbon I. The kinetics of adsorption from pulps.
J. S. Afr. Inst. Min. Metall. vol 84 no.2 1984
19. Le Roux J.D., Bryson A.W. and Young B.D., A Comparison of several kinetic models for the adsorption of gold cyanide.
J.S. Afr. Inst. Min. Metall., vol. 91 no. 3 1991
pp95 - 103.
20. Young B.D., The characterization of Particle Shape and Surface Texture and its impact on Mass and Momentum Transfer and Particle Abrasion.
PhD Thesis Univ of the Witwatersrand 1989.
21. Oldsue J.Y., Current Trends in Mixer Scale-up Techniques, Chapter 9, Mixing of Liquids by Mechanical Agitation : vol. 1, editors: Ulbrecht J.J and Patterson G.K. Gordon and Breach Science Publishers, 1985.
22. Johnstone R.E. and Thring M.W., Pilot Plant, Models, Scale-up Methods in Engineering MC Graw Hill 1957
23. Rushton J.H., The use of Pilot Plant Mixing Data
Chem Eng Prog. vol 47 no.9 Sept. 1951 pp 485 - 488

24. Baguley W., Adsorption Mixing Requirements for CIP and CIL Lecture 9. Carbon School, SAIMM, Jhb. 1985.
25. Cloete F.L.D. and Coetzee M.C.C., Calculating the Minimum Power Requirement for complete Suspension of Solids in a mixer.
Powder Technology 46 1986 pp 239 - 243
26. Coetzee M.C.C and Cloete F.L.D., A comparison of axial-flow impellers with inclined blade turbines in a baffled mixer.
J. S. Afr. Min. Metall. vol. 89 no.4 1989 pp 99 - 109.
27. Zwietering TH.N., Suspending of Solid particles in liquid by agitators.
Chem. Eng.Sci. vol.8 1958 pp244 - 253
28. Sauder H.J and Luckiewicz E.T., Practical Process Engineering--A working Approach to Plant Design.
McGraw Hill, 1987
29. Chudacek M.W., Solid Suspension Behaviour in Profiled and Flat Bottom Mixing Tanks.
Chem. Engng. Sci. vol.40 no.3, 1985 pp385 -392
30. Sterbacek Z. and Tausk P., Mixing in the Chemical Industry
Pergamon Press Ltd, 1965
31. Baker J.J. and Treybal R.E., Mass Transfer Coefficients for Solids suspended in Agitated Liquids .
AIChE J. vol 6 no.2, 1960 pp289 - 295
32. Treybal R.E., Mass Transfer Operations 3rd Edition
McGraw Hill, 1995

33. Oldshue J.Y., Fluid Mixing Technology, New York, Mc Graw-Hill, 1983.
34. Chudacek M.W., The relationships between Suspension Criteria, Mechanism of Suspension, Tank Geometry, and Scale-up Parameters in Stirred Tanks.
Ind. Eng. Chem. Fundam. 1986 pp391 - 401
35. Nienow A.W., The Dispersion of Solids in Liquids, Chapter 8 in Mixing of Liquids by Mechanical Agitation : vol. 1, editors: Ulbrecht J.J and Patterson G.K. Gordon and Breach Science Publishers, 1985.
36. Chapman C.M., Nienow A.W., Cooke M. and Middleton J.C., Particle-Gas-Liquid Mixing in Stirred Vessels, Part 1: Particle-Liquid Mixing.
Chem Eng Res Des, vol. 61 March 1983, pp71 - 81
37. Nienow A.W., The Suspension of Solid Particles, Chapter 16 in Harnby N., Edwards M.F. and Nienow A.W. (eds) Mixing in the Process in Industries. London Butterworth, 1985.
38. Nienow A.W. and Miles D., The Effect of Impeller/Tank Configuration on Fluid-Particle Mass Transfer.
Chem Eng J. vol. 15 1978 pp13 - 24.
39. Nienow A.W., The Mixer as a reactor: Liquid/Solid Systems, Chapter 18 in Harnby N., Edwards M.F. and Nienow A.W. (eds) Mixing in the Process in Industries. London Butterworth, 1985.
40. Latterman R.D., Quon J.E. and Gemmell R.S., Film transport coefficient in agitated suspensions of activated carbon.

41. Nagata S., *Mixing - Principles and Applications*
Kondansha Ltd Japan and Halstad Press USA 1975.
42. Mular A.L., *Empirical Modelling and Optimization of Mineral Processes*
Minerals Sci. Engng. vol.4, No.3, July 1972 pp 30 - 42
43. Press W.H., Flannery B.P., Teukolsky S.A. and Vetterling W.T. *Numerical Recipes - The Art of Scientific Computing*, Cambridge University Press N. York, 1986.
44. Discussions held with Professor Fatti, Department of Statistics, University of the Witwatersrand, 1991 - 1992.
45. Chudacek M.W., *Impeller Power numbers and Impeller Flow Numbers in Profiled Bottom Tanks.*
Ind. Eng. Chem. Process Des. Dev. 24, pp 858 - 867. 1985.
46. Van der Merwe P.F., *Fundamentals of the Elution of Gold Cyanide from Activated Carbon.*
PhD Thesis, University of Stellenbosch, 1991
47. Jordi R.G., *The Influence of Fine Suspended Solid Materials on the Adsorption of Gold Cyanide by Activated Carbon.*
MSc Dissertation, University of the Witwatersrand, 1989.
48. Moys M.H. and King R.P., *Estimation of the Parameters in the Distributed-Constant Flotation Model.* Report 1567, National Institute of

Metallurgy, 15 January 1974.

APPENDIX 1A

POWER DATA

Impeller diameter = 110 mm and Vessel diameter = 185 mm

Speed (rpm)	Mean Load Cell Reading (g)	Actual Load (g)	Measured Torque (Nm)	Frictional Torque (Nm)	Power (W)
200	30.00	32.88	0.0441	0.0320	1.59
250	33.83	37.08	0.0497	0.0320	2.14
270	41.83	45.77	0.0614	0.0320	2.64
300	50.50	55.21	0.0740	0.0320	3.33
400	63.50	69.37	0.0931	0.0354	5.38
500	76.75	83.81	0.1124	0.0354	7.74
550	94.17	102.78	0.1379	0.0354	9.98
600	108.75	118.67	0.1592	0.0354	12.23

Impeller diameter = 110 mm and Vessel diameter = 305 mm

Speed (rpm)	Mean Load Cell Reading (g)	Actual Load (g)	Measured Torque (Nm)	Frictional Torque (Nm)	Power (W)
300	30.00	32.88	0.0441	0.0434	2.75
400	49.50	54.12	0.0726	0.0527	5.20
450	64.33	70.27	0.0943	0.0525	6.92
500	72.17	78.81	0.1057	0.0460	7.94
600	104.50	114.03	0.1530	0.0560	13.13
700	171.50	187.01	0.2509	0.0618	22.92

Impeller diameter = 130 mm and Vessel diameter = 305 mm

Speed (rpm)	Mean Load Cell Reading (g)	Actual Load (g)	Measured Torque (Nm)	Frictional Torque (Nm)	Power (W)
200	54.50	59.57	0.0800	0.0461	2.64
300	83.33	91.04	0.1221	0.0434	5.20
350	97.00	105.86	0.1420	0.0358	6.52
400	101.75	111.03	0.1489	0.0485	8.27
500	123.83	135.08	0.1812	0.0561	12.43
600	178.17	194.27	0.2606	0.0467	19.31
650	259.50	282.86	0.3794	0.0313	27.96

Impeller diameter = 142 mm and Vessel diameter = 305 mm

Speed (rpm)	Mean Load Cell Reading (g)	Actual Load (g)	Measured Torque (Nm)	Frictional Torque (Nm)	Power (W)
200	54.33	59.39	0.0797	0.0650	3.03
250	66.17	72.28	0.0970	0.0612	4.14
300	71.00	77.54	0.1040	0.0630	5.25
400	129.50	141.26	0.1895	0.0806	11.31
500	252.00	274.69	0.3685	0.0450	21.65
600	370.33	403.59	0.5414	0.0895	39.64

Impeller diameter = 110 mm and Vessel diameter = 330 mm

Speed (rpm)	Mean Load Cell Reading (g)	Actual Load (g)	Measured Torque (Nm)	Frictional Torque (Nm)	Power (W)
300	31.63	34.66	0.0465	0.0315	2.45
400	56.00	61.20	0.0821	0.0315	4.76
500	92.33	100.78	0.1352	0.0556	9.99
550	114.83	125.29	0.1681	0.0556	12.88
600	126.00	137.46	0.1844	0.0556	15.08
650	133.67	145.81	0.1956	0.0631	17.61
700	150.75	164.42	0.2206	0.0631	20.79
800	240.83	262.54	0.3522	0.0631	34.79

Impeller diameter = 130 mm and Vessel diameter = 330 mm

Speed (rpm)	Mean Load Cell Reading (g)	Actual Load (g)	Measured Torque (Nm)	Frictional Torque (Nm)	Power (W)
250	33.67	36.88	0.0495	0.0434	2.43
300	76.67	83.72	0.1123	0.0434	4.89
350	92.33	100.78	0.1352	0.0716	7.58
390	134.33	146.52	0.1965	0.0716	10.95
500	139.25	151.88	0.2037	0.0763	14.66
550	176.83	192.81	0.2586	0.0763	19.29
600	212.93	232.03	0.3113	0.0763	24.35
650	255.75	278.78	0.3740	0.0763	30.65

Impeller diameter = 142 mm and Vessel diameter = 330 mm

Speed (rpm)	Mean Load Cell Reading (g)	Actual Load (g)	Measured Torque (Nm)	Frictional Torque (Nm)	Power (W)
200	37.25	40.78	0.0547	0.0484	2.16
250	68.17	74.46	0.0999	0.0484	3.88
300	90.33	98.59	0.1323	0.0650	6.20
350	129.50	141.26	0.1895	0.0650	9.33
400	198.25	216.15	0.2899	0.0741	15.25
500	234.83	255.99	0.3434	0.0741	21.86
550	308.17	335.88	0.4506	0.0741	30.22
640	408.17	444.80	0.5967	0.0741	44.95

Impeller diameter = 275 mm and Vessel diameter = 690 mm

Speed (rpm)	Mean Load Cell Reading (g)	Actual Load (g)	Measured Torque (Nm)	Frictional Torque (Nm)	Power (W)
149	283.50	309.03	2.12	0.126	35.04
171	309.50	337.35	2.31	0.126	43.62
200	360.50	392.90	2.70	0.126	59.19
261	447.50	487.67	3.35	0.126	95.01
283	498.00	542.69	3.72	0.126	113.98
309	563.00	613.49	4.21	0.126	140.31

Impeller diameter = 480 mm and Vessel diameter = 1200 mm

Speed (rpm)	Mean Load Cell Reading (g)	Actual Load (g)	Measured Torque (Nm)	Frictional Torque (Nm)	Power (W)
110	2037	2219.16	21.75	0.823	260.02
125	2051	2234.41	21.90	0.823	297.44
131	2154	2346.61	23.00	0.823	326.81
140	2161	2354.23	23.07	0.823	350.29
150	2433	2650.53	25.98	0.823	421.02
162	2502	2725.69	26.71	0.823	467.09

APPENDIX 1B

DATA FROM KINETIC TESTS

Impeller diameter = 110 mm: vessel diameter = 185 mm

Speed (rpm)	Time (min)	Conc. (ppm)	$\ln C/C_0$
200	0	5.09	0
	2	4.51	-0.1210
	4	4.41	-0.1434
	6	4.26	-0.1780
	8	3.96	-0.2510
	10	3.80	-0.2923
slope of line = -8.19×10^{-3}			
correlation coefficient = -0.978			
$k_f = 0.43 \times 10^{-5} \text{ ms}^{-1}$			

Impeller diameter = 110 mm: vessel diameter = 185 mm

Speed (rpm)	Time (min)	Conc. (ppm)	$\ln C/C_0$
250	0	4.23	0
	2	3.60	-0.1613
	4	3.50	-0.1894
	6	3.35	-0.2332
	8	2.71	-0.4453
	10	2.49	-0.5339
slope of line = -0.050647			
correlation coefficient = -0.972			
$k_f = 2.67 \times 10^{-5} \text{ ms}^{-1}$			

Impeller diameter = 110 mm: vessel diameter = 185 mm

Speed (rpm)	Time (min)	Conc. (ppm)	lnC/C ₀
270	0	5.01	0
	2	4.28	-0.1575
	4	3.88	-0.2556
	6	3.44	-0.3760
	8	3.08	-0.4855
	10	2.83	-0.5881
slope of line = -0.0571			
correlation coefficient = -0.997			
k _f = 3.00 x 10 ⁻⁵ ms ⁻¹			

Impeller diameter = 110mm: vessel diameter = 185 mm

Speed (rpm)	Time (min)	Conc. (ppm)	lnC/C ₀
300	0	5.87	0
	2	5.01	-0.1584
	4	4.12	-0.3540
	6	3.54	-0.5057
	8	3.42	-0.5402
	10	2.85	-0.7225
slope of line = -0.0791			
correlation coefficient = -0.9877			
k _f = 3.69 x 10 ⁻⁵ ms ⁻¹			

Impeller diameter = 110 mm: vessel diameter = 185 mm

Speed (rpm)	Time (min)	Conc. (ppm)	lnC/C ₀
400	0	4.38	0
	2	3.60	-0.1951
	4	3.12	-0.3392
	6	2.70	-0.4838
	8	2.34	-0.6269
	10	2.07	-0.7495
slope of line = -0.07406			
correlation coefficient = -0.997			
k _f = 3.90 x 10 ⁻⁵ ms ⁻¹			

Impeller diameter = 110 mm: vessel diameter = 185 mm

Speed (rpm)	Time (min)	Conc. (ppm)	lnC/C ₀
500	0	5.02	0
	2	4.30	-0.1548
	4	3.95	-0.2397
	6	3.30	-0.4195
	8	2.76	-0.5982
	10	2.31	-0.7762
slope of line = -0.0770			
correlation coefficient = -0.995			
k _f = 4.05 x 10 ⁻⁵ ms ⁻¹			

Impeller diameter = 110 mm: vessel diameter = 185 mm

Speed (rpm)	Time (min)	Conc. (ppm)	lnC/C ₀
550	0	5.10	0
	2	4.02	-0.2380
	4	3.45	-0.3909
	6	2.93	-0.5542
	8	2.57	-0.6853
	10	2.27	-0.8095
slope of line = -0.07932			
correlation coefficient = -0.993			
k _f = 4.17 x 10 ⁻⁵ ms ⁻¹			

Impeller diameter = 110 mm: vessel diameter = 185 mm

Speed (rpm)	Time (min)	Conc. (ppm)	lnC/C ₀
600	0	4.97	0
	2	3.92	-0.2373
	4	3.36	-0.3915
	6	2.86	-0.5387
	8	2.45	-0.7073
	10	2.22	-0.8059
slope of line = -0.07981			
correlation coefficient = -0.993			
k _f = 4.20 x 10 ⁻⁵ ms ⁻¹			

Impeller diameter = 110 mm: vessel diameter = 305 mm

Speed (rpm)	Time (min)	Conc. (ppm)	lnC/C ₀
300	0	6.63	0
	2	6.10	-0.0833
	4	5.60	-0.1688
	6	5.23	-0.2372
	8	4.88	-0.3065
	10	4.63	-0.3547
slope of line = -0.03588			
correlation coefficient = -0.996			
k _r = 1.89 x 10 ⁻⁵ ms ⁻¹			

Impeller diameter = 110 mm: vessel diameter = 305 mm

Speed (rpm)	Time (min)	Conc. (ppm)	lnC/C ₀
400	0	5.58	0
	2	4.96	-0.1178
	4	4.46	-0.2240
	6	3.87	-0.3659
	8	3.62	-0.4327
	10	3.24	-0.5436
slope of line = -0.05435			
correlation coefficient = -0.997			
k _r = 2.86 x 10 ⁻⁵ ms ⁻¹			

Impeller diameter = 110 mm: vessel diameter = 305 mm

Speed (rpm)	Time (min)	Conc. (ppm)	lnC/C ₀
450	0	5.85	0
	2	5.10	-0.1372
	4	4.57	-0.2469
	6	3.99	-0.3827
	8	3.45	-0.5281
	10	3.11	-0.6318
slope of line = -0.06302			
correlation coefficient = -0.999			
k _r = 3.36 x 10 ⁻⁵ ms ⁻¹			

Impeller diameter = 110 mm: vessel diameter = 305 mm

Speed (rpm)	Time (min)	Conc. (ppm)	$\ln C/C_0$
500	0	6.61	0
	2	5.65	-0.1569
	4	5.06	-0.2672
	6	4.35	-0.4184
	8	3.75	-0.5668
	10	3.29	-0.6977
slope of line = -0.06956			
correlation coefficient = -0.999			
$k_f = 3.66 \times 10^{-5} \text{ ms}^{-1}$			

Impeller diameter = 110 mm: vessel diameter = 305 mm

Speed (rpm)	Time (min)	Conc. (ppm)	$\ln C/C_0$
600	0	6.48	0
	2	5.56	-0.1531
	4	4.89	-0.2815
	6	4.26	-0.4195
	8	3.65	-0.5740
	10	3.12	-0.7309
slope of line = -0.0722			
correlation coefficient = -0.999			
$k_f = 3.80 \times 10^{-5} \text{ ms}^{-1}$			

Impeller diameter = 110 mm: vessel diameter = 305 mm

Speed (rpm)	Time (min)	Conc. (ppm)	$\ln C/C_0$
700	0	6.14	0
	2	5.24	-0.1585
	4	4.58	-0.2931
	6	3.76	-0.4904
	8	3.36	-0.6029
	10	2.90	-0.7501
slope of line = -0.07544			
correlation coefficient = -0.998			
$k_f = 3.97 \times 10^{-5} \text{ ms}^{-1}$			

Impeller diameter = 130 mm: vessel diameter = 305 mm

Speed (rpm)	Time (min)	Conc. (ppm)	lnC/C ₀
200	0	5.84	0
	2	5.59	-0.0438
	4	5.35	-0.0876
	6	5.16	-0.1238
	8	4.98	-0.1593
	10	4.72	-0.2029
slope of line = -0.02068			
correlation coefficient = -0.998			
k _f = 1.088 x 10 ⁻⁵ ms ⁻¹			

Impeller diameter = 130 mm: vessel diameter = 305 mm

Speed (rpm)	Time (min)	Conc. (ppm)	lnC/C ₀
300	0	5.87	0
	2	5.43	-0.0779
	4	5.00	-0.1604
	6	4.49	-0.2680
	8	4.26	-0.3206
	10	3.81	-0.4322
slope of line = -0.04281			
correlation coefficient = -0.997			
k _f = 2.253 x 10 ⁻⁵ ms ⁻¹			

Impeller diameter = 130 mm: vessel diameter = 305 mm

Speed (rpm)	Time (min)	Conc. (ppm)	lnC/C ₀
350	0	5.03	0
	2	4.15	-0.1923
	4	3.55	-0.3485
	6	3.30	-0.4215
	8	2.90	-0.5507
	10	2.78	-0.5930
slope of line = -0.05876			
correlation coefficient = -0.980			
k _f = 3.092 x 10 ⁻⁵ ms ⁻¹			

Impeller diameter = 130 mm: vessel diameter = 305 mm

Speed (rpm)	Time (min)	Conc. (ppm)	lnC/C ₀
400	0	5.11	0
	2	4.51	-0.1249
	4	3.95	-0.2575
	6	3.48	-0.3842
	8	3.07	-0.5095
	10	2.68	-0.6454
slope of line = -0.064393			
correlation coefficient = -0.9999			
$k_f = 3.389 \times 10^{-5} \text{ ms}^{-1}$			

Impeller diameter = 130 mm: vessel diameter = 305 mm

Speed (rpm)	Time (min)	Conc. (ppm)	lnC/C ₀
500	0	6.07	0
	2	5.23	-0.1489
	4	4.48	-0.3037
	6	3.95	-0.4296
	8	3.49	-0.5535
	10	2.91	-0.7352
slope of line = -0.07165			
correlation coefficient = -0.999			
$k_f = 3.771 \times 10^{-5} \text{ ms}^{-1}$			

Impeller diameter = 130 mm: vessel diameter = 305 mm

Speed (rpm)	Time (min)	Conc. (ppm)	lnC/C ₀
600	0	5.56	0
	2	4.82	-0.1606
	4	4.11	-0.3200
	6	3.57	-0.4609
	8	3.20	-0.5703
	10	2.60	-0.7779
slope of line = -0.075136			
correlation coefficient = -0.997			
$k_f = 3.954 \times 10^{-5} \text{ ms}^{-1}$			

Impeller diameter = 130 mm: vessel diameter = 305 mm

Speed (rpm)	Time (min)	Conc. (ppm)	$\ln C/C_0$
650	0	6.35	0
	2	5.37	-0.1676
	4	4.56	-0.3311
	6	4.07	-0.4448
	8	3.39	-0.6276
	10	2.87	-0.7941
slope of line = -0.07806			
correlation coefficient = -0.999			
$k_f = 4.108 \times 10^{-5} \text{ ms}^{-1}$			

Impeller diameter = 142 mm: vessel diameter = 305 mm

Speed (rpm)	Time (min)	Conc. (ppm)	$\ln C/C_0$
200	0	6.20	0
	2	5.87	-0.0547
	4	5.75	-0.0753
	6	5.46	-0.1271
	8	5.15	-0.1856
	10	5.01	-0.2131
slope of line = -0.02157			
correlation coefficient = -0.993			
$k_f = 1.135 \times 10^{-5} \text{ ms}^{-1}$			

Impeller diameter = 142mm: vessel diameter = 305 mm

Speed (rpm)	Time (min)	Conc. (ppm)	$\ln C/C_0$
250	0	6.03	0
	2	5.55	-0.0830
	4	5.28	-0.1328
	6	4.94	-0.1994
	8	4.49	-0.2949
	10	4.19	-0.3640
slope of line = -0.036033			
correlation coefficient = -0.997			
$k_f = 1.896 \times 10^{-5} \text{ ms}^{-1}$			

Impeller diameter = 142 mm: vessel diameter = 305 mm

Speed (rpm)	Time (min)	Conc. (ppm)	lnC/C ₀
300	0	5.89	0
	2	5.24	-0.1169
	4	4.82	-0.2005
	6	4.27	-0.3216
	8	3.80	-0.4383
	10	3.50	-0.5205
slope of line = -0.052683			
correlation coefficient = -0.998			
$k_t = 2.777 \times 10^{-5} \text{ ms}^{-1}$			

Impeller diameter = 142 mm: vessel diameter = 305 mm

Speed (rpm)	Time (min)	Conc. (ppm)	lnC/C ₀
400	0	6.07	0
	2	5.22	-0.1509
	4	4.65	-0.2665
	6	3.90	-0.4424
	8	3.43	-0.5708
	10	3.06	-0.6849
slope of line = -0.06943			
correlation coefficient = -0.998			
$k_t = 3.654 \times 10^{-5} \text{ ms}^{-1}$			

Impeller diameter = 142 mm: vessel diameter = 305 mm

Speed (rpm)	Time (min)	Conc. (ppm)	lnC/C ₀
500	0	6.08	0
	2	5.22	-0.1525
	4	4.59	-0.2811
	6	3.90	-0.4440
	8	3.36	-0.5931
	10	2.98	-0.7131
slope of line = -0.072146			
correlation coefficient = -0.999			
$k_t = 3.797 \times 10^{-5} \text{ ms}^{-1}$			

Impeller diameter = 142 mm: vessel diameter = 305 mm

Speed (rpm)	Time (min)	Conc. (ppm)	lnC/C ₀
600	0	6.25	0
	2	5.29	-0.1668
	4	4.61	-0.3044
	6	3.87	-0.4793
	8	3.27	-0.6478
	10	2.88	-0.7748
slope of line = -0.078456			
correlation coefficient = -0.999			
k _f = 4.129 x 10 ⁻⁵ ms ⁻¹			

Impeller diameter = 110 mm: vessel diameter = 330 mm

Speed (rpm)	Time (min)	Conc. (ppm)	lnC/C ₀
300	0	4.98	0
	2	4.87	-0.0223
	4	4.75	-0.0473
	6	4.63	-0.0729
	8	4.50	-0.1014
	10	4.36	-0.1330
slope of line = -0.01323			
correlation coefficient = -0.998			
k _f = 0.7 x 10 ⁻⁵ ms ⁻¹			

Impeller diameter = 110 mm: vessel diameter = 330 mm

Speed (rpm)	Time (min)	Conc. (ppm)	lnC/C ₀
400	0	5.10	0
	2	4.76	-0.0690
	4	4.33	-0.1537
	6	4.10	-0.2183
	8	3.98	-0.2480
	10	3.76	-0.3048
slope of line = -0.0302			
correlation coefficient = -0.987			
k _f = 1.59 x 10 ⁻⁵ ms ⁻¹			

Impeller diameter = 110 mm: vessel diameter = 330 mm

Speed (rpm)	Time (min)	Conc. (ppm)	lnC/C ₀
500	0	5.02	0
	2	4.7	-0.1433
	4	4.06	-0.2122
	6	3.72	-0.2997
	8	3.44	-0.3780
	10	3.14	-0.4692
slope of line = -0.0448			
correlation coefficient = -0.994			
k _t = 2.36 x 10 ⁻⁵ ms ⁻¹			

Impeller diameter = 110 mm: vessel diameter = 330 mm

Speed (rpm)	Time (min)	Conc. (ppm)	lnC/C ₀
550	0	5.60	0
	2	4.46	-0.1262
	4	3.92	-0.2553
	6	3.43	-0.3888
	8	3.06	-0.5095
	10	2.72	-0.6207
slope of line = -0.06267			
correlation coefficient = -0.9996			
k _t = 3.3 x 10 ⁻⁵ ms ⁻¹			

Impeller diameter = 110 mm: vessel diameter = 330 mm

Speed (rpm)	Time (min)	Conc. (ppm)	lnC/C ₀
600	0	5.07	0
	2	4.22	-0.1835
	4	3.57	-0.3508
	6	3.20	-0.4602
	8	2.86	-0.5725
	10	2.50	-0.7071
slope of line = -0.06874			
correlation coefficient = -0.995			
k _t = 3.62 x 10 ⁻⁵ ms ⁻¹			

Impeller diameter = 110 mm: vessel diameter = 330 mm

Speed (rpm)	Time (min)	Conc. (ppm)	lnC/C ₀
650	0	5.04	0
	2	4.15	-0.1943
	4	3.51	-0.3618
	6	3.11	-0.4828
	8	2.73	-0.6131
	10	2.47	-0.7132
slope of line = -0.07062			
correlation coefficient = -0.993			
k _f = 3.72 x 10 ⁻⁵ ms ⁻¹			

Impeller diameter = 110 mm: vessel diameter = 330 mm

Speed (rpm)	Time (min)	Conc. (ppm)	lnC/C ₀
700	0	5.06	0
	2	4.29	-0.1631
	4	3.72	-0.3057
	6	3.23	-0.4469
	8	2.80	-0.5898
	10	2.40	-0.7239
slope of line = -0.07344			
correlation coefficient = -0.9998			
k _f = 3.86 x 10 ⁻⁵ ms ⁻¹			

Impeller diameter = 110 mm: vessel diameter = 330 mm

Speed (rpm)	Time (min)	Conc. (ppm)	lnC/C ₀
800	0	4.99	0
	2	4.22	-0.1676
	4	3.88	-0.3045
	6	3.03	-0.4793
	8	2.61	-0.6481
	10	2.30	-0.7745
slope of line = -0.07811			
correlation coefficient = -0.999			
k _f = 4.13 x 10 ⁻⁵ ms ⁻¹			

Impeller diameter = 130 mm: vessel diameter = 330 mm

Speed (rpm)	Time (min)	Conc. (ppm)	$\ln C/C_0$
250	0	5.03	0
	2	4.95	-0.0160
	4	4.84	-0.0385
	6	4.75	-0.0573
	8	4.66	-0.0764
	10	4.57	-0.0959
slope of line = 9.7071×10^{-3}			
correlation coefficient = -0.999			
$k_f = 0.51 \times 10^{-5} \text{ ms}^{-1}$			

Impeller diameter = 130 mm: vessel diameter = 330 mm

Speed (rpm)	Time (min)	Conc. (ppm)	$\ln C/C_0$
300	0	4.99	0
	2	4.75	-0.0493
	4	4.56	-0.0901
	6	4.29	-0.1511
	8	4.15	-0.1843
	10	3.98	-0.2262
slope of line = -0.02281			
correlation coefficient = -0.998			
$k_f = 1.20 \times 10^{-5} \text{ ms}^{-1}$			

Impeller diameter = 130 mm: vessel diameter = 330 mm

Speed (rpm)	Time (min)	Conc. (ppm)	$\ln C/C_0$
350	0	5.04	0
	2	4.76	-0.0572
	4	4.29	-0.1611
	6	3.98	-0.2361
	8	3.71	-0.3064
	10	3.51	-0.3618
slope of line = -0.037594			
correlation coefficient = -0.996			
$k_f = 1.98 \times 10^{-5} \text{ ms}^{-1}$			

Impeller diameter = 130 mm: vessel diameter = 330 mm

Speed (rpm)	Time (min)	Conc. (ppm)	lnC/C ₀
390	0	5.08	0
	2	4.27	-0.1737
	4	3.84	-0.2798
	6	3.42	-0.3957
	8	3.03	-0.5167
	10	2.69	-0.6358
slope of line = -0.06177			
correlation coefficient = -0.997			
k _f = 3.25 x 10 ⁻⁵ ms ⁻¹			

Impeller diameter = 130 mm: vessel diameter = 330 mm

Speed (rpm)	Time (min)	Conc. (ppm)	lnC/C ₀
500	0	5.06	0
	2	4.16	-0.1959
	4	3.61	-0.3377
	6	3.12	-0.4835
	8	2.71	-0.6244
	10	2.40	-0.7459
slope of line = -0.07373			
correlation coefficient = -0.997			
k _f = 3.88 x 10 ⁻⁵ ms ⁻¹			

Impeller diameter = 130 mm: vessel diameter = 330 mm

Speed (rpm)	Time (min)	Conc. (ppm)	lnC/C ₀
550	0	4.97	0
	2	4.13	-0.1851
	4	3.58	-0.3281
	6	3.13	-0.4624
	8	2.76	-0.5882
	10	2.26	-0.7881
slope of line = -0.07549			
correlation coefficient = -0.997			
k _f = 3.97 x 10 ⁻⁵ ms ⁻¹			

Impeller diameter = 130 mm: vessel diameter = 330 mm

Speed (rpm)	Time (min)	Conc. (ppm)	$\ln C/C_0$
600	0	4.93	0
	2	4.05	-0.1966
	4	3.45	-0.3570
	6	3.02	-0.4901
	8	2.69	-0.6058
	10	2.23	-0.7933
slope of line = -0.07610			
correlation coefficient = -0.997			
$k_f = 4.00 \times 10^{-5} \text{ ms}^{-1}$			

Impeller diameter = 130 mm: vessel diameter = 330 mm

Speed (rpm)	Time (min)	Conc. (ppm)	$\ln C/C_0$
650	0	5.34	0
	2	4.34	-0.2074
	4	3.63	-0.3860
	6	3.22	-0.5058
	8	2.73	-0.6709
	10	2.42	-0.7915
slope of line = -0.07811			
correlation coefficient = -0.996			
$k_f = 4.11 \times 10^{-5} \text{ ms}^{-1}$			

Impeller diameter = 142 mm: vessel diameter = 330 mm

Speed (rpm)	Time (min)	Conc. (ppm)	$\ln C/C_0$
200	0	4.95	0
	2	4.91	-0.0080
	4	4.87	-0.0163
	6	4.75	-0.0412
	8	4.69	-0.0540
	10	4.56	-0.0821
slope of line = -8.19×10^{-3}			
correlation coefficient = -0.978			
$k_f = 0.43 \times 10^{-5} \text{ ms}^{-1}$			

Impeller diameter = 142 mm: vessel diameter = 330 mm

Speed (rpm)	Time (min)	Conc. (ppm)	$\ln C/C_0$
250	0	5.08	0
	2	4.95	-0.0259
	4	4.81	-0.0546
	6	4.63	-0.0928
	8	4.48	-0.1257
	10	4.29	-0.1690
slope of line = -0.1689			
correlation coefficient = -0.996			
$k_f = 0.89 \times 10^{-5} \text{ ms}^{-1}$			

Impeller diameter = 142 mm: vessel diameter = 330 mm

Speed (rpm)	Time (min)	Conc. (ppm)	$\ln C/C_0$
300	0	4.22	0
	2	3.93	-0.0759
	4	3.73	-0.1282
	6	3.36	-0.2326
	8	3.25	-0.2659
	10	2.94	-0.3662
slope of line = -0.03579			
correlation coefficient = -0.994			
$k_f = 1.88 \times 10^{-5} \text{ ms}^{-1}$			

Impeller diameter = 142 mm: vessel diameter = 330 mm

Speed (rpm)	Time (min)	Conc. (ppm)	$\ln C/C_0$
350	0	4.62	0
	2	3.82	-0.1901
	4	3.55	-0.2634
	6	3.23	-0.3579
	8	2.87	-0.4761
	10	2.66	-0.5521
slope of line = -0.05304			
correlation coefficient = -0.990			
$k_f = 2.79 \times 10^{-5} \text{ ms}^{-1}$			

Impeller diameter = 142 mm: vessel diameter = 330 mm

Speed (rpm)	Time (min)	Conc. (ppm)	lnC/C ₀
400	0	5.07	0
	2	4.25	-0.3764
	4	3.65	-0.3286
	6	3.23	-0.4509
	8	2.84	-0.5795
	10	2.50	-0.7071
slope of line = -0.06953			
correlation coefficient = -0.998			
k _f = 3.66 x 10 ⁻⁵ ms ⁻¹			

Impeller diameter = 140 mm: vessel diameter = 330 mm

Speed (rpm)	Time (min)	Conc. (ppm)	lnC/C ₀
500	0	5.03	0
	2	4.18	-0.1851
	4	3.62	-0.3289
	6	3.17	-0.4617
	8	2.78	-0.5930
	10	2.30	-0.7825
slope of line = -0.07527			
correlation coefficient = -0.998			
k _f = 3.96 x 10 ⁻⁵ ms ⁻¹			

Impeller diameter = 142 mm: vessel diameter = 330 mm

Speed (rpm)	Time (min)	Conc. (ppm)	lnC/C ₀
550	0	5.10	0
	2	4.14	-0.2085
	4	3.47	-0.3851
	6	3.07	-0.5076
	8	2.62	-0.6661
	10	2.31	-0.7920
slope of line = -0.0779			
correlation coefficient = -0.996			
k _f = 4.10 x 10 ⁻⁵ ms ⁻¹			

Impeller diameter = 142 mm: vessel diameter = 330 mm

Speed (rpm)	Time (min)	Conc. (ppm)	$\ln C/C_0$
640	0	4.99	0
	2	3.93	-0.2388
	4	3.37	-0.3925
	6	2.86	-0.5566
	8	2.47	-0.7032
	10	2.17	-0.8327
slope of line = -0.08173			
correlation coefficient = -0.995			
$k_f = 4.30 \times 10^{-5} \text{ ms}^{-1}$			

Impeller diameter = 275 mm: vessel diameter = 690 mm

Speed (rpm)	Time (min)	Conc. (ppm)	$\ln C/C_0$
309	0	2.77	0
	2	2.34	-0.1686
	4	1.98	-0.3358
	6	1.71	-0.4824
	8	1.50	-0.6134
	10	1.33	-0.7337
slope of line = -0.073564			
correlation coefficient = -0.998			
$k_f = 3.87 \times 10^{-5} \text{ ms}^{-1}$			

Impeller diameter = 275 mm: vessel diameter = 690 mm

Speed (rpm)	Time (min)	Conc. (ppm)	$\ln C/C_0$
283	0	2.66	0
	2	2.22	-0.1808
	4	1.91	-0.3312
	6	1.69	-0.4536
	8	1.46	-0.5999
	10	1.29	-0.7237
slope of line = -0.071403			
correlation coefficient = -0.998			
$k_f = 3.76 \times 10^{-5} \text{ ms}^{-1}$			

Impeller diameter = 275 mm: vessel diameter = 690 mm

Speed (rpm)	Time (min)	Conc. (ppm)	lnC/C ₀
261	0	2.73	0
	2	2.29	-0.1757
	4	1.97	-0.3263
	6	1.72	-0.4620
	8	1.52	-0.5856
	10	1.35	-0.7042
slope of line = -0.069806			
correlation coefficient = -0.997			
k _r = 3.67 x 10 ⁻⁵ ms ⁻¹			

Impeller diameter = 275 mm: vessel diameter = 690 mm

Speed (rpm)	Time (min)	Conc. (ppm)	lnC/C ₀
200	0	2.71	0
	2	2.35	-0.1425
	4	2.08	-0.2646
	6	1.85	-0.3818
	8	1.74	-0.4431
	10	1.53	-0.5717
slope of line = -0.055393			
correlation coefficient = -0.995			
k _r = 2.92 x 10 ⁻⁵ m ⁻¹			

Impeller diameter = 275 mm: vessel diameter = 690 mm

Speed (rpm)	Time (min)	Conc. (ppm)	lnC/C ₀
171	0	2.80	0
	2	2.48	-0.1214
	4	2.25	-0.2187
	6	2.05	-0.3118
	8	1.90	-0.3878
	10	1.75	-0.4700
slope of line = -0.046319			
correlation coefficient = -0.997			
k _r = 2.44 x 10 ⁻⁵ ms ⁻¹			

Impeller diameter = 275 mm: vessel diameter = 690 mm

Speed (rpm)	Time (min)	Conc. (ppm)	lnC/C ₀
149	0	2.59	0
	2	2.42	-0.0679
	4	2.17	-0.1769
	6	2.06	-0.2290
	8	1.90	-0.3098
	10	1.68	-0.4329
slope of line = -0.04203			
correlation coefficient = -0.994			
k _f = 2.21 x 10 ⁻⁵ ms ⁻¹			

Impeller diameter = 480 mm: vessel diameter = 1200 mm

Speed (rpm)	Time (min)	Conc. (ppm)	lnC/C ₀
162	0	4.18	0
	2	3.53	-0.1690
	4	3.09	-0.3021
	6	2.78	-0.4079
	8	2.43	-0.5424
	10	2.13	-0.6742
slope of line = -0.06567			
correlation coefficient = -0.998			
k _f = 3.46 x 10 ⁻⁵ ms ⁻¹			

Impeller diameter = 480 mm: vessel diameter = 1200 mm

Speed (rpm)	Time (min)	Conc. (ppm)	lnC/C ₀
150	0	4.17	0
	2	3.72	-0.1142
	4	3.20	-0.2648
	6	2.75	-0.4163
	8	2.45	-0.5318
	10	2.24	-0.6214
slope of line = -0.064447			
correlation coefficient = -0.997			
k _f = 3.39 x 10 ⁻⁵ ms ⁻¹			

Impeller diameter = 480 mm: vessel diameter = 1200 mm

Speed (rpm)	Time (min)	Conc. (ppm)	lnC/C ₀
140	0	2.72	0
	2	2.48	-0.0924
	3	2.31	-0.1634
	4	2.13	-0.2445
	5	2.03	-0.2926
	6	1.91	-0.3535
	7	1.76	-0.4353
	slope of line = -0.062634		
correlation coefficient = -0.997			
k _r = 3.30 x 10 ⁻⁵ ms ⁻¹			

Impeller diameter = 480 mm: vessel diameter = 1200 mm

Speed (rpm)	Time (min)	Conc. (ppm)	lnC/C ₀
131	0	4.57	0
	2	3.98	-0.1382
	3	3.75	-0.1978
	4	3.57	-0.2469
	5	3.39	-0.2987
	6	2.21	-0.3532
	7	3.06	-0.4011
	slope of line = -0.056456		
correlation coefficient = -0.997			
k _r = 2.97 x 10 ⁻⁵ ms ⁻¹			

Impeller diameter = 480 mm: vessel diameter = 1200 mm

Speed (rpm)	Time (min)	Conc. (ppm)	$\ln C/C_0$
125	0	2.80	0
	2	2.52	-0.1054
	3	2.43	-0.1417
	4	2.36	-0.1710
	5	2.24	-0.2231
	6	2.17	-0.2548
	7	2.11	-0.2829
	slope of line = -0.040087		
correlation coefficient = -0.995			
$k_f = 2.10 \times 10^{-5} \text{ ms}^{-1}$			

Impeller diameter = 480 mm: vessel diameter = 1200 mm

Speed (rpm)	Time (min)	Conc. (ppm)	$\ln C/C_0$
110	0	3.89	0
	2	3.65	-0.0637
	3	3.57	-0.0858
	4	3.51	-0.1028
	5	3.45	-0.1200
	6	3.36	-0.1465
	7	3.30	-0.1645
	slope of line = -0.02269		
correlation coefficient = -0.993			
$k_f = 1.19 \times 10^{-5} \text{ ms}^{-1}$			

APPENDIX 2A

DETERMINATION OF THE FRICTIONAL TORQUE IN THE TORQUE MEASURING EQUIPMENT - Small Vessels

PART 2A.A BACKGROUND

In the tests on the 185, 305 and 330 mm diameter vessels, the friction generated by the four ball bearings in the thrust bearing that supported the turntable would oppose the torque applied to the table by the mixing vessel. To determine this opposing torque, τ_{fric} measurements were conducted after each kinetic test. As shown in Figure 2A.1, a torque was applied to the turntable using known weights. Some difficulties were experienced in getting reproducible results. The system that was found to be most reliable is the one shown in the figure.

A torque was applied to the turntable by means of a weight suspended from the turntable by a string over a polished bar. The string between the turntable and the bar was stretched and the weight was allowed to take up the tension. With this arrangement T_2 is greater than T_1 . These tensions are related by the formula:

$$\frac{T_1}{T_2} = e^{-\mu\beta} \quad 2A.1$$

where μ is the bollard friction and β is the angle of contact of the string over the bar ($= \pi/2$ radians in this case).

The applied torque, τ_{app} is therefore given by:

$$\tau_{app} = F_T d_s = T_2 d_s = T_1 d_s e^{\mu\beta} \quad 2A.2$$

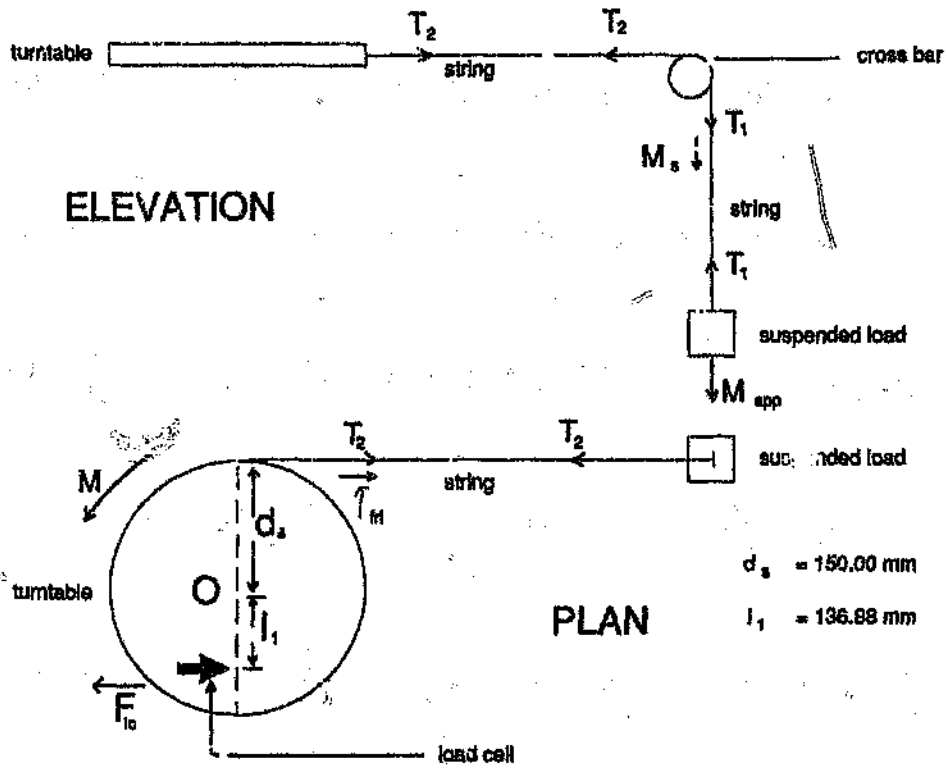


Figure 2A.1: Schematic diagram for the determination of the static frictional torque in the set-up for the 185, 305 and 330 mm diameter vessels

The load cell provides an opposing torque, τ_{lc} , which is given by:

$$\tau_{lc} = F_{lc}L_1 \quad 2A.3$$

where F_{lc} is the force measured by the load cell.

Because of the way the system was set up the applied torque decreased from the initial tension (imposed by stretching the string) down to the equilibrium value where:

$$T_2 = T_1 e^{\mu\theta} \quad 2A.4$$

It took about ten minutes for this equilibrium to be reached - the string slipping on the bar until the system had reached this state. The consequence of this was that the force F_{lc} decreased with time and as the system moved to equilibrium, the turntable moved marginally as shown by the arrow M. The direction of table motion is important because the frictional torque in the table bearing would oppose such motion.

At equilibrium therefore,

$$\tau_{lc} = \tau_{frl} + \tau_{app} \quad 2A.5$$

$$M_{lc}gl_1 = \tau_{frl} + (M_{app} + M_s)gd_s e^{\mu\theta} \quad 2A.6$$

$$M_{lc} = INTT + GRADT (M_{app} + M_s) \quad 2A.7$$

where M_{app} , M_s and M_{lc} are respectively the masses of the weights, the string between the bar and the weight recorded by the load cell and g is the acceleration due to gravity ($= 9.81 \text{ ms}^{-2}$).

By measuring M_{lc} for a range of weights M_{app} , it is possible to determine the intercept with the M_{lc} axis (INTT) and the gradient of the curve (GRADT). The Bollard friction was determined in a separate experiment

- the value obtained was 0.22 (see Part 2A.B) - but can also be found from the GRADT using Equation 2A.8:

$$\mu = \frac{1}{\beta} \ln\left(\frac{l_1 \text{GRADT}}{d_s}\right) \quad 2A.8$$

Thereafter τ_{fri} can be determined from Equation 2A.9:

$$\tau_{fri} = gl_1(INTT) \quad 2A.9$$

PART 2A.B BOLLARD FRICTION

The value of the Bollard friction, μ , was estimated by suspending the weights from the load cell directly - as shown in Figure 2A.2. From this it can be seen that

$$\frac{T_2}{T_1} = e^{-\mu\beta} \quad 2A.10$$

and so

$$M_{lc} = (M_{app} + M_s) e^{-\mu\beta} \quad 2A.11$$

The data obtained is shown in Table 2A.1. (NOTE: the values of M_{lc} are negative because the string was pulling on the load cell.)

Table 2A.1: Data for determination of Bollard Friction

$M_{app} + M_s$ (g)	401.029	302.729	203.029	151.929
M_{lc} (g)	-286.29	-216.57	-145.78	-110.91
$M_{app} + M_s$ (g)	103.029	73.229	24.729	
M_{lc} (g)	-74.96	-53.18	-19.41	

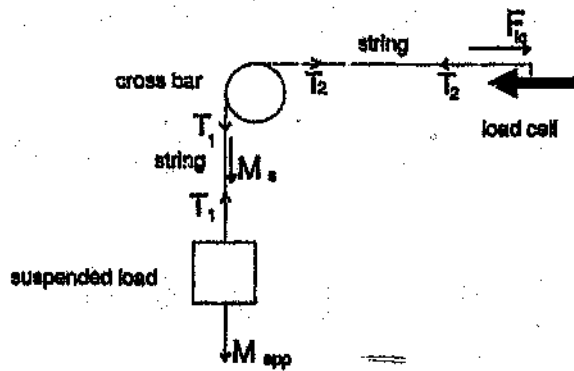


Figure 2A.2: Schematic diagram for the determination of Bollard friction on the cross bar

The regression equation for this data was found to be

$$-M_{lc} = 1.91 + 0.709(M_{app} + M_s) \quad 2A.12$$

from which $\mu = 0.219$.

PART 2A.C EXAMPLE OF FRICTIONAL TORQUE CALCULATION

Table 2A.2: Friction data for kinetic test on the 305 mm diameter vessel and impeller diameter of 110 mm at 300 rpm.

$M_{app}+M_s$ (g)	401.033	302.733	203.033	151.933
M_{lc} (g)	606.96	488.22	343.34	270.35
$M_{app}+M_s$ (g)	103.033	73.233	24.733	
M_{lc} (g)	175.58	128.74	61.20	

Table 2A.2 indicates the data obtained after the kinetic test on the 305 mm diameter vessel with 110 mm diameter impeller at 300 rpm. The regression equation for this data with a correlation coefficient of 0.998 is

$$M_{lc} = 30.254 + 1.48(M_{app} + M_s) \quad 2A.13$$

From which $\tau_{frl} = 30.254 \times 9.81 \times 13.688 \times 10^{-5} \text{ Nm}$
 $= 0.0406 \text{ Nm}$.

PART 2A.D CHECK ON THE VALUE OF THE BOLLARD FRICTION

The regression equations for the frictional torque that were obtained after each kinetic test were examined. The mean value of GRADT in these equations was $1.419g^{-1}$, the minimum and maximum values being respectively $1.33g^{-1}$ and $1.57g^{-1}$.

Using Equation 2A.8 the values for μ calculated from these equations have a range (minimum to maximum) of 0.123 to 0.229 with a mean of 0.165. These values are of similar magnitude to the value of 0.219 determined in an independent experiment as described in Part 2A.B.

The relative standard deviation on GRADT was about 4% giving a relative standard deviation on the Bollard friction of about 15%. There are two reasons why this high value (15%) is not a cause of concern. Firstly, the tests were done at different times over a period of months. Therefore the frictional conditions in the different experiments were very likely to be slightly different. Secondly, the value of the Bollard friction affects the estimate of τ_{fr} very little indeed because the value of M_s is very small.

APPENDIX 2B

DETERMINATION OF THE FRICTIONAL TORQUE IN THE TORQUE MEASURING EQUIPMENT - Large Vessels

PART 2B.A BACKGROUND

The basis for determining the frictional torque in the torque measuring system for the large vessels (690 and 1200 mm diameter) was very similar to that described in Appendix 2A. The only difference arose from the scale of the equipment and the different configuration used. The frictional torque was expected to be fairly high because the systems were more robust and in the case of the 1200 mm diameter vessel, two bearings were used in the system - one to support the drive system and the other to stabilise the impeller. Figure 2B.1 illustrates the system used.

Measurements to determine the frictional torque were conducted several times during the series of kinetic tests. Unfortunately the range of weights that were used was too small and very inconsistent results were obtained. The measurements were repeated after the kinetic tests had been completed and the results reported below were obtained.

Unlike in the measurements on the small vessel system, the tension in the vertical section of the cord (T_1 in Figure 2B.1) was greater than the tension in the horizontal part of the cord (T_2 in the figure). Consequently, during a measurement of the frictional torque the force registered by the load cell increased slightly until equilibrium was reached. This meant that motion within the bearings was in the direction indicated by arrow M in Figure 2B.1 and the associated frictional torque acted in concert with the torque exerted by the

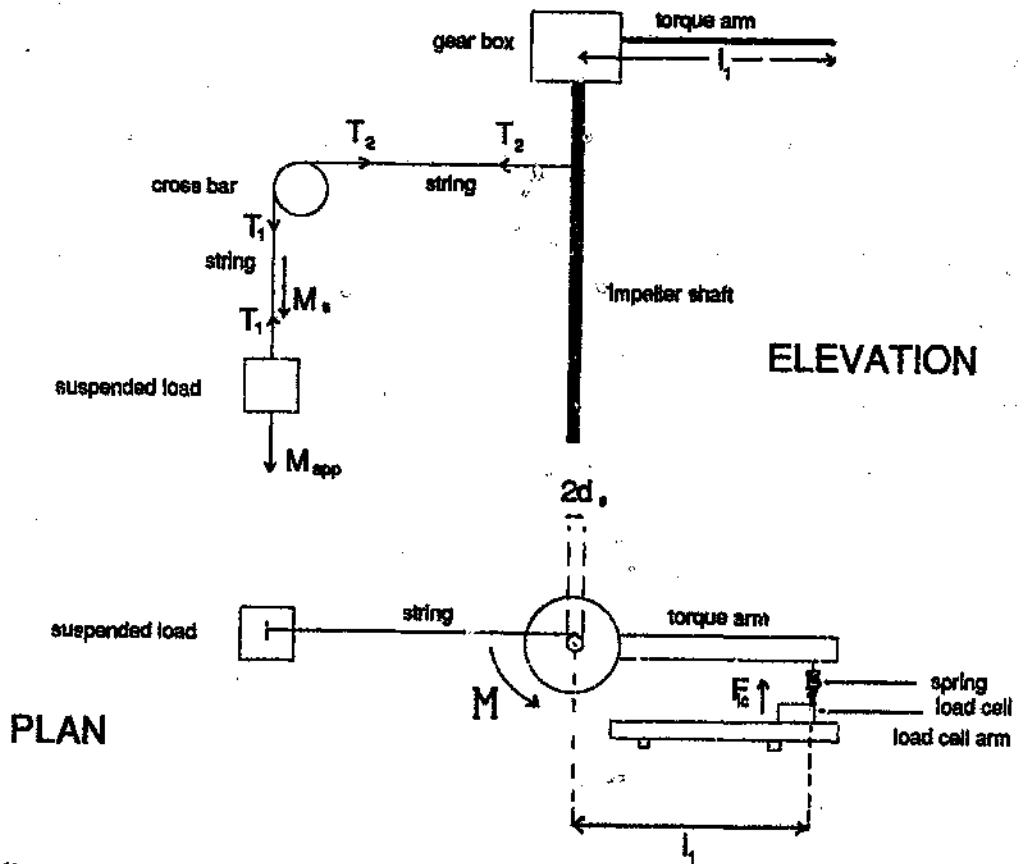


Figure 2B.1: Schematic diagram for the determination of the static frictional torque in the set-up for the 690 and 1200 mm diameter vessels

load cell. Therefore:

$$\tau_{lc} + \tau_{frt} = \tau_{app} \quad 2B.1$$

$$T_2 = T_1 e^{-\mu\beta} \quad 2B.2$$

$$M_{lc} g l_1 = (M_{app} + M_s) g d_s e^{-\mu\beta} - \tau_{frt} \quad 2B.3$$

In this case $l_1 = 700$ mm and $d_s = 26$ mm for the 690 mm vessel system and $l_1 = 1000$ mm and $d_s = 15$ mm for the 1200 mm vessel system.

The load cell was not set at zero during these tests but at an initial reading of M_0 when not under load. The actual load measured by the load cell, M_{lc} , was therefore the difference between M_0 and the registered load M_{reg} . (M_{reg} was always smaller than M_0 because the system was pulling on the load cell. Therefore:

$$M_{lc} = M_0 - M_{reg} \quad 2B.4$$

$$M_{reg} = M_0 + \frac{\tau_{frt}}{g l_1} - (M_{app} + M_s) g d_s e^{-\mu\beta} \quad 2B.5$$

Plotting M_{reg} against $M_{app} + M_s$ will give value for the intercept, INTT, and gradient, GRADD, as follows:

$$INTT = M_0 + \frac{\tau_{frt}}{g l_1} \quad 2B.6$$

$$GRADD = - \frac{d_s e^{-\mu\beta}}{l_1} \quad 2B.7$$

from which

$$\tau_{frt} = (INTT - M_0) g l_1 \quad 2B.8$$

$$\mu = \frac{1}{n} \ln \left(-GRADD \frac{l_1}{d_s} \right)$$

2B.9

PART 2B.B 690 mm Vessel

The data from one set of measurements is shown below:

Table 2B.1: Friction data (690 mm Vessel)

$M_{app} + M_s$ (kg)	2.00	5.06	7.18	10.50
M_{reg} (g)	-1438.65	-1510.33	-1558.15	-1620.03

$M_{app} + M_s$ (kg)	12.00	14.42
M_{reg} (g)	-1646.72	-1701.18

$$M_0 = -1420.90 \text{ g}$$

The regression line for this data is

$$M_{reg} = -1402.59 - 0.02071(M_{app} + M_s) \quad 2B.10$$

The regression coefficient is -0.9989. From Equations 2B.8 to 2B.10 the frictional torque and coefficient of friction for this set of data were found to be 0.1257 Nm and 0.3719 respectively. Taking the mean values from four sets of measurements the following values were obtained:

$$\tau_{fri} \text{ (690 mm vessel)} = 0.126 \text{ Nm and}$$

$$\mu = 0.37$$

The relative standard deviation on τ_{fri} was 0.8% and on μ was 1.2%.

PART 2B.C 1200 mm Vessel

The data from one set of measurements is shown below:

Table 2B.2: Friction data (1200 mm vessel)

$M_{app}+M_s$ (kg)	13.37	20.10	25.90	31.34
M_{reg} (g)	-1413.16	-1454.56	-1503.86	-1541.70

$M_{app}+M_s$ (kg)	42.87
M_{reg} (g)	-1666.76

$$M_0 = -1370.13 \text{ g}$$

The regression line for this data is

$$M_{reg} = -1286.18 - 8.6 \times 10^{-3}(M_{app} + M_s) \quad 2B.11$$

The regression coefficient is -0.993. From Equations 2B.8, 2B.9 and 2B.11 the frictional torque and coefficient of friction for this set of data were found to be 0.8236 Nm and 0.364 respectively. Taking the mean values from four sets of measurements the following values were obtained:

$$\tau_{frl} \text{ (1200 mm vessel)} = 0.823 \text{ Nm and}$$

$$\mu = 0.364$$

The relative standard deviation on τ_{frl} was 0.7% and on μ was 2.9%.

PART 2B.D CHECK ON BOLLARD FRICTION

As a means of checking the data reported above, the values of the Bollard Friction that were obtained may be compared. It can be seen that the two mean values (0.37 and 0.364) are very close. The range of weights used was different in the two series of tests - 2.00 to 14.42 kg

for the 650 mm vessel, and 13.37 to 42.87 kg for the 1200 mm vessel. The measurements that have been made are therefore seen to be consistent.

APPENDIX 3A

BI-LINEAR MODEL - THEORY

The plots of k_f vrs speed or power input take the form of the graph shown in Figure 3A.1. The two straight lines intercept each other at x_c and the slopes of the two lines before and after x_c are β and γ respectively.

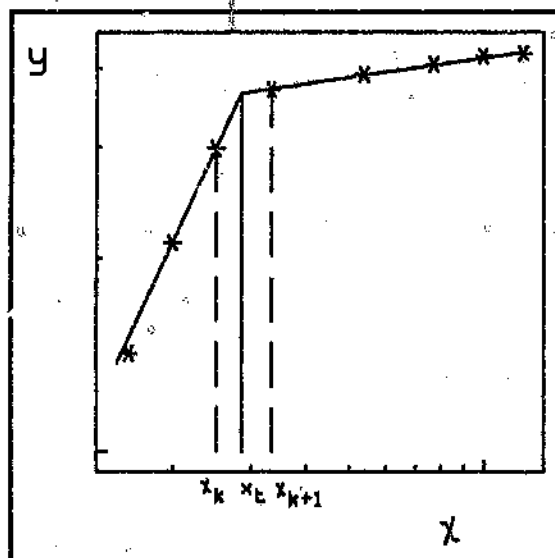


Figure 3A.1: A sketch of the relationship between the film mass transfer coefficient and the power input for agitation during the adsorption of aurocyanide onto activated carbon

$$\text{Model: } \begin{aligned} y &= \alpha + \beta x && \text{for } x \leq x_c \\ &= \alpha + \beta x_c + \gamma (x - x_c) && \text{for } x > x_c \end{aligned} \quad (1)$$

$$= \delta + \gamma x \quad (2)$$

where $\delta = \alpha + (\beta - \gamma) x_t$

Residual sum of squares S is the sum of S_L , the sum of the squares of the residuals at the left side of x_t , and S_R , the corresponding value for the right side of x_t , so that:

$$S_L = \sum_{i=1}^k (y_i - \alpha - \beta x_i)^2 \quad (4)$$

and

$$S_R = \sum_{i=k+1}^n (y_i - \alpha - \beta x_t - \gamma(x_i - x_t))^2 \quad (5)$$

where k is such that $x_k \leq x_t < x_{k+1}$

SOLUTION OF THE MODEL EQUATION

Minimising S_R with respect to γ , by finding the partial derivative of S_R with respect to the parameter γ ,

$$\frac{\partial S_R}{\partial \gamma} = -2 \sum_{i=k+1}^n (x_i - x_t) (y_i - \alpha - \beta x_t - \gamma(x_i - x_t)) \quad (6)$$

$$= -2 \left[\sum_{i=k+1}^n (x_i - x_t) y_i - (\alpha + \beta x_t) \sum_{i=k+1}^n (x_i - x_t) - \gamma \sum_{i=k+1}^n (x_i - x_t)^2 \right]$$

For $\frac{\partial S_R}{\partial \gamma} = 0$, $\gamma = \gamma$

$$\gamma = \frac{\sum_{i=k+1}^n (x_i - x_t) y_i - (\alpha + \beta x_t) \sum_{i=k+1}^n (x_i - x_t)}{\sum_{i=k+1}^n (x_i - x_t)^2}$$

$$= \frac{B - (\alpha + \beta x_t) C}{A}$$

$$\text{where } A = \sum_{i=k+1}^n (x_i - x_t)^2, \quad B = \sum_{i=k+1}^n (x_i - x_t) y_i, \quad C = \sum_{i=k+1}^n (x_i - x_t)$$

$$S_R = \sum_{i=k+1}^n (y_i - \alpha - \beta x_t)^2 - 2\gamma \sum_{i=k+1}^n (y_i - \alpha - \beta x_t) (x_i - x_t) + \gamma^2 \sum_{i=k+1}^n (x_i - x_t)^2$$

$$= \sum_{i=k+1}^n (y_i - \alpha - \beta x_t)^2 - 2\gamma B + 2\gamma (\alpha + \beta x_t) C + \gamma^2 A$$

$$= \sum_{i=k+1}^n (y_i - \alpha - \beta x_t)^2 - 2\gamma B + 2\gamma (\alpha + \beta x_t) C + \gamma^2 A$$

$$S_{R|\gamma} = \sum_{i=k+1}^n (y_i - \alpha - \beta x_t)^2 - \left[\frac{B - (\alpha + \beta x_t) C}{A} \right] [2B - 2(\alpha + \beta x_t) C + (B + (\alpha + \beta x_t) C)]$$

$$= \sum_{i=k+1}^n (y_i - \alpha - \beta x_t)^2 - \frac{[B - (\alpha + \beta x_t) C]^2}{A}$$

$$S_{|\gamma} = \sum_{i=1}^k (y_i - \alpha - \beta x_i)^2 + \sum_{i=k+1}^n (y_i - \alpha - \beta x_t)^2 - \frac{[B - (\alpha + \beta x_t) C]^2}{A}$$

$$S_{|\gamma} = S_2 + S_{R|\gamma}$$

Minimising $S_{|\gamma}$ with respect to α and β ,

$$\frac{\partial S_{|\gamma}}{\partial \alpha} = -2 \left[\sum_{i=1}^k (y_i - \alpha - \beta x_i) + \sum_{i=k+1}^n (y_i - \alpha - \beta x_t) \right] - \frac{2}{A} [B - (\alpha + \beta x_t) C] (-C)$$

$$= -2 \left[\sum_{i=1}^n (y_i - n\alpha - \beta \sum_{i=1}^k \chi_i + (n-k)x_c - \frac{CB}{A} + \frac{C^2\alpha}{A} + \frac{C^2x_c\beta}{A}) \right]$$

$$= -2 \left[\sum_{i=1}^n y_i - \frac{CB}{A} + \alpha \left(\frac{C^2}{A} - n \right) + \beta \left(x_c \left(\frac{C^2}{A} - n + k \right) - \sum_{i=1}^k \chi_i \right) \right]$$

$$\frac{\partial S_{1\gamma-\gamma}}{\partial \beta} = -2 \left[\sum_{i=1}^k \chi_i (y_i - \alpha - \beta \chi_i) + x_c \sum_{i=k+1}^n (y_i - \alpha - \beta x_c) - \frac{Cx_c}{A} (B - (\alpha + \beta x_c) C) \right]$$

$$= -2 \left[\sum_{i=1}^k \chi_i y_i - \alpha \sum_{i=1}^k \chi_i - \beta \sum_{i=1}^k \chi_i^2 + x_c \sum_{i=k+1}^n y_i - \alpha x_c (n-k) - \beta x_c (n-k) - \frac{Cx_c B}{A} + \frac{\alpha C^2 x_c}{A} + \frac{\beta C^2 x_c^2}{A} \right]$$

$$= -2 \left[\sum_{i=1}^k \chi_i y_i + x_c \sum_{i=k+1}^n y_i - \frac{Cx_c B}{A} + \alpha \left(\frac{C^2 x_c}{A} - \sum_{i=1}^k \chi_i - x_c (n-k) \right) + \beta \left(\frac{C^2 x_c^2}{A} - \sum_{i=1}^k \chi_i^2 - x_c^2 (n-k) \right) \right]$$

$$\text{For } \frac{\partial S_{1\gamma-\gamma}}{\partial \alpha} = \frac{\partial S_{1\gamma-\gamma}}{\partial \beta} = 0, \quad \alpha = \hat{\alpha}, \quad \beta = \hat{\beta}$$

$$\Rightarrow \begin{pmatrix} \hat{\alpha} \\ \hat{\beta} \end{pmatrix} = \begin{pmatrix} \frac{C^2}{A} - n & x_c \left(\frac{C^2}{A} - n + k \right) - \sum_{i=1}^k \chi_i \\ x_c \left(\frac{C^2}{A} - n + k \right) - \sum_{i=1}^k \chi_i & x_c^2 \left(\frac{C^2}{A} - n + k \right) - \sum_{i=1}^k \chi_i^2 \end{pmatrix}^{-1}$$

$$* \begin{pmatrix} \frac{CB}{A} - \sum_{i=1}^n y_i \\ x_c \left(\frac{CB}{A} - \sum_{i=k+1}^n y_i \right) - \sum_{i=1}^k \chi_i y_i \end{pmatrix}$$

$$S_{\min|x} = \frac{\sum_{i=1}^k (y_i - \hat{\alpha} - \hat{\beta}x_i)^2 + \sum_{k=1}^n (y_i - \hat{\alpha} - \hat{\beta}x_i)^2}{(B - (\hat{\alpha} + \hat{\beta}x_i)C)^2}$$

This last equation is minimised with respect to x_i , by iteration. Depending on the accuracy required, the minimum sum of squares of the residuals gives the best fit values of x_i , α , β , γ and δ .

APPENDIX 3B

C COMPUTER PROGRAM FOR THE ESTIMATION OF PARAMETERS
 IN THE BI-LINEAR MODEL

C LEAST SQUARES PROGRAM FOR THE BI-LINEAR REGRESSION
 MODEL

```
REAL *8  X(50),Y(50),ALPHA,BETA,GAMMA,DELTA,SSMIN
REAL *8  XTURN,XSTART,STEPSZ
INTEGER *4  NORD,I, IANS,NOSTEP
CHARACTER *80  INNAME,OUTNAME
```

C OPENING FILES

```
WRITE(*,*)'PLEASE SUPPLY THE NAME OF THE FILE THE
& X-Y VALUES'
```

```
WRITE(*,*)
```

```
READ(*,'(A80)') INNAME
```

C

```
OPEN(10,FILE=INNAME,STATUS='OLD')
```

```
WRITE(*,*)'WHAT IS THE NAME OF THE OUTPUT FILE'
```

```
WRITE(*,*)
```

```
READ(*,'(A80)') OUTNAME
```

```
OPEN(8,FILE=OUTNAME,STATUS='NEW')
```

C

```
WRITE(*,*)'PLEASE INPUT VALUE FOR NORD'
```

```
READ(*,*) NORD
```

C 100 FORMAT(I2)

C WRITE (*,*)'PLEASE INPUT VALUES FOR X AND Y'

```
READ(10,*) (X(I),Y(I),I=1,NORD)
```

C

C READ(5,101) (X(I),I=1,NORD)

C READ(5,101) (Y(I),I=1,NORD)

C 101 FORMAT(6F2.2)

```
WRITE(*,*)'WRITE 1 IF YOU WANT LOG TRANSFER OF
$ X-Y, OTHERWISE 0'
```

```
C WRITE (*,*) 'INPUT IANS'  
  READ(*,*) IANS
```

```
C 111 FORMAT(I2)
```

```
C TRANSFORMING THE VALUES
```

```
  IF (IANS .NE. 1) GO TO 10  
  DO 1 I = 1,NORD  
  1 Y(I) = ALOG(Y(I))  
10 CONTINUE
```

```
C  
  IF (IANS .NE.1) GO TO 11  
  DO 13 I =1,NORD
```

```
13 X(I) = ALOG(X(I))  
11 CONTINUE  
2 CONTINUE
```

```
  WRITE(*,102)
```

```
102 FORMAT('WRITE LOWEST VALUE, STEPSIZE AND # OF  
!STEPS FOR TRIAL TURNING POINTS')
```

```
  READ(*,*) XSTART, STEPSZ, NOSTEP
```

```
  XTURN = XSTART - STEPSZ
```

```
  DO 3 I=1,NOSTEP
```

```
  XTURN = XTURN + STEPSZ
```

```
  CALL TURNPT(NORD, X, Y, XTURN, ALPHA, BETA, GAMMA,  
&DELTA, SSMIN)
```

```
  WRITE(*,105) XTURN, ALPHA, BETA, GAMMA, DELTA, SSMIN
```

```
  WRITE(8,105) XTURN, ALPHA, BETA, GAMMA, DELTA, SSMIN
```

```
105 FORMAT(T2,F8.4,T14,E12.6,T27,E12.6,T40,E12.6,T53,  
@E12.6,T66,E14.6)
```

```
3 CONTINUE
```

```
  WRITE(*,106)
```

```
106 FORMAT(/T2,'WRITE 1 IF YOU WANT ANOTHER TRY,  
!OTHERWISE 0')
```



```

      READ(*,*) IANS
C 107 FORMAT(I2)
      IF (IANS .EQ. 1) GO TO 2
      CLOSE(8)
      CLOSE(10)
      STOP
      END

C      THIS IS THE END OF THE MAIN PROGRAM

C      SUBROUTINE BEGINS

      SUBROUTINE TURNPT(NORD, X, Y, XTURN, ALPHA, BETA, GAMMA,
#DELTA, SSMIN)
      REAL *8 X(NORD), Y(NORD), A(2,2), B(2),
*ALPHA, BETA, GAMMA
      REAL *8 DELTA, SSMIN, DFIX, SUM, TERM
      REAL*8 XTURN, ASUM, BSUM, CSUM, DSUM, ESUM,
@FSUM, GSUM, HSUM
      INTEGER *4 I, ILOW, NORD

      ASUM = 0.
      BSUM = 0.
      CSUM = 0.
      DSUM = 0.
      ESUM = 0.
      FSUM = 0.
      GSUM = 0.
      HSUM = 0.
      K = 0
      DO 1 I = 1, NORD
      K = K + 1
      IF (X(K) .GT. XTURN) GO TO 2
1 CONTINUE
2 K = K - 1
      DO 3 I = 1, K
      DSUM = DSUM + X(I)

```

```

ESUM = ESUM + X(I)**2
FSUM = FSUM + X(I)*Y(I)
3 HSUM = HSUM + Y(I)
ILOW = K + 1
DO 4 I = ILOW, NORD
DIFX = X(I) - XTURN
ASUM = ASUM + DIFX **2
BSUM = BSUM + DIFX *Y(I)
CSUM = CSUM + DIFX
GSUM = GSUM + Y(I)
4 HSUM = HSUM + Y(I)
TERM = CSUM **2/ASUM - NORD
A(1,1) = TERM
A(1,2) = XTURN *(TERM + K) - DSUM
A(2,1) = A(1,2)
A(2,2) = XTURN **2*(TERM + K) - ESUM
B(1) = CSUM *BSUM/ASUM - HSUM
B(2) = XTURN *(CSUM * BSUM/ASUM -GSUM) - FSUM
A(1,2) = A(1,2)/A(1,1)
B(1) = B(1)/A(1,1)
A(2,2) = A(2,2) - A(1,2)*A(2,1)
B(2) =B(2) - B(1)* A(2,1)
BETA = B(2)/A(2,2)
ALPHA = B(1) - B(2)*A(1,2)/A(2,2)
DELTA = ALPHA + BETA * XTURN
GAMMA = (BSUM - DELTA * CSUM)/ASUM
DELTA = DELTA - GAMMA * XTURN
SUM = 0.
DO 5 I = 1,K
5 SUM = SUM + (Y(I) -ALPHA - BETA * X(I)) ** 2
DO 6 I = ILOW, NORD
6 SUM = SUM + (Y(I) - ALPHA - BETA *XTURN) ** 2
SSMIN = SUM -GAMMA ** 2 * ASUM
RETURN
END

```

APPENDIX 4A

FITNESS OF THE BI-LINEAR MODEL

The residual sum of squares of a model fit provides a quantitative measure of the fitness of the model.

For the models:

$$y = \alpha + \beta x + \varepsilon \quad \text{for } x \leq x_c \quad 4A.1$$

$$= \delta + \gamma x + \varepsilon \quad \text{for } x > x_c$$

Analysis of the variance summarizes information related to the sources of variation in the data as:

$$DATA = MODEL FIT + RESIDUAL \quad 4A.2$$

This variation is quantified by squaring and summing the deviations as:

$$SST = SSM + SSR \quad 4A.3$$

where SST is the total variation, SSM is the variation due to the model, SSR is the variation due to the error (residual).

Algebraically Equation 4A.3 is equal to:

$$\sum (y_i - \bar{y})^2 = \sum (\hat{y}_i - \bar{y})^2 + \sum (y_i - \hat{y}_i)^2 \quad 4A.4$$

where y_i = experimental data i , \bar{y} = mean of the experimental data and \hat{y}_i = the predicted value of y_i using the model.

The value for SSR is the SSMIN obtained during the regression described in Appendix 3B (results of the bi-linear regression program). Therefore SST can be calculated from Equation 4A.4, and SSM may be found by difference. The squared multiple correlation coefficient R^2 , gives the proportion of the total variation of the data which is explained by the model. The nearer R to 1,

the more significant the fit of the model to the data.
It is given by:

$$R^2 = \frac{SSM}{SST}$$

4A.5

The Fortran program used to do this is outlined in Appendix 4B. The values of R are given in Table 5.1 in Chapter 5.

APPENDIX 4B

C **COMPUTER PROGRAM TO DETERMINE THE FITNESS OF THE
BI-LINEAR MODEL.**

C A PROGRAM FOR TESTING THE ADEQUACY OF THE
C BI-LINEAR REGRESSION MODEL BY CALCULATING THE
C REGRESSION CORRELATION (EFFICIENT

```
REAL *8 X(10),Y(10),SSMIN,SY
REAL *8 YM,SST,SSM,RSQ
INTEGER *4 I
CHARACTER *80 INNAME,OUTNAME
```

C OPENING FILES

```
WRITE(*,*)'PLEASE SUPPLY THE NAME OF THE FILE OF  
! THE X-Y VALJES'
```

```
WRITE(*,*)
READ(*,'(A80)') INNAME
```

C

```
OPEN(10,FILE=INNAME,STATUS='OLD')
WRITE(*,*) 'WHAT IS THE NAME OF THE OUTPUT FILE'
WRITE(*,*)
READ(*,'(A80)') OUTNAME
OPEN(8,FILE=OUTNAME,STATUS='NEW')
```

C

```
READ INPUT
WRITE(*,*) 'WHAT IS THE NUMBER OF RECORDS (X-Y  
* VALUES)'
```

```
READ(*,*) N
DO 10 I = 1,N
READ(10,*) X(I),Y(I)
```

10 CONTINUE

C

```
CALCULATING Y-MEAN
SY = 0.0
```

```

DO 12 I = 1,N
SY = SY + LOG(Y(I))
12 CONTINUE
YM = SY/N

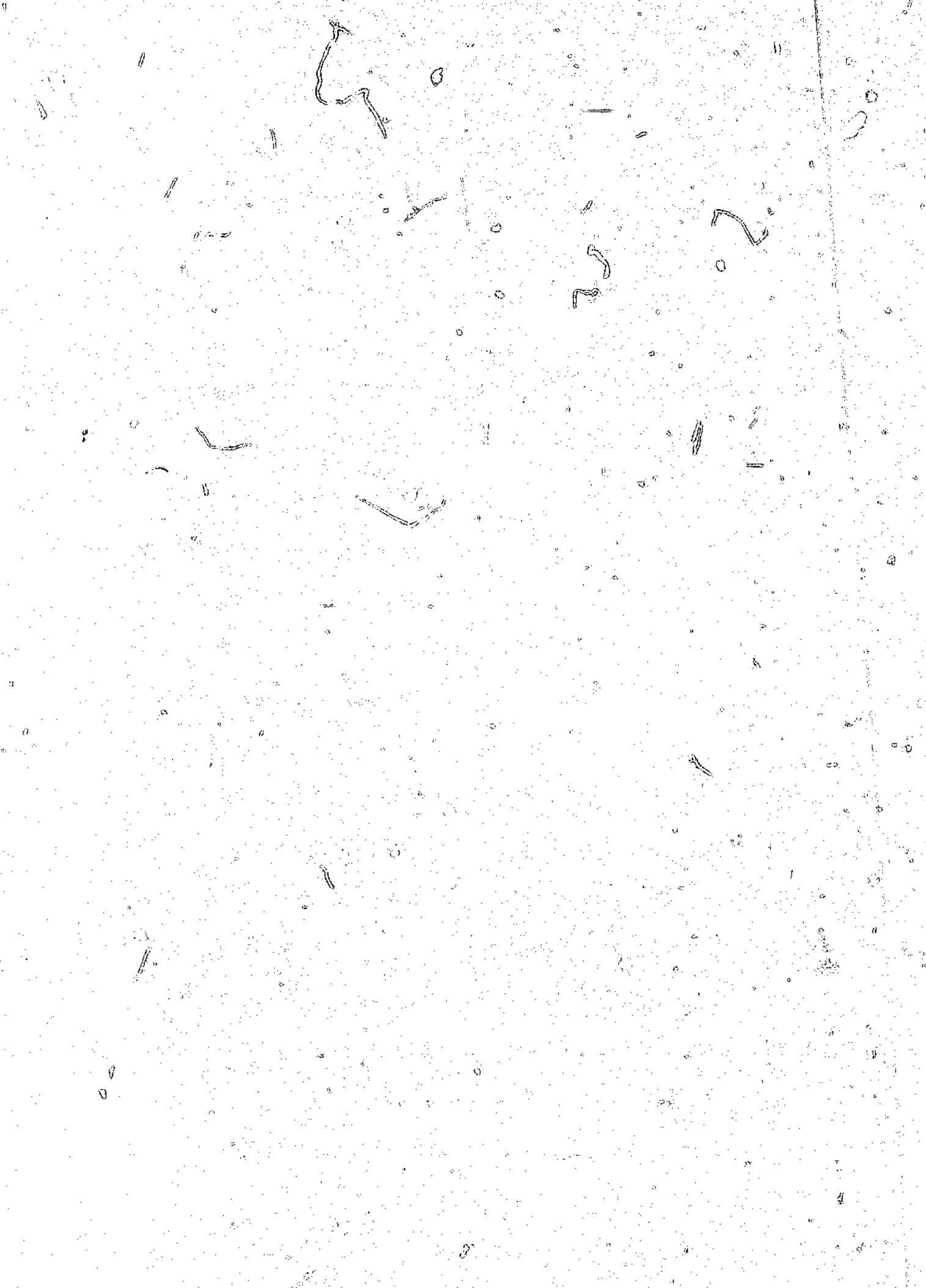
SST = 0
DO 15 I = 1,N
SST = SST + (LOG(Y(I)) - YM)**2
15 CONTINUE
WRITE(8,*)
C WRITE(8,51) SST

SSM = SST - SSMIN

RSQ = SSM/SST
22 WRITE(8,52) RSQ
WRITE(*,52) RSQ
52 FORMAT(T2,E12.6)
CLOSE(10)
CLOSE(8)

STOP
END

```



Author: Afewu, Kodjo Isaac.

Name of thesis: Scale-up in carbon-in-pulp adsorption process systems.

PUBLISHER:

University of the Witwatersrand, Johannesburg

©2015

LEGALNOTICES:

Copyright Notice: All materials on the University of the Witwatersrand, Johannesburg Library website are protected by South African copyright law and may not be distributed, transmitted, displayed or otherwise published in any format, without the prior written permission of the copyright owner.

Disclaimer and Terms of Use: Provided that you maintain all copyright and other notices contained therein, you may download material (one machine readable copy and one print copy per page) for your personal and/or educational non-commercial use only.

The University of the Witwatersrand, Johannesburg, is not responsible for any errors or omissions and excludes any and all liability for any errors in or omissions from the information on the Library website.